A Statistical Approach to Solar Photovoltaic Module Lifetime Prediction

by

Joseph Mathurin Kuitche

A Dissertation Presented in Partial Fulfillment
of the Requirements for the Degree
Doctor of Philosophy

Approved November 2014 by the
Graduate Supervisory Committee:

Rong Pan, Co-Chair
Govindasamy TamizhMani, Co-Chair
Douglas C. Montgomery
Teresa Wu

ARIZONA STATE UNIVERSITY

December 2014

ABSTRACT

The main objective of this research is to develop an approach to PV module lifetime prediction. In doing so, the aim is to move from empirical generalizations to a formal predictive science based on data-driven case studies of the crystalline silicon PV systems. The evaluation of PV systems aged 5 to 30 years old that results in systematic predictive capability that is absent today. The warranty period provided by the manufacturers typically range from 20 to 25 years for crystalline silicon modules. The end of lifetime (for example, the time-to-degrade by 20% from rated power) of PV modules is usually calculated using a simple linear extrapolation based on the annual field degradation rate (say, 0.8% drop in power output per year). It has been 26 years since systematic studies on solar PV module lifetime prediction were undertaken as part of the 11-year flat-plate solar array (FSA) project of the Jet Propulsion Laboratory (JPL) funded by DOE. Since then, PV modules have gone through significant changes in construction materials and design; making most of the field data obsolete, though the effect field stressors on the old designs/materials is valuable to be understood. Efforts have been made to adapt some of the techniques developed to the current technologies, but they are too often limited in scope and too reliant on empirical generalizations of previous results. Some systematic approaches have been proposed based on accelerated testing, but no or little experimental studies have followed. Consequently, the industry does not exactly know today how to test modules for a 20 – 30 years lifetime.

This research study focuses on the behavior of crystalline silicon PV module technology in the dry and hot climatic condition of Tempe/Phoenix, Arizona. A three-phase approach was developed: (1) A quantitative failure modes, effects, and criticality analysis (FMECA) was developed for prioritizing failure modes or mechanisms in a given environment; (2) A time-series approach was used to model

environmental stress variables involved and prioritize their effect on the power

output drop; and (3) A procedure for developing a prediction model was proposed for

the climatic specific condition based on accelerated degradation testing

DEDICATION

In memory of

    my father, Victor Founta;

    and my sister, Appolline Chantal Kengne …

ACKNOWLEDGEMENTS

TABLE OF CONTENTS

LIST OF TABLES

LIST OF FIGURES

xiii

CHAPTER I

INTRODUCTION

1.1   Why PV Reliability is important

For nearly two decades now, the photovoltaic (PV) industry has been growing at a very high rate. In the last decade, the total cumulative PV capacity increased at an average of 49% per year; reaching 135-GW installation at the end of 2013 (Figure 1). Between 1983 and 1999 (Figure 2), PV shipments grew by about 15%, with nearly 150MW produced in 1998 and 200MW in 1999 (Wang, et al., 2011). Even though fossil fuels still constitute about 80% of today's world energy, the percentage of the total energy consumption from solar has been on the rise: At the end of 2013, the solar power plants account for 5.3% of German electricity consumption, 7% in Italy, and 3% in Belgium, Bulgaria, Czech Republic, Greece and Spain (IEA, 2014).
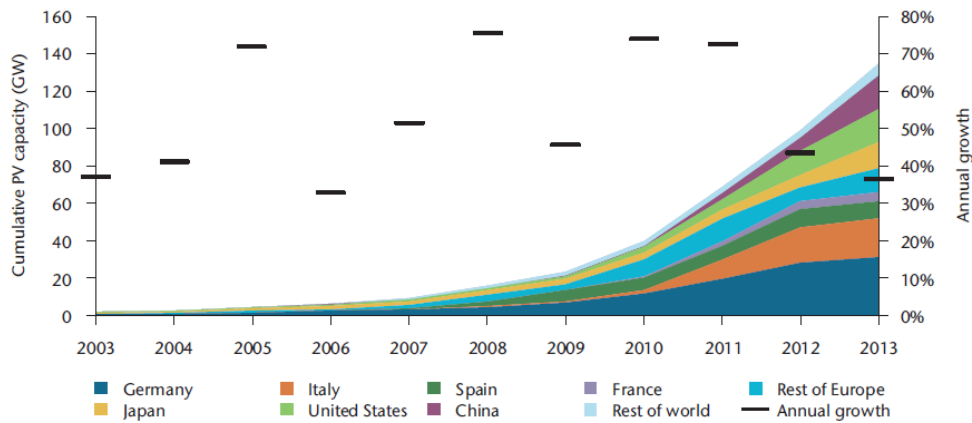
Figure 1: Global Cumulative Growth of PV Capacity [source: IEA, 2014]

The sustainable success of the PV industry depends on the long term performance of the systems in the field. Unreliable and poor quality products would adversely affect the market growth. It is no secret that, as Wohlgemuth, et al. (2005) put it, "the long-term reliability and durability of PV modules is critical to the cost-effectiveness and commercial success of the PV".

1

For a long time, the penetration of the PV technology was hampered by its high investment cost and questions on the return on investment (ROI). Researchers have developed new techniques to optimize manufacturing processes and, as a result, reduce the costs. For instance, over the past six years, PV system costs have drop by 10-15% in California, 21% in Japan for residential systems, and a staggering 30-44% in Italy. In the meantime, manufacturers have used field return data to develop accelerated stress tests that could help ensure long term durability of the product. Nowadays, many manufacturers offer 25-30 years warranty on their crystalline silicon PV modules with 80-70% retention of the initial/rated power output. Moreover, PV applications have moved from small, stand-alone systems to large, grid-connected systems as solar energy has increasingly gained attention amid the need for energy independence. According to IEA, off-grid systems account today for only about 2% of the market segment while grid-connected systems account for nearly 98%; of which 20% residential and 30% commercial rooftop systems, 10% industrial and 40% utility ground-based systems.

The levelized cost of energy (LCOE) is used today as preferred metric to compare solar energy costs to that from conventional energy sources. According to (Darling, et al., 2011), the LCOE can be thought of as the price at which energy must be sold to break even over the lifetime of the technology. (Wang, et al., 2011) identify two set of information required for the LCOE calculation: (1) system cost items, payment method, financing and incentives; and (2) performance parameters and case study location.

A PV system performance is primarily dictated by the site solar resource, the PV module durability, and the inverter reliability. It is well known that the failure rate of inverters is much higher than PV modules. However, it turns out that the energy production by the overall system during its lifetime is not strongly sensitive to

variations in inverter failure or inverter disturbances as compared to the degradation of PV modules because of their quick replacement and repairs (Atcitty, et al., 2011). PV modules are generally seen as the most reliable component of PV systems. As Vasquez and Rey-Stolle (2008) pointed out, issues resulting from degradation of individual modules were not typically taken into serious consideration. However, with large grid-connected power stations, customers have become more sensitive to power losses over time and the need for a reliability model based on degradation have become of utmost importance. The PV system performance ratio (PR), which accounts for the various losses in the system, is typically estimated to be between 80% and 90% on average throughout the year. Just a few underperforming modules can make a serious negative impact at both the string and system level performances. A web article published by Burgess in the April 2012 issue of Renewable Energy World (Burgess, 2012) emphasized this view: "In a world where large solar assets are built with 80 percent debt leverage or more, a one percent change in output can equate to a 10 percent change in the ROI for the investors. The importance of an unanticipated drop in the performance ratio from 0.8 to 0.66 would probably wipe out any anticipated return from the project. This potential future variability has a major impact on site financial viability, but more importantly on the attractiveness of solar as an investable asset class. A key objective of the industry should be to increase the entitlement level for Performance Ratio (PR) beyond the 0.80 level and reduce the long-term risk of assets drifting off that entitlement level. This would: (1) reduce the overbuild and hence initial capital outlay; (2) reduce the levelized cost of electricity for the site; (3) increase the ROI for the investors; and (4) reduce the long-term financial risk, thus attracting financial backing and possibly reducing insurance premiums." Standards & Poor's (S&P), a global authority in credit quality, identifies 8 finance criteria for utility-scale PV projects. Two of the criteria are based on technology reliability and resource availability. The S&P report indicates

that all the PV technologies rely on accelerated testing for measuring and claiming useful lives of approximately 25 years.

1.2   Challenges in PV Reliability Studies

The anticipated lifetime of PV modules spans several decades. The construction materials and design are constantly changing to reduce LCOE and the stakeholders cannot wait for decades to identify the failure modes and mechanisms of these new modules. A PV module lifetime prediction study requires the use of accelerated aging tests to duplicate observed field reliability issues. Unfortunately, there is little or no systematically field monitored data or independent accelerated test data available to support most of the warranty claims.

The basic concept is based on the hypothesis that the products will behave the same way in the short period of time under the right levels of increased stress as they do in a longer period of time when used at normal stress.

The purpose of accelerated aging tests (AAT) for photovoltaic (PV) modules is to shorten the test time by using simulated test conditions, which are more severe than the actual field operating conditions, to replicate actual field failure modes and mechanisms. As shown in Figure 2 below, only 4% (7 GW) of the modules were installed before 2007, 38% (62 GW) were installed between 2007 and 2011, and 58% (95 GW) is expected to be installed by 2015. Therefore, the required actual failure data and degradation data to develop an appropriate accelerated aging testing program has to come from the field data of the 4% modules which were installed before 2007. It is to be recognized that only a tiny fraction of the module data from the 4% modules (installed before 2007) is available for the degradation data analysis (due to availability of metered kWh data). If the construction materials and design of 4% modules produced before 2007 are the same as that of the recent (2007-2011) and the future (2012-2015) modules, then developing accelerated testing

4

programs for the recent/new modules based on the old modules' field failure and degradation data become reasonably simple. However, this is based on the assumption that statistically significant field degradation data are available from a large number of PV systems installed in varied (hot-dry, hot-humid and cold-dry) climatic conditions. The development of an accelerated testing program for the new/recent modules becomes very challenging if the construction materials and design are not the same (and it is the case now) and if the changes are projected to be significantly influencing (positively or negatively) the field failure and degradation rates based on some preliminary accelerated testing such as accelerated qualification testing. The type, extent, limits and sequence of the accelerated stress tests of qualification standards have been stipulated with two goals in mind: (i) accelerate the same failure mechanisms as observed in the field but without introducing other unknown failures that do not occur in the actual field; and (ii) Induce/accelerate these failure mechanisms in a reasonably short period of time, say 60-90 days, to reduce testing time and cost. A background literature review on the history of qualification testing and on the failure rates in the qualification testing programs can be obtained elsewhere (Osterwald and McMahon, 2008).
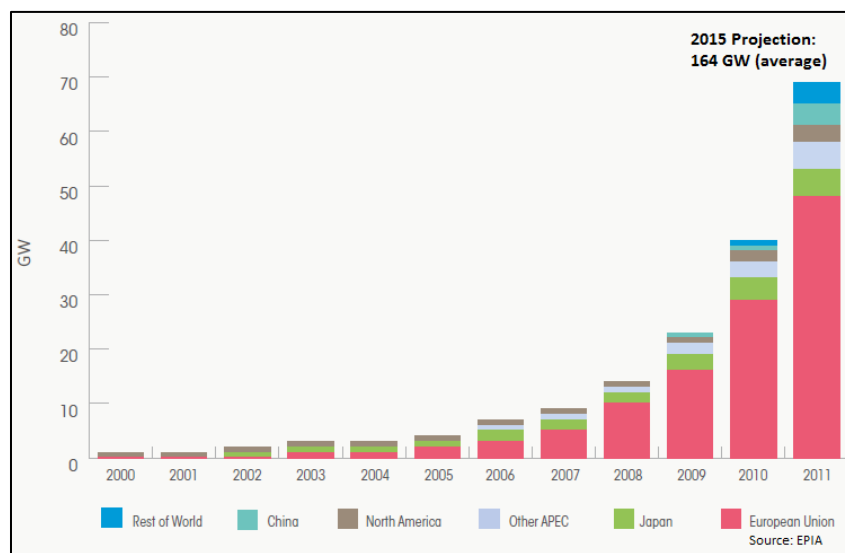
Figure 2: Installed PV Capacity

In order to reduce the cost and keep up with the product development pace with ever evolving new materials and designs, accelerated tests need to be carried out with minimum sample size and at the shortest testing time.

Another equally important and related challenge stemmed from the variety of climate zones. There are many different terrestrial environments in which PV modules are or could be deployed. A map of climate zones in the United States is shown in Figure 3.
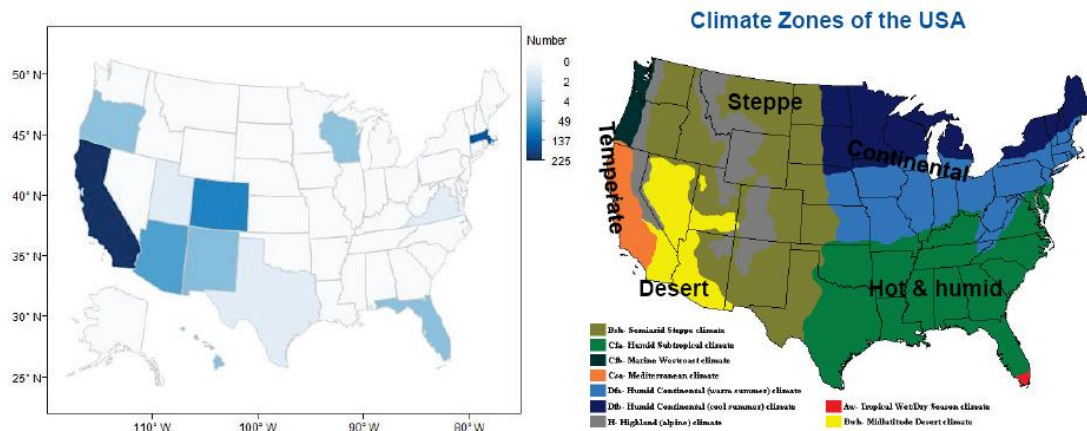
Figure 3: Climatic Conditions under which PV Modules can Operate (Jordan, 2011)

The reliability and durability data obtained from accelerated tests should be able to allow the PV module manufacturers to predict product lifetimes and build confidence in their warranty periods. To achieve that, these data must be correlated to field performance data. Such correlation would require the determination of acceleration factors associated with common failure modes.

1.3 Motivations & Objectives

Reviewed literature on PV field performance show an average degradation rate of 0.8%/year, with the median at 0.5%/year (Jordan & Kurtz, 2012); which, at the surface, seems fairly encouraging. However, this does not address the basic reliability issues in the PV community: how do PV reliability engineers test to

determine the number of years for the warranty? How do PV customers choose the PV module that will last longer? How do PV investors know that they're making a safe investment of $1 billion (if the modules fail after 10 years, the warranty will be worthless because the company will be gone)? How do the insurance companies determine rates for insuring PV installations? How do the PV manufacturers differentiate their product from other products? (NREL Workshop, 2013).

The warranty period provided by the manufacturers typically ranged from 20 to 30 years for crystalline silicon modules. As shown in Figure 4, the warranty length roughly increased by 5 years every 6 years between 1987 and 1999. This coincided with the introduction of the PV safety, design, and qualification standards in the early 1987. These standards, known today as IEC61215 for c-Si modules, IEC61646 for thin film, IEC61730 & ANSI UL1703 for safety; have been instrumental in helping improve the quality of PV products and, as a result, reducing early failure – or "infant mortality" and stirring the growth of the industry for the past 2 decades. Passing the qualification test means the product has met a specific set of requirements and is much more likely to survive in the field and not have design flaws that lead to infant mortality. Unfortunately, as experimentally determined by Wohlgemuth (2011), a large number of modules (eight out of ten models from various manufacturers studied in his work) appear to be currently designed and manufactured just to meet the pass requirements of qualification standards of (IEC 61215, 2005; IEC 61646, 2008). The qualification tests are not meant to test PV modules for the end-of-life (wear-out) failure mechanisms; however, they do an excellent job of identifying design, materials, and process flaws that are likely to lead to premature failure (infant mortality) (Wohlgemuth and Kurtz, 2011). The qualification testing involves a set of well-defined accelerated stress tests (irradiation, environmental, mechanical and electrical) with strict pass/fail criteria based on extended functionality/performance, minimum safety/insulation, and detailed visual

requirements. The qualification testing does not, as anticipated, identify all the possible actual lifetime/reliability field failures; however, it does identify the major/catastrophic design quality issues which would initially occur in the field. Therefore, it may be concluded that the qualification tests are the minimum requirements to initiate comparative or lifetime/reliability testing but they cannot be considered as lifetime or reliability tests because they do not cover the failures related to wear out mechanisms. In other words, the modules which do not meet the qualification testing requirements may not be considered for reliability testing.
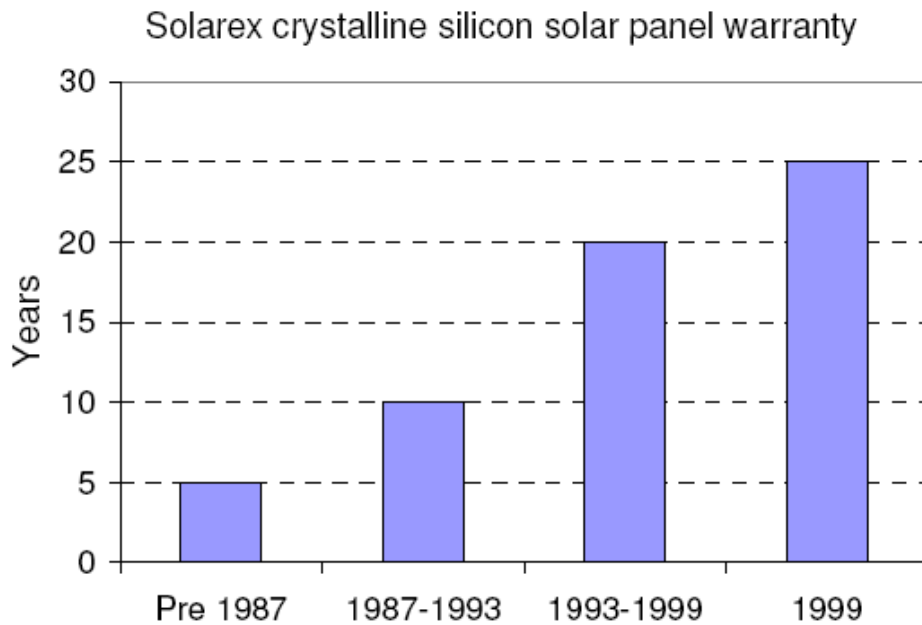
Figure 4: Trend in Solar Panel Warranty Length (SunPower, 2011)

Another motivating factor is the cost of PV modules. According to IEA, The prices of cells and modules fell rapidly from $4/Watt in 2008 to $0.8/Watt in 2012; and there is considerable body of evidence that the costs of cells and modules, whether of c-Si or thin film, will decline further as deployment increases and technology improves in the next two decades. It is believed that for PV modules to reach grid parity, costs must continue to come down. Figure 5 shows that module costs are expected to fall

to $0.3/Watt - $0.4/Watt by 2035. The question is whether new lower cost products have equivalent lifetimes and durability. The emergence of the global PV market has coincided with rapid reductions in the costs of modules and systems. As PV modules go from a specialty product to a commodity with many new suppliers, will their products continue to perform well?

Then there is the technological factor: Crystalline silicon (c-Si) modules, whether single- (sc-Si) or multi-crystalline (mc-Si), currently dominate the PV market with around 90% share. Alternative PV technologies, including thin films, had been expected to gain an increasing share of the market, but instead their share shrank from 15% in 2009 to about 10% in 2013 [IEA, 2014].
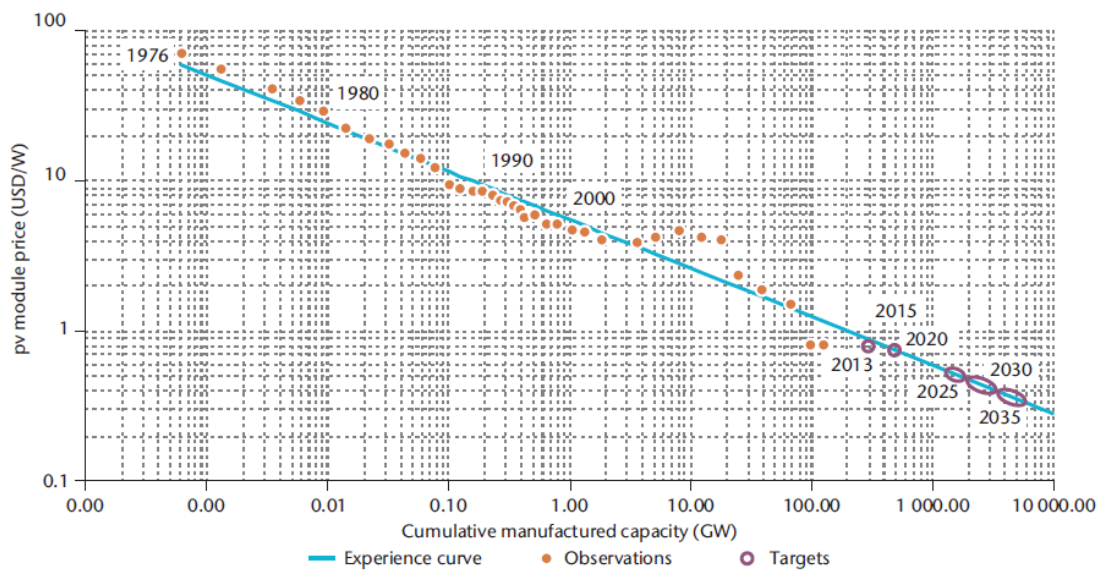
Figure 5: Module Prices Projections to 2035 (IEA, 2014)

In summary, there is no formal protocol/procedure, norms or labels that would tell customers about the behavior, performance and longevity of various PV products in specific environments. As Wohlgemuth and Kurtz (2011) point out, "We do not know how to test modules for a 25-year lifetime." Thus, the lifetime prediction of solar modules is still a difficult task and has not been systematically and comprehensively

studied since the 11-year Flat-Plate Solar Array (FSA) project of JPL (Jet Propulsion Laboratory) ended in 1986. The main objective of this research is to develop an approach to PV module lifetime prediction. In doing so, the aim is to move from empirical generalizations to a formal predictive science based on data-driven case studies of the crystalline silicon PV systems. The evaluation of PV systems aged 5 to 30 years old result in systematic predictive capability that is absent today.

This research study focuses on the behavior of crystalline silicon PV module technology in the dry and hot climatic condition of Tempe/Phoenix, Arizona. Our main objectives are threefold: (1) develop a methodology for identifying the dominant failure/degradation modes for modules installed in a given climate based on the data collected from the aforementioned geographical area; (2) determine the environmental stress variables involved and prioritize their effect on the power output drop; and (3) develop a strategy to derive a life prediction model from the design and execution of accelerated tests

1.4   Research Plan

In this research, we propose a systematic approach to lifetime prediction of PV modules in a hot and dry climatic condition. We start with key assumptions: "Accelerated stress tests from the qualification tests are designed to address the identified field failure modes" (Wohlgemuth and Kurtz, 2011). This is necessary for setting our initial conditions. Three phases were envisioned:

Phase I - Investigation of field failure modes and correlation to performance output parameters: The long-term field failure data of various PV systems are evaluated for the identification of field failure or degradation modes, and they are correlated to the present day performance data of the system or modules in order to determine the dominant mode(s). This is the focus of Chapter 3.

Phase II - Investigation of environmental factors affecting the PV degradation: The weather data in solar panel testing sites are gathered and analyzed to determine the effects of use environmental stresses. Empirical models are developed to quantify the stress effects on performance output. Based on this study, recommendations can be made on how to simulate the identified stress variables, and how to increase stress levels without introducing failure modes that are not seen in the field. Chapter 4 covers this investigation.

Phase III - Accelerated Degradation test for lifetime prediction: The accelerated degradation tests for predicting module life in Phoenix, Arizona will be designed and experimented. This study is presented in Chapter 5.

The relevant literature is presented next in Chapter 2.

CHAPTER II

RELIABILITY OF PHOTOVOLTAIC MODULE: LITERATURE REVIEW

2.1   Field Failure/Degradation Modes and Mechanisms

Field Failure and Degradation Rates

As shown in Table 1, the performance loss of a grid-tied PV system could be caused by various non-failure factors and non-module degradation factors. In order to accurately determine and report the annual degradation rates and mismatch of PV modules, it is extremely important to isolate and remove the influence of all other factors. Table 1 was generated primarily from information in a paper published by Sandia (King, Boyson, & Kratochvil, 2002). Another recent study carried out by Sandia serves as a good example of how to isolate and remove the influence of all the factors (which are not related to module durability issues) that determine module degradation rates (Granata, Boyson, Kratochvil, & Quintana, 2009). As shown in Figure 6, the module degradation rate can be as high as 4%/year, but the median and average degradation rates are only 0.5%/year and 0.8%/year, respectively (Jordan & Kurtz, 2011).

Table 1: De-Rating Factors Involved in the Energy Production of Grid-Tied PV Systems (Based on Data from King, Boyson, & Kratochvil, 2002)

Influence of Module and System Level Factors on AC-Energy Production		
Factor	**Range (%)**	**Issue**
Module orientation	-25 to +30	Installation issue
Array utilization losses (MPPT)	-30 to -5	Inverter issue
Module power specification	-15 to 0	Performance overrating issue
Module temperature coefficients	-10 to -2	Performance issue
Module (array) degradation (%/yr)	**-7 to -0.5**	**Durability issue**
Module Vmp vs. Irradiance	-5 to +5	Performance issue
Module soiling (annual average)	-10 to 0	Site and tilt angle issue
Angle-of-incidence optical losses	-5 to 0	Performance issue
Module mismatch in array	**-5 to 0**	**Durability variation issue**
Solar spectral variation	-3 to +1	Performance issue

Note: MPPT is maximum power point tracking; Vmp is voltage at maximum power point.

The list of the module failures presented in Table 2 may seem to be very long, but in reality the crystalline silicon modules have a very impressive track record with only negligibly small field failure issues and warranty returns. As shown in Figure 7, most of the PV systems fail not due to modules but due to inverters (IEA-PVPS-TASK2, 2007).
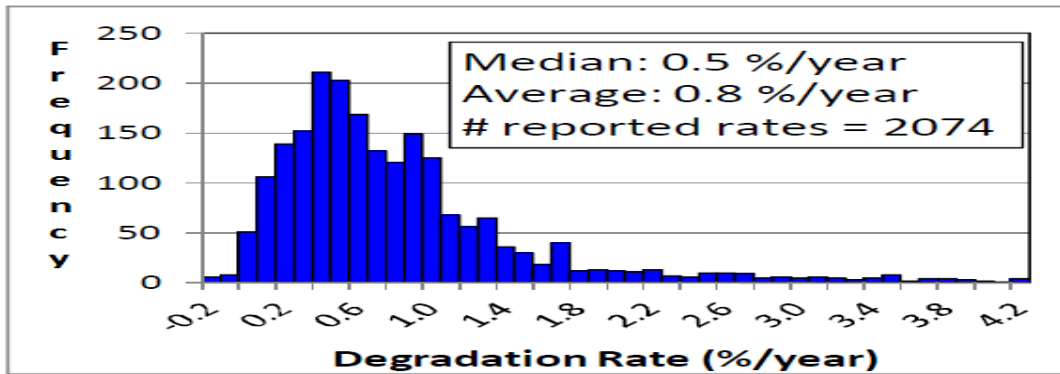
Figure 6: Annual Degradation of PV Modules (Jordan & Kurtz, 2011).
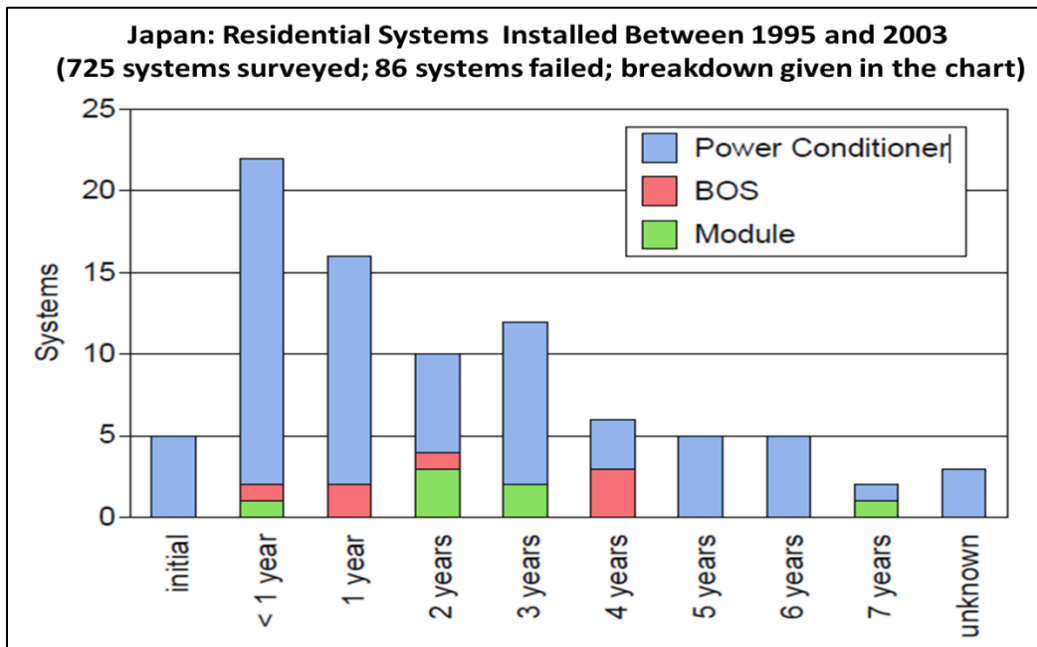
Figure 7: Failure Rates of Inverters, Modules, and BOS in Residential PV Systems (IEA-PVPS-TASK2, 2007).

As noted earlier in this report, the inverters are replaced or repaired in a short period of time with less impact on lifetime energy production of the PV systems. The

temporary energy production loss due to inverter failures during the lifetime of PV systems would be much less than the permanent energy production loss due to higher degradation rates of PV modules. The impact of higher degradation rate on the lifetime (and energy production) of PV modules would be dramatic, as shown in Figure 8 (Osterwald & McMahon, 2009).
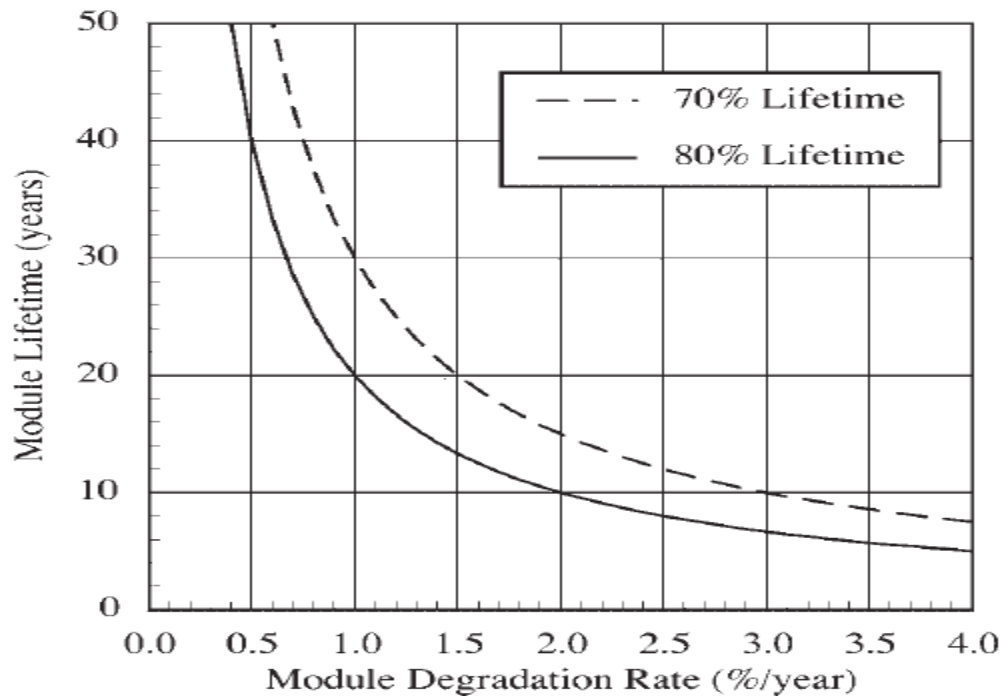
Figure 8: Serious Impact of Higher Degradation Rate on the Lifetime of PV Modules (Osterwald & McMahon, 2009).

Based on various publications, Wohlgemuth summarized recently reported field failure and warranty return rates for crystalline silicon modules (Wohlgemuth, 2012) as follows:

- less than 0.1% of annual field failure rate on 10-year-old qualified (per qualification standards) modules,

- 0.005% of annual field failure rate on up to 5-year-old modules (only six module failures out of 125,000 modules from 11 different manufacturers),

- 0.13% warranty return rate on 1994-2005 modules (one failure every 4200 module-years of operation), and

- 0.01% annual return rate on 2005-2008 modules.

Therefore, it may be concluded that the lifetime of PV modules is typically dictated by the degradation rates rather than failure rates. However, it is to be noted that the multiple failure modes over time could have cumulative influence on the degradation rates of the PV modules. For example, cracked cells and failed bypass diodes can electro-thermally accelerate degradation rates.

Field Failure and Degradation Modes

Failure and degradation modes and mechanisms of PV modules are dictated by their design/packaging/construction and the field environment in which they operate. As shown in Figure 9, the design/construction of PV modules has gone through a dramatic change since 1975 (Ross, 2012). The design and component changes include cell type (from monocrystalline silicon [mono-Si] to polycrystalline silicon [poly-Si] and mono-Si along with various thin-film technologies), superstrate (from silicone to glass), encapsulant (from silicone to ethylene vinyl acetate [EVA]), substrate (from fiberglass board to polymeric backsheet), cell string (from one to multiple), interconnect between cells (from one to multiple), and bypass diode (from none to multiple). An excellent representation of design evolution between 1975 and 1984 is shown in Figure 10 (Ross, 2012).
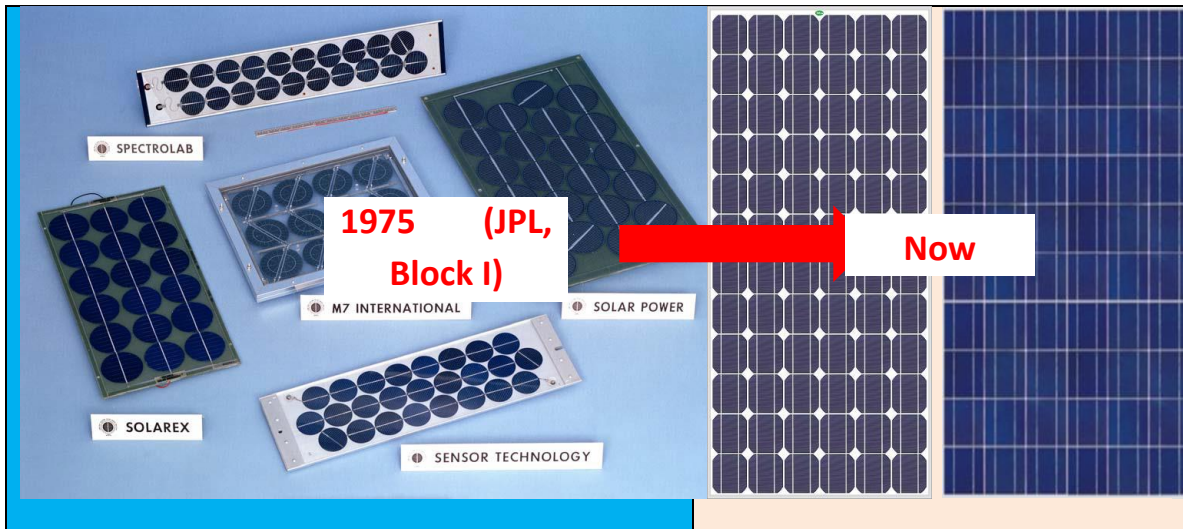
Figure 9: Evolution of PV Module Design since Mid-1970s (Ross, 2012).

Figure 10: Evolution of PV Module Construction since 1975 (Ross, 2012).

The failure or degradation modes in PV modules indicate symptoms, whereas failure or degradation mechanisms represent the course for arriving at these symptoms. The field failures and degradation losses may be classified as reliability failures and durability losses, respectively. An extensive list of graphic and photographic representations and examples of field failure and degradation modes are not provided here, but can be obtained from the tutorials of various IEEE Photovoltaic Specialists Conferences. The typical field failure and degradation modes of crystalline-silicon PV modules in the field are shown in Table 2. This classification

table was generated primarily based on information from tutorial material presented

at the 2011 IEEE Photovoltaic Specialists Conference (Wohlgemuth, 2011). As stated

earlier, the lifetime of PV modules is typically dictated by the degradation rates

rather than failure rates, although the failure modes and rates could significantly

influence the degradation rates of the PV modules.

Table 2: Failures and Degradation Modes of PV Modules

Failure Modes (Leading to immediate warranty returns)	Degradation Modes (Leading to power degradation toward warranty limit)

- Broken interconnects (leading to arcing, backskin burns or glass shattering or power loss higher than warranty limit)
- Solder bond failure
(leading to backskin burns or glass shattering)
- Severe corrosion
(leading to backskin burns or power loss higher than warranty limit)
- Chipped cells (leading to hotspots or power loss higher than warranty level)
- Encapsulant delamination (leading to power loss higher than warranty level)
- Broken glass (leading to safety issue)
- Hotspots (leading to backsin burning and safety issue or power loss higher than warranty limit)
- Ground faults (leading to safety issue or power loss higher than warranty limit)
- Junction box failures (arcing or ground faults)
- Connector failures (leading to safety issue)
- Structural failures (leading to safety issue)
- Bypass diode failures (leading to safety issue due to hot spot or power loss higher than warranty limit due to string loss)

- Gradual cracking of interconnects (leading to power degradation limit)
- Gradual solder bond failure (leading to power degradation limit)
- Slow corrosion (leading to metallization discoloration and power degradation limit)
- Gradual cracking of cells (leading to power degradation)
- Gradual encapsulant discoloration (leading to power degradation)
- Gradual (photo)electrochemical degradation of semiconducting and/or metallic materials
(potential induced degradation leading to power degradation)
- Gradual backsheet warping (leading to power degradation)
- Gradual increase of module mismatch (leading to power degradation)
- Strongly adhering and gradual hardening of soil layer on superstrate (leading to slow cumulative/permanent increase in annual power degradation) or weakly adhering and rain/wind cleaning of soil layer (leading to fixed/temporary annual degradation due to non-cumulative reversible annual rain effect)

Field Failure and Degradation Modes, Mechanisms, Causes, and Effects

A failure mechanism is responsible for one or more failure modes. A failure mechanism could be triggered by one or more failure causes and a failure mode could trigger one or more failure effects. The field failure analysis approach for PV modules may be represented as shown in the following sequence:

Failure Mechanism (Cause) → Failure Mode (Effect)

Example:

Thermo-mechanical fatigue (Expansions-Contractions) → Broken interconnects (Arcing)

As shown in Table 3, a single failure mechanism may be triggered by one or more failure causes leading to one or more failure modes with each failure mode leading to one or more failure effects. Some failure modes are caused by compound mechanisms instead of just a single mechanism. In the fault tree analysis, all the causes for every failure mode are systematically identified.

For details on the failure and degradation modes and mechanisms, see Wohlgemuth's tutorial materials from the 2011 IEEE Photovoltaic Specialists Conference (Wohlgemuth, 2011).

Table 3: Field Failure and Degradation Modes and Mechanisms Along with Cause and Effect on PV Modules

Cautionary Note: To differentiate the reliability issues from the durability issues, this table is broken up into two sections—Failure Modes (reliability issues) and Degradation Modes (durability issues). Most of the degradation modes (presented in the second part of the table) can lead to failure modes (presented in the first part of the table) if they go far enough. In other words, most of the failure modes are also caused by the slow degradation modes, which

could later become severe, leading to failure modes. For example, one broken interconnect on a cell that has two interconnects in a three-string module will reduce power due to degradation mode but not result in a failure mode as it is still within the warranty limit. However, when both the interconnect ribbons on a cell are broken, the diode will turn on and the module will lose ~ 1/3 of its power, leading to failure as the power drop in the module exceeds the warranty limit. Therefore, the difference between failure mode and degradation mode should be fully understood before assigning a specific field issue under failure mode or degradation mode category.

Field Failure Modes and Mechanisms

Failure Mode	Failure Cause	Failure Effect	Failure Mechanism
Broken interconnects	• Thermal expansion and contraction of interconnects* • Flexing due to wind load or snow load* • Difference in thermal expansion coefficient as compared to substrate/superstrate** • Larger cells** • Thicker ribbon** • Kinks in ribbon** • No stress relief in ribbon**	• Arcing (due to short distance between the broken ribbons) • Backskin burns (due to joule heated hotspots) • Ground fault due to backskin burns (due to water access) • Power drop beyond warranty limit due to severe series resistance or diode activation	• Thermo-mechanical fatigue
Solder bond failure	• Thermal expansion and contraction*	• Backskin burns (due to joule	• Thermo-mechanical fatigue

20

	• Metal segregation* • Flexing due to wind load* • Vibration during shipment (poor packaging)* • Electrical cycle (day/night or sunny/cloudy)* • Less number of solder bonds per cell (per tabbing ribbon)** • Absence of redundancy for non-cell solder bonds** • No stress relief for interconnects** • Use of non-softer ribbon** • Poor quality of solder bonds (alloy/process)**	heated hotspots) • Ground fault due to backskin burns (due to water access) • Shattered glass (due to hotspots) • Power drop beyond warranty limit due to severe series resistance	
Corrosion	• Moisture ingress through backsheet or laminate edges* • Presence of higher ambient temperature along with humidity* • High system voltage due to sunlight	• Hotspot induced backskin burns • Hotspot induced broken glass • Power drop beyond warranty limit due to severe series resistance	• Chemical corrosion (metallic and semiconducting components during nighttime), electrochemical corrosion (metallic components during

	presence* • Higher ionic conductivity of encapsulant due to moisture** • Higher moisture absorption of encapsulant** • Metallization (alloy) sensitivity to moisture** • Interconnect (alloy)** sensitivity to moisture		daytime), or photoelctrochemical corrosion (semiconducting components during daytime) between cells or between cell and frame
Broken cells	• Difference in thermal expansion and contraction of cell components* • Vibration during shipment (poor packaging)* • Wind/snow load* • Larger cells** • Thinner cells** • Larger modules** • Cell chipping**	• Drop in power beyond acceptable/warranty limits (due to increase in crack length and chipping away active cell area; it is to be noted that broken cells often only result in a small power loss not a module failure) • Hotspots (due to reverse bias	• Thermo-mechanical fatigue

			heating)
Encapsulant delamination	• Sensitivity of adhesive bonds to ultraviolet (UV) light at higher temperatures or to humidity in the field* • Poor adhesive bonds at the interfaces during processing (glass/encapsulant; cell/encapsulant; backsheet/encapsulant)** • Contamination from the material (Excess Na in glass or acetic acid from encapsulant)**	• Moisture ingress • Enhanced encapsulant conductivity and interface conductivity (enhanced chemical/ electrochemical/ photoelectrochemical corrosion) • Major transmission loss • Power drop beyond warranty limit due to optical decoupling and moisture ingress induced corrosion	• Photothermal reaction (interface bonds breakage due to UV and temperature) • Chemical reaction (interface bond breakage because of humidity or contaminants)
Broken glass	• Primary cause may probably be attributed to flying pebbles from cutting the grass • Hotspots or arcs due to broken interconnects or solder bonds because of thermal expansion / contraction*	• Ground fault • Enhanced corrosion due to moisture access during rainy and humid days • Dramatic drop in power during rainy days (short circuiting)	• Thermo-mechanical fatigue

	• Thermal gradient within glass (for annealed glass)* • Vandalism (rock throwing)** • Failure of support structure** • Misuse of support structure** • Not following manufacturer's mounting instruction** • Process induced stress (only annealed glass)** • Defective supply chain **		
Hotspots	• Thermal expansion/contraction of interconnects or solder bonds* • Shadowing** • Faulty cell or cells in a string** • Low shunt resistance cells** • Failure of bypass diode**	• Backskin burns • Decrease in power • Shattered glass • Encapsulant bubbling (localized) • Encapsulant discoloration (localized) • Power drop beyond warranty limit	• Thermo-mechanical fatigue or purely electrical
Junction box failures	• Thermal expansion/contraction	• Arcing (inside junction box)	• Thermo-mechanical fatigue

	of junction box circuit* • Thermal expansion/contraction of junction box attachment/adhesive* • Water access to the junction box circuit beneath the junction box due to poor attachment with backskin (workmanship issue)** • Junction box without proper pottant or drainage** • Water access to the junction box circuit through breathable hole**	• Ground fault • Corrosion • Power drop beyond warranty limit due to severe increase in series resistance	
Ground fault	• Installation error (sharp metallic penetration from mounting structure to active cell circuit)**	• Arcing with potential fire	• Not applicable
Backsheet warping/detaching / cracking/crumbling	• Poor adhesion between encapsulant and backsheet • Moisture ingress through backsheet	• Ground fault under wet conditions (due to water access to active circuit and frame;	• Chemical reaction weakening interface bonds (due to higher ambient temperature and/or humidity)

	and/or laminate edges • Polymer disintegration over time	however, note that the backsheet issues do not usually result in module failure)	
Connector failures	• Thermal expansion and contraction* • UV/heat/humidity* • Installation error** • Incompatible male/female parts**	• Arcing • High voltage exposure risk (worse in flat roof puddles!) • Contact resistance energy loss • Connector lifetime reduction (due to higher operating temperature; worse in hot-sunny location rooftops)	• Thermo-mechanical fatigue • Chemical corrosion
Structural failures	• Wind load* • Snow load* • Not following manufacturer's mounting instruction** • Inappropriate frame adhesive** • Inappropriate frame profile** • Inappropriate mounting	• Module breakage • Frame deformation	• Mechanical fatigue

	locations on the frame**		
	• Inadequate installer training**		
	• Insufficient glass thickness**		
Bypass diode failures	• Thermal expansion and contraction*	• Open circuit failure of the bypass diode may not result in any noticeable change in module output	• Thermal fatigue
	• Insufficient diode rating**	• Without a functional bypass diode the module will be susceptible to hot spot problems and arcing if an open circuit occurs within the circuit protected by that bypass diode	
	• Insufficient heat dissipation inside junction box**	• Short circuit failure of the bypass diode will lead to a loss of the power (beyond warranty limit) produced by	

		the cells being protected by the failed diode.	

Degradation Modes and Mechanisms			
Degradation Mode	Degradation Cause	Degradation Effect	Degradation Mechanism
Gradual cracking of interconnects	• Thermal expansion and contraction of interconnects* • Flexing due to wind load or snow load* • Difference in thermal expansion coefficient as compared to substrate** • Larger cells** • Thicker ribbon** • Kinks in ribbon** • No stress relief in ribbon**	• Slow decrease in power (due to increase in series resistance) but within warranty limit	• Thermo-mechanical fatigue
Slow corrosion	• Moisture ingress through backsheet or laminate edges* • Presence of higher ambient temperature along with humidity* • High system voltage due to sunlight presence* • Higher ionic conductivity of encapsulant due to	• Increase in series resistance and decrease in power but within warranty limit	• Chemical corrosion (metallic and semiconducting components during nighttime), electrochemical corrosion (metallic components during daytime), or photoelctrochemical

	moisture** • Higher moisture absorption of encapsulant** • Metallization (alloy) sensitivity to moisture** • Interconnect (alloy)** sensitivity to moisture		corrosion (semiconducting components during daytime) between cells or between cell and frame
Gradual cell breaking	• Difference in thermal expansion and contraction of cell components as compared to superstrate/substrate* • Vibration during shipment (poor packaging)* • Wind/snow load* • Larger cells** • Thinner cells** • Larger modules** • Cell chipping**	• Slow decrease in power (due to decrease in shunt resistance) but within warranty limit	• Thermo-mechanical fatigue
Gradual encapsulant discoloration	• UV exposure at higher operating temperatures* • Reduced breathability** • Higher UV concentration* • Inappropriate additives in EVA**	• Transmission loss • Reduced current/power but may not be affecting fill factor or warranty limit • Cosmetic/visual	• Photothermal reaction (in the presence of UV and higher module temperature)

		change	
Gradual electrochemical corrosion or cation migration to the semiconductor surface/junction	• Moisture ingress through backsheet or laminate edges** • Higher ionic conductivity of encapsulant due to moisture** • Higher moisture absorption of encapsulant** • Metallization (alloy) sensitivity to moisture** • Interconnect (alloy) sensitivity to moisture**	• Series resistance increase and/or shunt resistance decrease depending on bias polarity and climatic conditions • Potential induced degradation leading to power loss but within warranty limit	• Electrochemical corrosion (metallic components during daytime) or photoelctrochemical corrosion (semiconducting components during daytime are more sensitive to electrochemical reactions under light) between cells or between cell and frame
Gradual solder bond failures	• Thermal expansion and contraction* • Flexing due to wind load** • Vibration during shipment (poor packaging)** • Electrical cycle (day/night or sunny/cloudy)* • Small number of solder bonds per cell (per tabbing ribbon)** • Absence of redundancy for non-cell solder bonds**	• Bussbar discoloration • Power decrease within warranty limit due to series resistance increase	• Thermo-mechanical fatigue

	• No stress relief for interconnects** • Use of non-softer ribbon** • Poor quality of solder bonds (alloy/process)**		
Gradual backsheet warping/detaching / cracking/crumbling	• Poor adhesion between encapsulant and backsheet** • Moisture ingress through backsheet and/or laminate edges** • Polymer disintegration over time**	• Slow power degradation (due to corrosion of cell and circuit components) but within warranty limit	• Chemical reaction weakening interface bonds (due to higher ambient temperature and/or humidity)
Gradual module mismatch	• Difference in degradation rate between field-aged modules in a string caused by poor production quality control**	• Slow power loss at the string/array level (due to operation away from each module's maximum power point) but within warranty limit	• Not applicable
Gradual soiling	• Low tilt angle of modules in soiling-prone locations with infrequent rainfall*	• Slow transmission loss • Reduced current/power	• Strongly adhering and gradual hardening of soil layer on superstrate or weakly adhering

		but may not be affecting fill factor or warranty limit • Cosmetic/visual change	and rain/wind cleaning of soil layer (leading to fixed/temporary annual degradation due to non-cumulative reversible annual rain effect)

Notes: * Environmental Cause
      ** Material/Design/Process/Construction Cause

A detailed visual inspection checklist, developed by the National Renewable Energy Laboratory (NREL) (Wohlgemuth, 2011) for recording field failures is presented in Appendix A. For the purposes of statistical and physical modeling of the power plants, these field issues may be segregated into two categories—Module Failures and Module Degradation—as indicated in Table 3. Descriptions of destructive and non-destructive techniques to evaluate the degradation mechanisms of long-term field-exposed modules can be found in (Sakamoto & Oshiro, 2005; Sandia, 1999; Quintana, et al., 2000; King, et al., 2000; Emery, 2003; Veldman, et al., 2011).

    2.2   Environmental Stress Factors

The lifetime of PV modules is a function of a few key major field stresses such as temperature, humidity, UV light, and system voltage.

The maximum stress levels or duration used during the accelerated tests (AT) should not introduce failure modes that do not occur in the field (commonly called foolish failure modes). In order to determine the maximum stress level and duration during AT, it is necessary to identify the use stress level and failure mechanism in the field.

The limits for testing time, cycle, and stress level need to be determined for various stresses including temperature, humidity, UV, and voltage.

An assessment of environmental data for the years 1965 to 1974 at nine different geographic locations in the United States was conducted under the FSA project (Kolyer and Mann, 1977). They used the concept of "environmental cell" to characterize the environmental conditions for solar arrays and identify environmental factors and levels that can be used in accelerated testing. An "environmental cell" is defined by a set of environmental variables and their ranges. An example assuming 3 environmental variables of interest (say, temperature, relative humidity, and irradiance) could be a cell defined by the ranges 20°C to 30°C for temperature, 800 W/m² to 1000 W/m² for irradiance, and 40% to 50% RH. If the range of temperature is partitioned into 4 intervals, that of relative humidity is partitioned into 2, and the range of irradiance is partitioned 3 intervals, then we end up with a cube consisting of 24 environmental cells representing 24 static conditions. Using this concept, descriptive statistic can be used to analyze multi-years weather data and determine the frequency and duration of an environmental condition. The expected number of exposure hours E can be forecast as follows:

$$E = \frac{NKT}{H}$$

Where

N = observed number of occurrences of a cell in a historical time period H,

K = data collection interval (in hours),

T = forecast time period.

Gaines, et al. (1977) identifies the major environmental factors affecting the life of PV modules: ultraviolet (UV) radiation, oxygen, moisture, temperature, chemical pollutants such as SO_2, dirt accumulation, and abrasion. Dumbleton and Haillant (2011) use temperature and radiation data for the outdoor environments to estimate

acceleration factors between used and simulated environments. Laronde, Charki, and Bigaud (2010) discuss the empirical influence of temperature variations on the reliability of photovoltaic modules using Arrhenius and Weibull models.

Because the qualification tests defined in the IEC 61215 and IEC 61646 standards were developed based on failure modes identified in the field, the limits identified in these standards may be used as starting points (Wohlgemuth & Kurtz, 2011). Again, the accelerated test levels should not alter the actual field failure mechanisms. For example, the limits identified in the standard thermal cycling test (85°C/-40°C; 200 cycles) and DH test (85°C/85% relative humidity [RH]; 1,000 hours) may be increased provided the failure modes and failure mechanisms of both field failures and accelerated test failure are identical.

Stress Level and Duration Limits: Temperature

The temperature cycling is a major stress test done on PV modules to determine the ability of the module to withstand thermal mismatch, fatigue, and other stresses caused by repeated changes of temperature.

Due to substantial difference in the thermal coefficients of expansion between the silicon wafer and the tinned-copper ribbon, bowing and breaking of the thinner wafers could occur if the ribbons are soldered continuously along the screen-printed bus lines on the silicon wafer or just soldered too close to the edge of the cell on front and back (Dhere, 2005). A joint paper published by Sandia and NREL indicates that the changes in solder-joint geometry caused by thermomechanical fatigue reduce the number of redundant solder-joints leading to increased series resistance and decreased performance (Quintana, King, McMahon, & Osterwald, 2002). The stress level and duration limit related to the temperature stress can be increased three ways: the duration of the thermal cycling test can be increased just by increasing the number of cycles at the standard cycle rate of less than 100°C per

hour; the stress frequency during the thermal cycle test can be increased by increasing the cycle rate; the stress limit can be increased by increasing the temperature range.

Low cycle rate: Based on the outdoor exposure via comparison to field data and via modeling of weather data, the two hundred normal/standard thermal cycles (between 85°C and -40°C) that are used in the qualification testing have been equated to 10 to 11 years (Wohlgemuth & Kurtz, 2011). For a lifetime of 20 years, additional thermal cycling is required. If the normal 200 cycles equals 10 years of field exposure, then 500 cycles would represent 25 years, assuming linear dependence of power drop on the number of cycles (Wohlgemuth & Kurtz, 2011). The results obtained in another study, presented in Figure 11 (Herrmann et al., 2010), appear to indicate a linear dependence of power drop with the number of cycles during normal thermal cycling (NTC). If one assumes 20% power drop from the original is the durability/warranty requirement for thermal cycling, all seven but one (Figure 13) have met the warranty requirement up to 800 cycles at a temperature difference of 125°C (from -40°C to 85°C). Therefore, the required number of NTC for the lifetime determination may be calculated assuming linear degradation (for example, 0.5%-2.4% power drop per year) in the field and the linear degradation in the accelerated thermal cycling test and/or using the Coffin-Manson model.
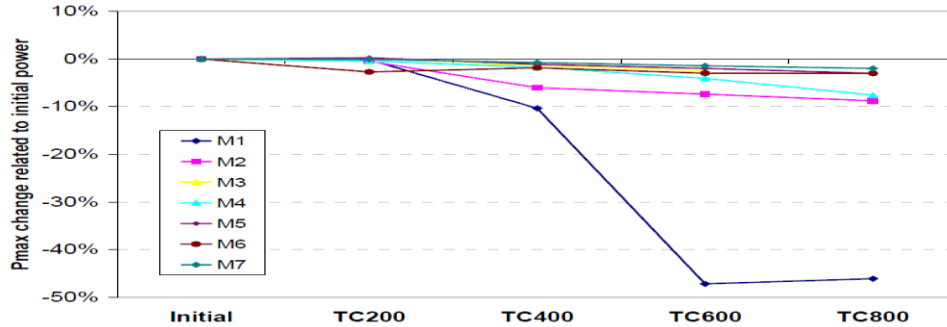
Figure 11: Cycle Limit for Thermal Cycling Stress (Herrmann et al., 2010).

High cycle rate: A rate of 60°C/hour is commonly used in military specifications and 180°C/hour in space component specification (Hoffman & Ross, 1978). In order to reduce the cycling duration, another research group has attempted to use a rapid thermal cycling (RTC) method with a cycling rate of 400°C/hour (Aoki, Okamoto, Masuda, & Doi, 2010). This study has indicated a power loss of 37% and the failure of solder bonds within 500 cycles as indicated in the impedance study shown in Figure 12. During this 500 cycling period, the testing was paused three times (see Figure 12) and the module was maintained at room temperature, apparently, for the stress relaxation/annealing. Unfortunately, this rapid thermal cycling method has apparently been applied on only one sample with no comparison to the standard/normal cycling method on an identical sample. An extensive normal thermal cycling (NTC) study carried out by BP Solar on a specific crystalline silicon module type indicated that the interconnect and solder bond failure from thermal cycling is not likely to be the lifetime limiting failure mechanism for this specific module type (Wohlgemuth, 2008). If the solder bond failure from thermal cycling was not likely to be the lifetime limiting failure mechanism in the field, the failure observed in the RTC method within 500 cycles may be attributed to the thermal shock imposed on the solder bonds (Wohlgemuth & Kurtz, 2011). It may be possible to conclude that RTC at 400°C/hour rate may be a good screening test but it may not

be an appropriate lifetime test; however, it may be worth exploring the RTC method with a large number of identical samples comparing NTC (perhaps at various cycling rates of 180, 300, and 400°C per hour cycle rates) and RTC failure modes and mechanisms. This comparative study might determine the upper limit for the cycling rate so the testing time can be significantly reduced.
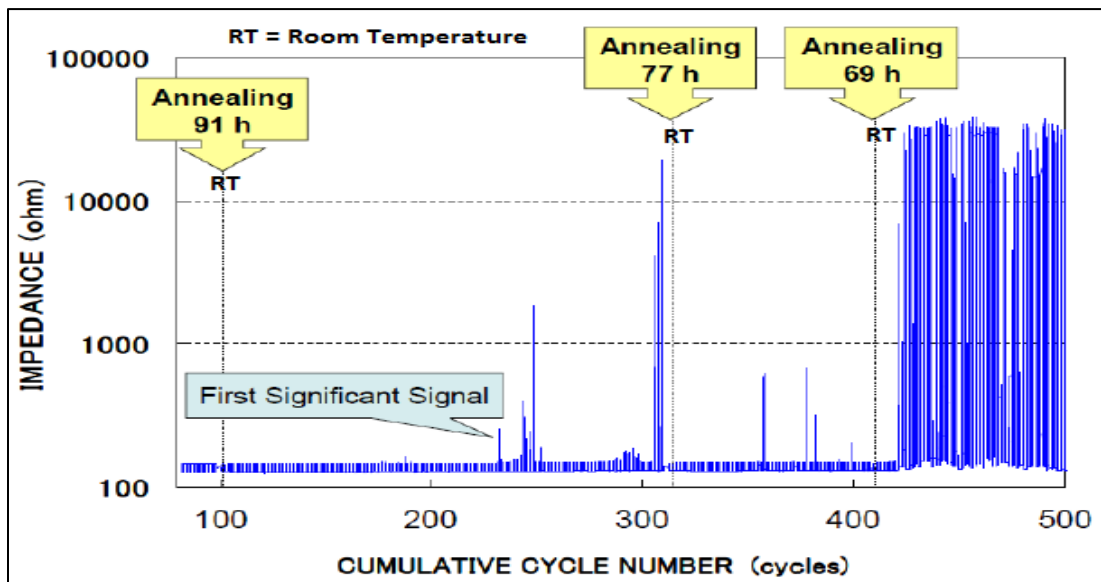
Figure 12: Variation of Impedance of during Rapid Thermal Cycling at 400°C/hour Rate (Aoki, et al., 2010).

High temperature range: As shown in Figure 13A, a study performed by SunPower indicates that the solder bond degradation cannot be differentiated between tin/lead (SnPb) and tin/silver (SnAg) if the number of thermal cycles is less than about 500 cycles at standard temperature range of -40°C and 90°C (Meydbray, Wilson, Brambila, Terao, & Daroczi, 2008). This plot also indicates that the SnPb solder bonds experience non-linear degradation with a dramatic increase after about 500 cycles whereas SnAg solder bonds experience linear degradation even up to 2000 cycles. In order to reduce the testing time (or number of cycles), SunPower performed testing on the solder bonds of these alloys at an increased upper temperature limit of 125°C (high temperature) instead of 90°C and the results are

presented in Figure 13B. The required number of cycles for the lifetime determination can be calculated based on the linear and non-linear degradation behaviors of these soldering alloys. However, it is to be noted that, at this upper temperature limit of 125°C, the module encapsulant will be affected leading to other failures that are not seen in the field.
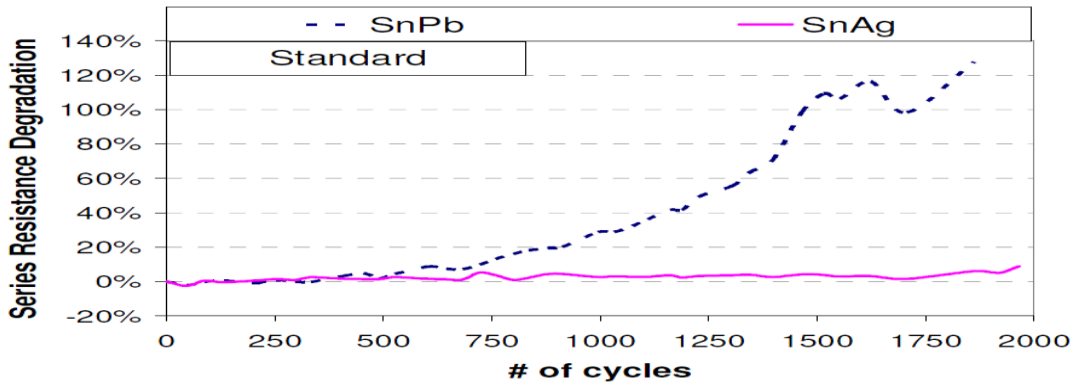
Figure 13A: Cycle Temperature of -40°C and 90°C.
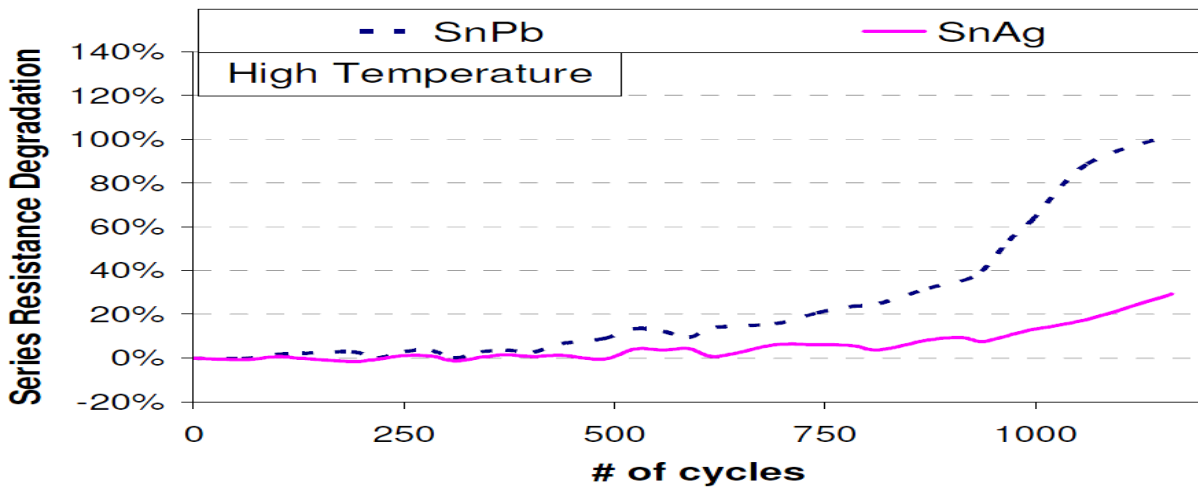
Figure 13B: Cycle Temperature of -40°C and 125°C

Figure 13: Performance Degradation of PV modules at the Cycle Temperature

(Meydbray, et al., 2008)

Stress Level and Duration Limits: Humidity

The DH test is another major stress test done on PV modules to determine the ability of the module to withstand the effects of long-term penetration of humidity. The encapsulant that has been laminated and cured on a flat glass will have reasonable bond strength in a dry environment, but may delaminate when exposed to a humid environment. As shown in Figure 14 (Arco Solar M55 module installed in approximately 1986 and apparently removed after about 10 years of operation in Austin – Texas), the delamination will lead to moisture ingress and subsequent corrosion of cell components. As shown in Figure 19, the same Arco Solar M55 module in a hot-dry climatic condition undergoes encapsulant browning only instead of encapsulant browning and delamination.
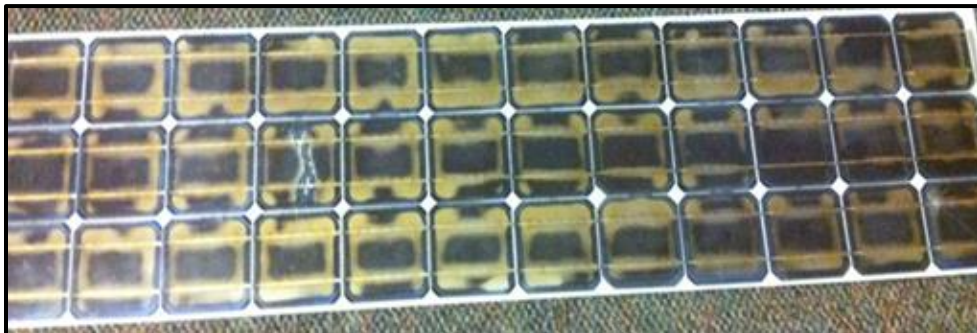
Figure 14: Encapsulant Browning, Delamination and Moisture Ingress Induced Corrosion of Cell Components in a Hot-Humid Condition (Photo Courtesy: Bill Kaszeta, PVRI).

Currently, the DH testing condition of 85°C/85%RH is extensively used in the qualification standards and by the industry. The hot-humid environment used in this test for 1,000 hours could weaken the interfaces including backsheet/junction box and glass/encapsulant. A recent study indicated that 5.5% (10 out of 183) of the modules that were subjected to this test failed in the post-wet resistance test (TamizhMani et al., 2012). As shown in Figure 15, a detailed diagnostic test revealed

that these post-wet resistance failures were due to the weakened interfaces of junction box attachment and laminate edge sealant failure.
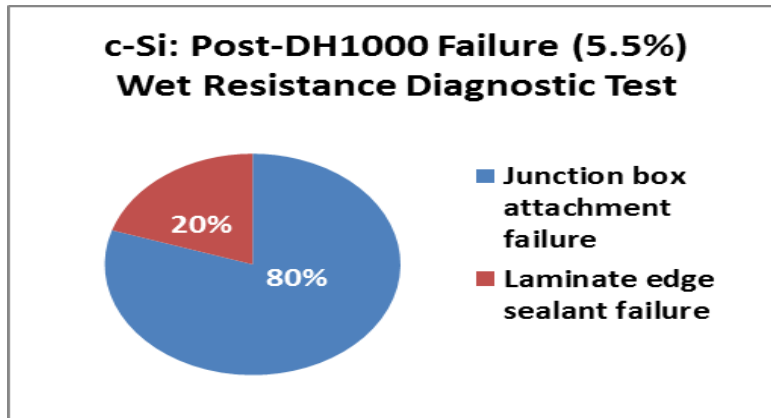
Figure 15: Post-DH Diagnostic Wet Resistance Test Revealing Weak Interfaces (TamizhMani et al., 2012).

The stress limit and duration for this test was chosen by JPL in the early 1980s based on a review of nominal module operating conditions in the field and the limitation of the encapsulant material to operate at elevated temperatures. Therefore, a temperature value of 85°C was selected by JPL as a first choice because it was comfortably below the 100°C limit for most encapulant materials but high enough to provide rational test durations of less than six months. The combined 85°C/85%RH test condition was selected for the module testing because it was commonly used by the semiconductor industry and the cell level reliability research groups.

Module: The effects of high RH on the low temperature (early morning) glass surface of the PV modules could lead to potential induced degradation (discussed in the next section). However, the RH value inside the laminate and at the interfaces within the package is not necessarily the ambient RH and it is expected to be extremely limited inside the package during daytime due to high operating temperatures of the modules and to very limited moisture ingress from the laminate edges or transport

through the typical backsheets. In the current accelerated DH testing of IEC 61215, a relative humidity on the glass surface is maintained at 85% when the cell temperature is at 85°C. This condition never happens in the field and it is difficult to judge what outdoor exposure the 1,000-hour exposure at 85°C/85%RH represents (Wohlgemuth & Kurtz, 2011).

In order to determine acceleration factors between actual field data and the accelerated test data (for example, 85°C/85%RH for 1,000 hours), an extensive experimental work based on the recent/current PV module designs and a detailed modeling study needs to be carried out similar to the study published by JPL in 1984 (Otth & Ross, 1983).

The typical meteorological year (TMY) database of United States and other countries provides weather data including hourly RH, irradiance, ambient temperature, and wind speed. Based on the hourly irradiance, ambient temperature, and wind speed, the hourly module temperature can be calculated using JPL, Sandia, or IEC models (Otth & Ross, 1983; IEC68153-2, Draft; King, Boyson, & Kratochvill, 2004). The JPL model (Otth & Ross, 1983) is reproduced below:

$$T_M = T_a + (0.325 - 0.01V)S \tag{1}$$

$$RH = (P_d/P_M) * 100 \tag{2}$$

Where

T_M = module operating temperature °C

T_a = ambient dry-bulb air temperature °C

T_d = ambient dewpoint temperature °C

V= wind velocity m/s

S = irradiance level mW/cm^2

RH = module relative humidity, %

P_M = $P(T_M)$ = water saturation pressure at temperature T_M

P_d = $P(T_d)$ water saturation pressure at temperature T_d

and where P (T_d) and P(T_M) are evaluated from:

$$\log_{10}[P(T)/218.17] = [B(3.2438 + 0.005868\,B + (0.00227\,B)^3)] / [(T + 273.15)$$

$$(1 + 0.002188\,B)]$$

Where B = 374.12 - T

If the reaction rate with respect to temperature and/or humidity doubles for every 10-unit (10°C or 10%RH) following a conventional Arrhenius model, then one can calculate the acceleration factor for EVERY hour using JPL models shown below (Otth & Ross, 1983). In these models, 1%RH is considered to be equivalent to 1°C as was determined based on an experimental study of one degradation mechanism performed by another research group and referenced by JPL (Desombre, 1980). Based on these models, it is now possible to calculate the equivalent accelerated time required for each TMY/field-hour. Because the equivalent accelerated time for each field-hour is known, one can integrate the equivalent accelerated time for one year or twenty years.

$$t_i = \Delta_i * 2^{(T_i - 60)/10} \tag{3}$$

and

$$t_i = \Delta_i * 2^{(T_i + RH_i - 100)/10} \tag{4}$$

Where

Δ_i = duration of field – exposure interval i (1 Hr)

t_i = duration at 60°C , 40% RH to yield same aging as i

T_i = module temperature during interval i °C.

RH_i = module relative humidity during interval i%

Based on the above models, JPL constructed the plots, shown in Figure 16A and Figure 16B, for Phoenix (hot-dry), Miami (hot-humid), and Boston (cold-dry or temperate) climatic conditions. If temperature is the only aging factor for the PV modules, then the AT at 85°C for 4,000, 8,000 and 10,000 hours is calculated to be equivalent to 20 years of lifetime in Boston, Miami, and Phoenix, respectively (Figure

42

16A). If combined temperature and humidity are the only aging factors for the PV

modules, then the AT at 85°C and 85% RH for 100, 350 and 700 hours should be

equivalent to 20 years of lifetime in Phoenix, Boston, and Miami, respectively (Figure

16B).
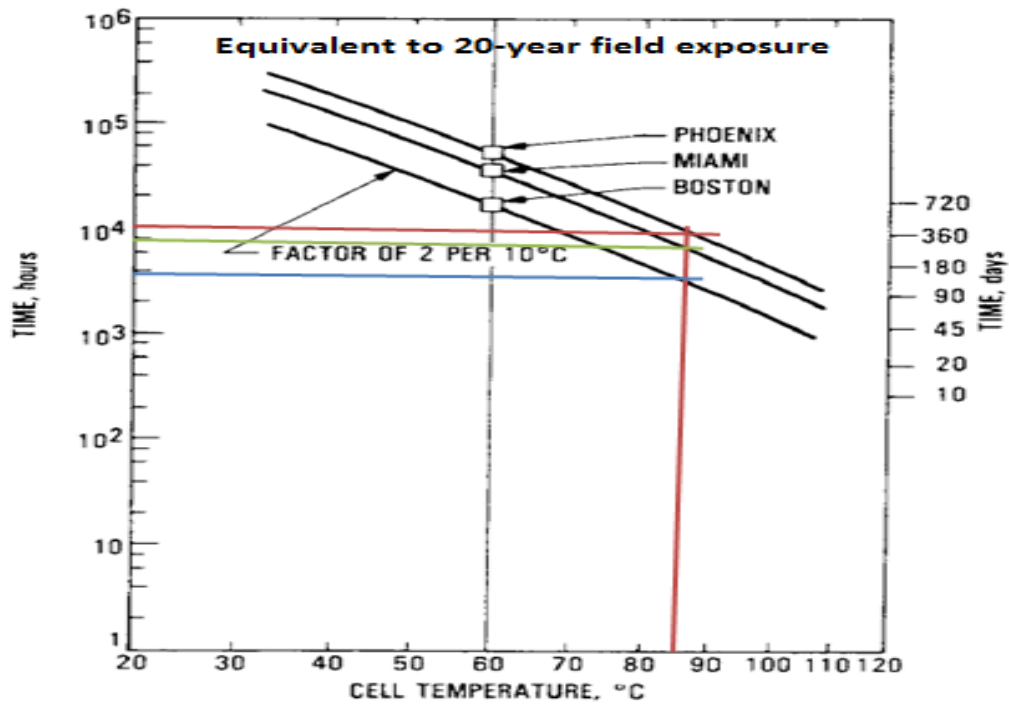
Figure 16A: At 85°C for 4,000, 8,000 and 10,000 hours
should be equivalent to 20 years of lifetime in
Boston, Miami, and Phoenix, respectively.
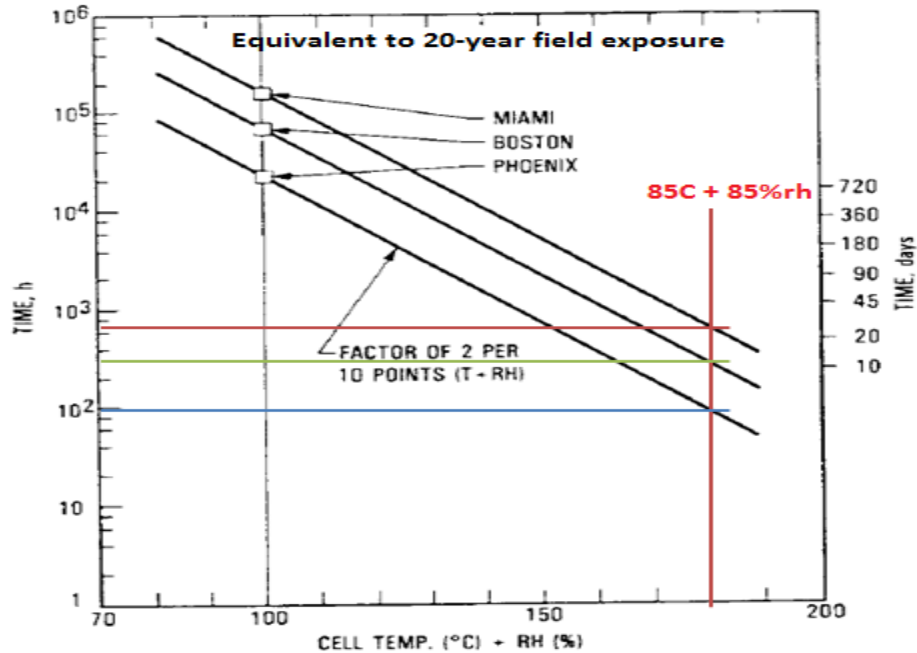
Figure 16B: At 85°C and 85% RH for 100, 350, and 700 hours
should be equivalent to 20 years of lifetime in
Phoenix, Boston, and Miami, respectively.

Figure 16: Accelerated Testing Equivalent to 20-Year Field Exposure

Similar to the thermal cycling test, an approach may be taken to determine the

required number of hours for the DH testing. As shown in Figure 17, for conventional

screen-printed polycrystalline silicon technologies, it takes about 3,000 hours of DH

testing (at 85°C/85%RH) to reach a 20% power loss, the level of degradation

typically specified in the 25-year warranty (Wohlgemuth, 2008). However, it is again

cautioned that the failure mode seen after 3,000 hours at 85°C/85%RH is not

something that is commonly seen in field exposed modules because the modules

tend to dry out (both at the surface and in the bulk) in the real world at this high

temperature of 85°C. It appears that the 85°C/85%RH test condition uses unrealistic

conditions—the 85°C/85%RH test condition appears to be a good screening test (for

qualification or comparative testing) but not a good (too severe!) weathering test

condition (for lifetime testing). Therefore, there is a need to match the field failure

mechanisms and modes in the lifetime accelerated DH testing using a range of

44

temperature and humidity levels. Also, it is yet to be objectively demonstrated that the modules that have experienced less than 20% degradation over 3,000 hours at 85°C/85%RH would have lasted 25 years in the field even if the difference in the failure modes/mechanisms between AT and field testing is ignored.
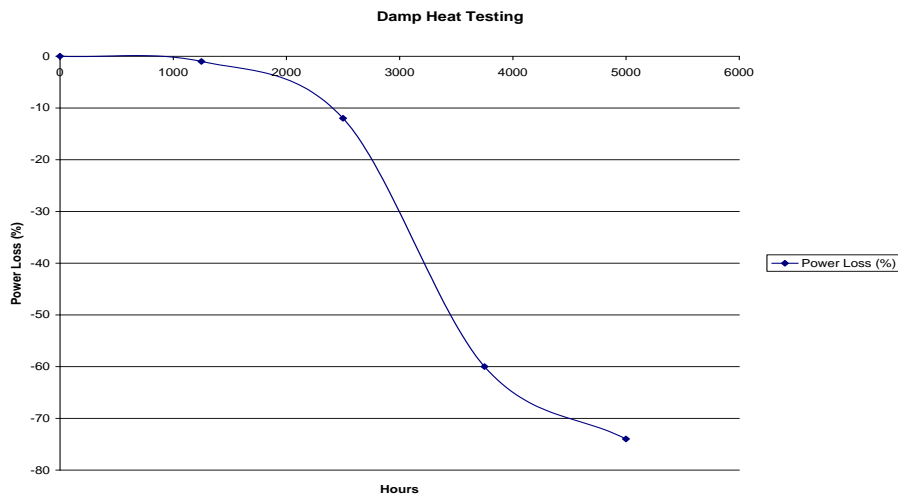
Figure 17: Maximum Duration Limit for Damp Heat Stress of PV Modules.

Backsheets and Encapsulants: The water vapor permeation (moisture ingress) rate through backsheets leads to many failure modes in PV modules and it is related to the change in the molecular weight of the backsheet polymer. For example, the molecular weight of a polyethylene terepthalate (PET) backsheet decreases during hot-humid field exposure through hydrolysis. As shown in Figure 18, a comparison of molecular weight decrease between field aged PET for 15 years at Rokko (Japan) and DH tested PET samples seems to indicate that the standard DH testing at 85°C/85%RH for 1,000 hours is equivalent to 45 years in the field (Eguchi, 2011). It is important to note that the phase change temperature of polymeric materials should not be exceeded when determining the upper and lower temperature limits for the accelerated tests. Because the 85°C limit used in the DH test is higher than the phase change temperature for PET, the above mentioned linear correlation should be used with caution.

45
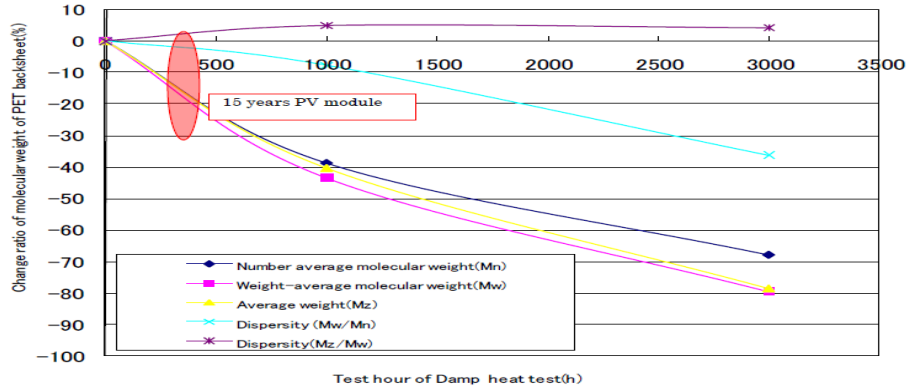
Figure 18: Loss of Molecular Weight of PET Backsheet during Extended Damp Heat

Test (Eguchi, 2011).

Based on the module operating temperatures at various climatic conditions and the

indoor accelerated tests, Fraunhofer Institute ISE research group has calculated the

required DH stress time limit for encapsulant and backsheet materials (Kohl, 2009).

Depending on the reaction mechanism, the activation energy from one polymer to

the other may differ. For example, the activation energies calculated for tedlar-

polyester-tedlar (TPT) backsheet and EVA, thermoplastic polyurethane, and polyvinyl

butyral encapsulants are 42, 34, 31, and 56 kJ/mole, respectively. This paper

indicates that the DH test at the stress limit of 85°C/85%RH may need to be

performed on EVA (activation energy of 34 kJ/mole) for a calculated time of about

1.5 years (13,000 hours) and about 0.5 year (4,000 hours) for a service lifetime of

25 years in a tropic and desert climatic conditions, respectively. Similarly, for TPT,

the calculated stress time at 85°C/85%RH stress limit for 25 years' service life in a

desert condition is about 1,100 hours. If the activation energy is higher than the

ones reported above, then the equivalent testing time at 85°C/85%RH would be

dramatically lower as shown in this plot. It is to be noted that the calculated AT time

presented in this work is based on the activation energy only without clearly

identifying the corresponding actual field failure modes and mechanisms which are

accelerated in the AT. An ongoing study at NREL seems to indicate that the PET

layers undergo hydrolysis failure mechanism in the field. Based on the chemical

kinetics involved in the hydrolysis process, this work calculates that the 1,000 hours

of DH testing at 85°C/85%RH is equivalent to about 300 years in Bangkok, one of

the highest hot-humid climatic condition sites in the world.

Stress Level and Duration Limits: UV

The UV test is another important stress test done on PV modules to identify those

materials and adhesive bonds that are susceptible to UV degradation. Typically, the

UV absorbers are added in the encapsulant to keep UV from reaching the

cell/encapsulant interfaces and the adhesives. Almost all modules contain EVA

encapsulant and it does not discolor in UV. There are UV tolerant EVA formulae being

sold today without UV absorbers (at least for front EVA). It is to be noted that the

encapsulant discoloration occurs not due to the discoloration of EVA or UV absorbing

additives but due to the other additives in EVA (anti-oxidants, curing systems, etc.

that degrade in UV and cause discoloration) (Holley, Agro, Galica, & Yorgensen,

1996; Shigekuni & Kumano, 1997)

As shown in Figure 19 (Arco Solar M55 modules installed in 1985 and still operating

after 26+ years in Phoenix - Arizona), the discoloration of encapsulant is a common

degradation mode due to UV exposure in the field, especially in hot-dry desert

climatic conditions. As shown in Figure 14, the same Arco Solar M55 module in a

hot-humid climatic condition undergoes encapsulant browning and delamination

instead of just encapsulant browning.

Figure 19: Encapsulant Browning Due to UV in a Hot-Dry Condition.

Based on the UV content of about 5.5% of the global irradiance in desert climatic conditions, the total UV-dose in desert conditions is calculated to be about 120 kWh/m^2/year (or about 3,000 kWh/m^2 over 25 years (Kohl, 2011). The UV absorbing additives used in EVA may chemically differ from one EVA manufacturer to the other and hence all EVAs cannot be considered the same. Before initiating the accelerated UV lifetime testing, two important things should be taken into account—selection of the UV source and selection of test sample construction.

The spectra of artificial UV sources strongly differ from the solar UV spectrum. Therefore, different aging behaviors of samples with different UV sources/lamps have to be expected and appropriately accounted by using appropriate light sources (for example, xenon arc lamps) and correct optical filters. The extent of discoloration of encapsulant is dictated by two competing reactions: discoloration by UV light; bleaching by diffused oxygen through substrate or superstrate (Gonzalez, Liang, & Ross, 1985; Holley, Agro, Galica, & Yorgensen, 1996). Figure 20 (Arco Solar M55 modules installed in 1985 and still operating after 26+ years in Phoenix – Arizona) clearly differentiates how the UV discoloration reaction dominates at the center of the cells and how the oxygen bleaching reaction (using diffused oxygen through the backsheet) dominates at the cell edges and cell cracks. Because the crystalline silicon (c-Si) wafers/cells do not allow oxygen to diffuse through and the inter-cell area is very limited in the current commercial modules (due to high packing density of square or scrounded cells as compared to round cells), the oxygen bleaching counter reaction of the encapuslant on the cell surfaces (which primarily dictate the power output) is very limited in current commercial modules.
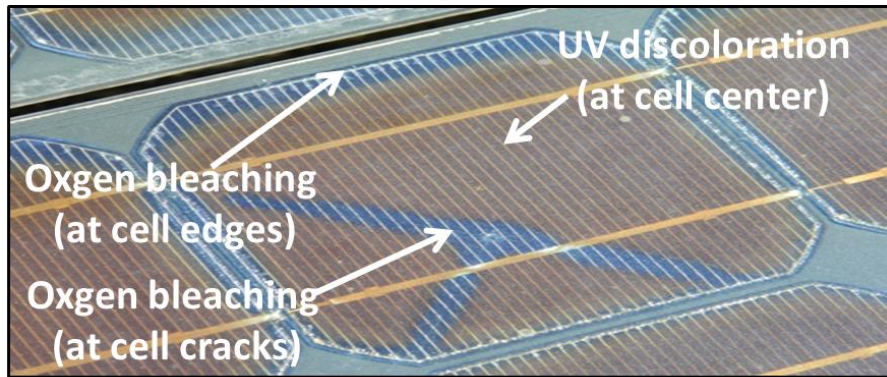
Figure 20: Encapsulant Browning Due to UV and Bleaching around the Cells and Cell-
Cracks Due to Oxygen Diffusion thru Backsheet and Cracks in a Hot-Dry Condition.

Figure 21 provides results of a specific EVA, called EVA-1 (Shioda, 2011). The

modules based on EVA-1 were exposed in the field over 20 years and showed little

(at the center and cell-gaps) or no (at the edges) activity loss of additives. The

construction of these modules appears to be: glass/EVA/Cell/EVA/polymer backsheet

with aluminum foil. Freshly constructed samples of the same EVA-1 were tested in

the lab at 110°C and 60 W/m^2 UV irradiance (equivalent to UV dosage in natural

sunlight) using a construction of glass/EVA/glass. When EVA-1 was tested in the lab

at a UV irradiance tripled in intensity compared with that of natural sunlight (180

W/m^2) but at the same temperature of 110°C, the additives appear to have lost part

of their activity without simulating the actual field failure mechanism. The

temperature dependent EVA discoloration reaction rate without including oxygen

bleaching counter reaction rate and the corresponding acceleration factor may be

modeled using the Arrhenius equation (Gonzalez, Liang, & Ross, 1985). In order to

evaluate the adhesion strength of EVA due to UV exposure over 20 years, it is

necessary to continuously expose the test samples, with high UV transmittance glass

in a typical weatherometer (2.5 UV suns at 60°C and 60%RH) for 6 to 7 months

(Kempe, 2008). BP Solar reported the use of a UV-exposure at 90°C for 26 weeks

[6.5 months] to verify a 25-year lifetime (Wohlgemuth, Cunningham, Monus, Miller,

49

& Nguyen, 2006). The temperature limit (60-90°C) and the relevance of humidity presence (0-60%RH) with respect to encapsulant browning and delamination still need to be investigated.

(A): Field Exposed—Glass/EVA/Cell/EVA/Backsheet construction

(B): Field Exposed—Glass/EVA/Cell/EVA/Backsheet

(C): Accelerated UV Exposure—Glass/EVA/Glass construction
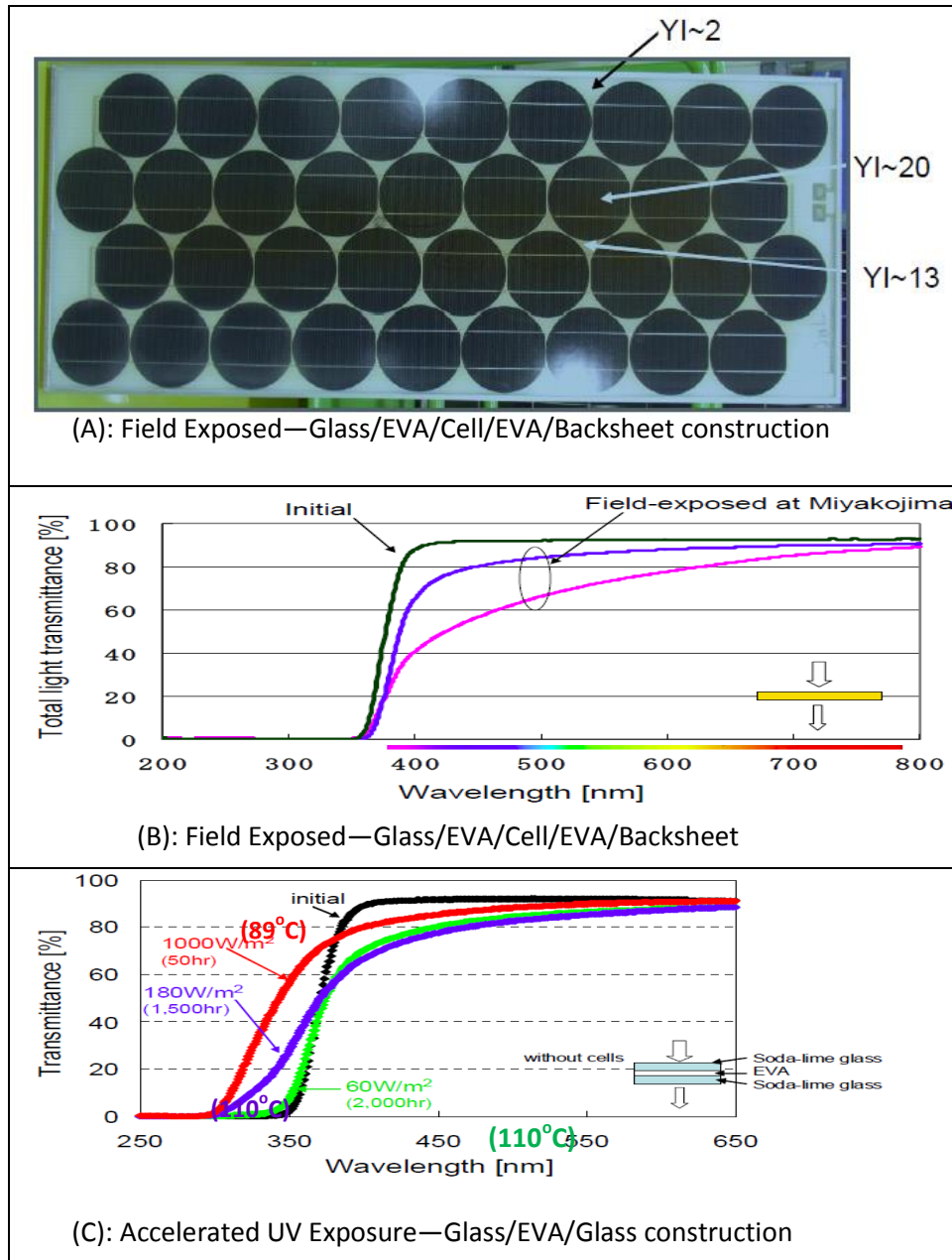
Figure 21: Acceleration Limit for UV Stress on Glass/EVA/Glass Sample (Shioda, 2011).

Stress Level and Duration Limits: Humidity-Freeze

The purpose of this test is to determine the ability of the module to withstand the effects of high temperature and humidity followed by sub-zero temperatures. In the humidity-freeze test, the modules are cycled once a day for 10 days between -40°C and 85°C/85%RH. The hot-humid environment (causing absorption of moisture) followed by sub-zero temperature (causing expansion of the absorbed water as it freezes) used in this test detects weakness of the interfaces including backsheet/junction box and glass/encapsulant. A recent study indicated that 8.8% (11 out of 125) of the modules that were subjected to this test failed in the post-wet resistance test (TamizhMani et al., 2012). Similar to the DH test, the post-wet resistance failures were attributed to the weakened interfaces of junction box attachment and laminate edge sealant failure.

The humidity-freeze test was initially developed by JPL and the object of this test was to force moisture into the module and observe mechanical and moisture-induced corrosion via visual inspection. This stress test is usually done for 10 cycles between -40°C and +85°C in a sequence after short UV (15 kWh) and thermal cycling (50 cycles) pre-conditioning stresses. If there is an insufficient cross-linking or adhesion between interfaces (glass/encapsulant, encapsulant/cell, backsheet/encapsulant and junction box/backsheet in c-Si modules, and glass/edge sealant/glass in thin-film modules), this screening test can quickly identify these issues. This test is not considered to be a lifetime test and it does not necessarily need to be extended beyond 10 cycles. This test sequence has proven to be extremely sensitive and important in the qualification testing programs to pre-screen the adhesion strength of junction boxes to the backsheet of c-Si modules and the edge sealants of thin-film modules (the qualification test results of several thousands of modules are discussed in the next section).

Stress Level and Duration Limits: Voltage

Potential induced degradation (PID) due to high system voltages in hot-humid climates can be a major degradation mechanism in PV modules, and it adversely affects the performance of PV modules due to combined effects of two or more of the following factors: system voltage, superstrate/glass surface conductivity, encapsulant conductivity, and silicon nitride anti-reflection coating property. As shown in Figures 22A and 22B, a module can experience different types and extent of degradation depending on the grounding configuration, polarity, and module position in the string (Pingel et al., 2010).
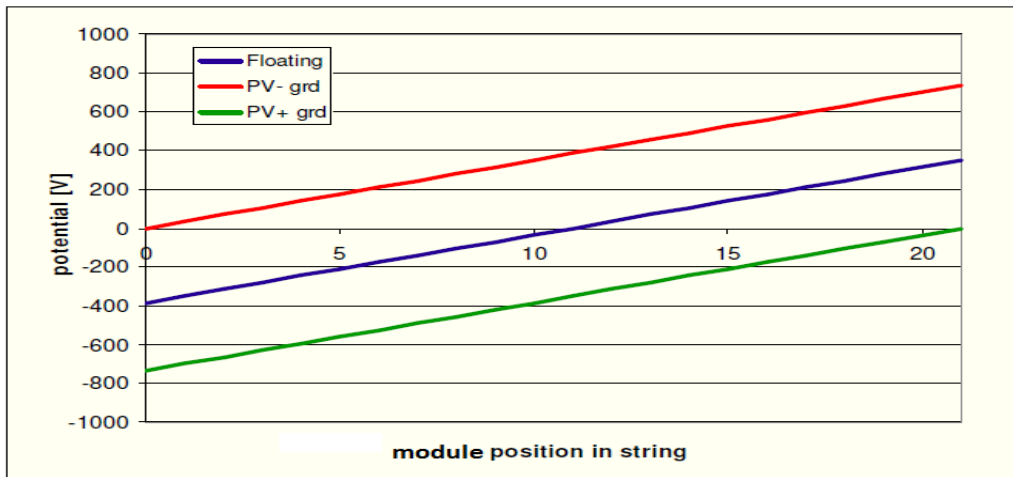
Figure 22A: Floating Arrays with Both Positive and Negative Polarities and Grounded Arrays with either Negative or Positive Polarity.
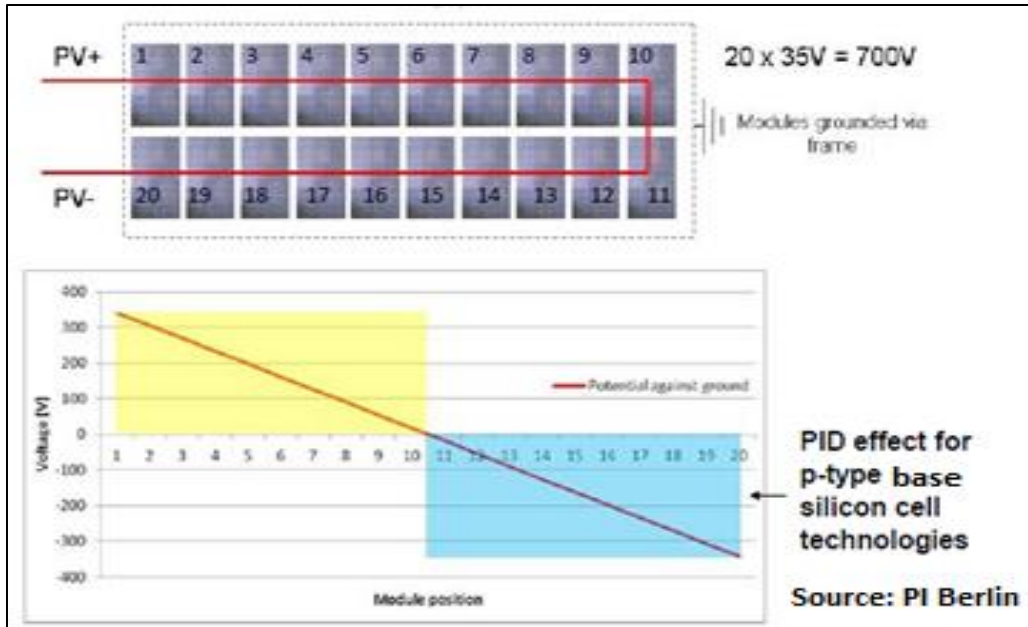
Figure 22B: An Example of a Floating Array with both Bias Polarities

Figure 22: Floating Arrays (Pingel et al., 2010)

As shown in the simplified diagram of Figure 23, the high system voltages (600-1500 V) in the PV systems could lead to leakage current between the cell/active circuit and the ground and hence could cause gradual performance degradation depending on the cell bias type and magnitude of leakage current. PID can be increased by increasing applied/system voltage, operating temperature, or electrical conductivity between cell/active circuit and module frame through surface conductivity (for example, condensed water layer on the glass surface), interfacial conductivity (for example, between cell and encapsulant) and/or bulk conductivity (for example, through encapsulant).
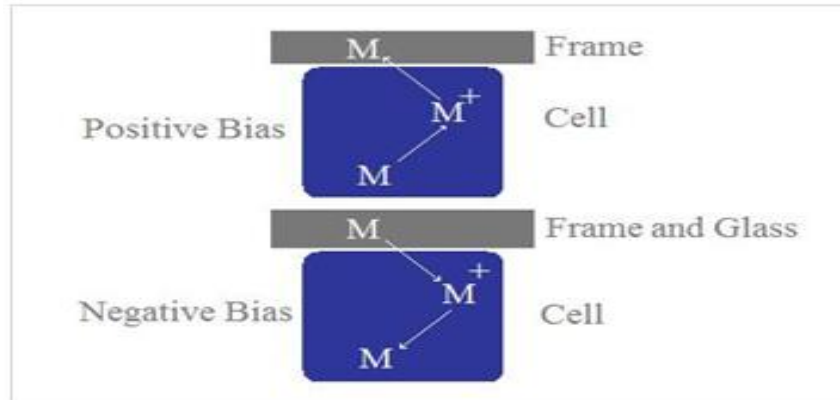
Figure 23: A Representation of Electrochemical Activity between the Frame/Glass

and Cell.

The original research on the electrochemical degradation of c-Si and thin-film modules was initiated by JPL in 1980s (JPL, 1986). A renewed interest in this research, now named PID, was motivated by a few recent field issues related to electrochemical degradation of thin-film and crystalline silicon modules (Dhere, Pethe, & Kaul, 2010; Hacke et al., 2011). Figure 24 indicates that an accelerated factor of 427 for PID can be obtained for the hot-humid use condition in Florida at -600 V by stressing the modules at 60°C and 85%RH for 96 hours (Hacke, 2012). This stress condition is estimated to be equivalent to about 4.7 years of the field use condition of Florida. For a 20-year lifetime, this linearly translates to 400 hours of PID stress testing at 60°C and 85%RH. The higher stress levels at or above 70°C and 70% RH, lead to high chemical activity of water that leads to degradation modes such as silicon nitride degradation and series resistance increases that are not seen in the field (Hacke et al., 2012). Therefore, it is important to eliminate PID stress conditions of the AT that induce electrochemical activities not seen in the field.
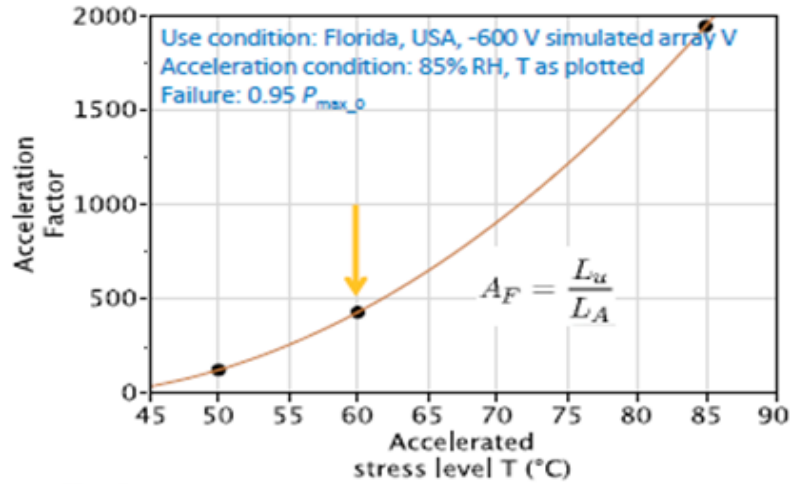
Figure 24: PID Acceleration Factor Dependence on Stress Temperature Level (Hacke, 2012).
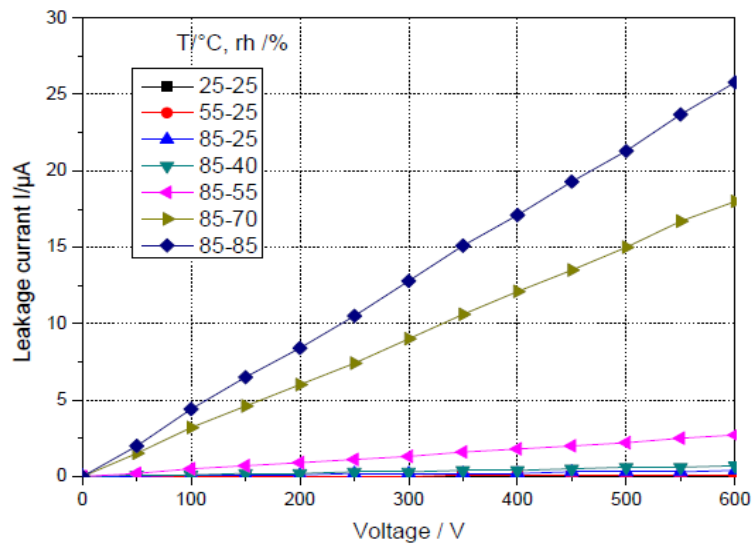
Figure 25: Linear Dependence of Current on Stress Voltage, and the Combined Voltage, Temperature, and Humidity Effects on the Leakage Current of a Module (Hoffmann & Koehl, 2012).

In chemical kinetics, the activation energy (in joules per mole) influences the chemical reaction rate (in moles per second) whereas in electrochemical kinetics the overpotential (in volts) influences the electrochemical reaction rate (in amps). Depending on the overpotential magnitude, either the Butler-Volmer (zero overpotential), Stern-Geary (low overpotential), or Tafel (high overpotential)

55

equation may be applied (Revie, 2000; Greene, 1986). The low overpotential (called polarization overpotential due to polarization resistance, Rpol) is composed of activation overpotential (or electrochemical activation energy) and ohmic overpotential. The ohmic overpotential (due to ohmic resistance, Rohmic) in a PV module is caused by the bulk resistance of encapsulant, bulk resistance of glass, surface resistance of glass (primary ohmic drop), and the interface between glass and encapsulant. The activation overpotential (due to activation resistance, Ract) in a PV module is caused by the interface between the electrode (active cell circuit) and electrolyte (encapsulant). The linear plot shown in Figure 25 above appears to be caused by both ohmic overpotential and activation overpotential. Because the ohmic overpotential in a PV module is extremely high as compared to the activation overpotential, the effect of activation overpotential is completely masked. In order to determine the activation overpotential and isolate it from the ohmic overpotential, it may be necessary to use the electrochemical impedance technique.

Figure 26 indicates that the module surface relative humidity is close to zero when the sun is shining in a hot-humid climatic condition (Hacke et al., 2011). During the sunny hot part of the day, the entire voltage is expected to drop on the glass surface with negligibly small voltage drop in the bulk and cell/encapsulant interface, leading to an absence of any PID during the sunny hot part of the day. The field data shown in this figure imply that the degradation may mostly occur first thing in the morning or after a rainstorm when there is high humidity and before the module has time to dry out in the sun. This situation may be simulated in the AT using a conductive carbon layer on the glass surface.
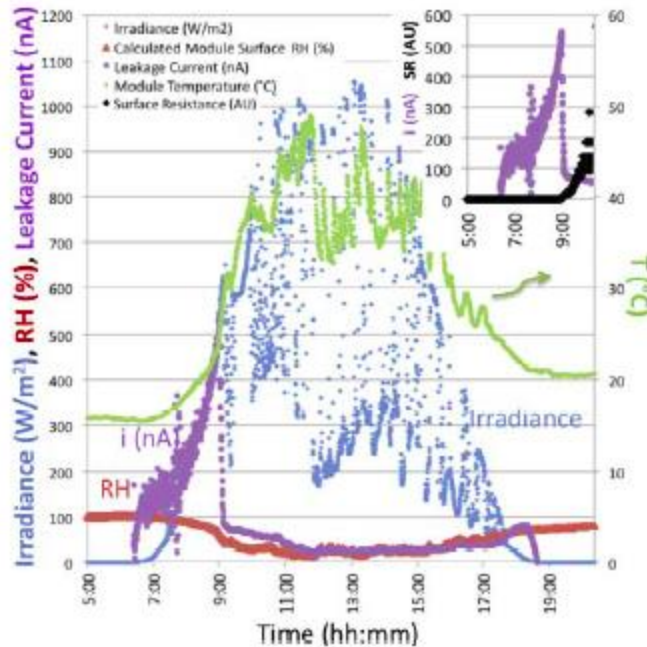
Leakage current to ground, irradiance, calculated module surface relative humidity (RH), and module temperature over a one-day period in Florida. The module is horizontally mounted, the active layer is biased to scale logarithmically with irradiance to a maximum voltage of −600 V with the module leads connected to a load resistor to maintain approximately P_{max}. The leakage current is highest when morning dew is on the module face and the surface resistance (SR) is low (inset). When the module is dry, the current most closely follows the calculated module surface RH.

Figure 26: When Sun is Shining, the Module Surface Relative Humidity is close to Zero even in a Hot-Humid Climatic Condition (Hacke et al., 2011).

Figure 27 shows the results of a simulated experiment with the interruption of surface conductivity using a carbon layer (Tatapudi, 2012). These PID experiments were performed on the thermal cycling (TC) (thermal cycling 200) and DH (DH 85°C/85%RH) pre-stressed modules rather than fresh modules to simulate the field aged modules going through PID stress. As shown in Figure 27, the ohmic resistance could be increased (or PID eliminated) to a very high level by interrupting the surface conductivity of the glass near the frame edges using either hydrophobic coating, glass surface modification with water repellent properties, or thick edge sealants for the frame attachment. In the high surface conductivity PID test (surface

fully carbon coated), the primary ohmic drop occurs in the bulk and interfaces similar to first thing in the morning or after a rainstorm in the field. In the disrupted surface conductivity PID test (surface partially carbon coated), the primary ohmic drop occurs on the glass surface similar to the sunny hot part of the day. This plot also indicates that the pre-DH-stressed modules degrade at much higher level than the pre-TC stressed modules possibly due to increase in the bulk conductivity of the encapsulant because of moisture ingress during the 1,000 hour DH test. It is important to note that no PID effect has been reported on the fresh modules if the cells do not have the silicon nitride antireflection coating. Recent studies on the fresh modules indicate that the PID effect is mostly, if not entirely, reversible if reverse voltage (positive voltage) is applied on c-Si with p-base (Hacke et al., 2011). This probably implies that the irreversible electrochemical reaction involving cell metallization may not occur on the fresh modules during PID stress testing. However, the irreversible electrochemical reaction involving cell metallization may occur if the module had been pre-stressed at 85°C/85%RH for 1,000 hours (TamizhMani, 2012). This study seems to indicate that both reversible and irreversible degradation mechanisms may be operating on the DH pre-stressed modules. It is not yet clear whether PID involves only the silicon nitride (SiN) layer or both the SiN layer and the cell metallization in the actual field aged modules. This requires further investigations and characterizations of the field aged modules in hot-humid climatic conditions.
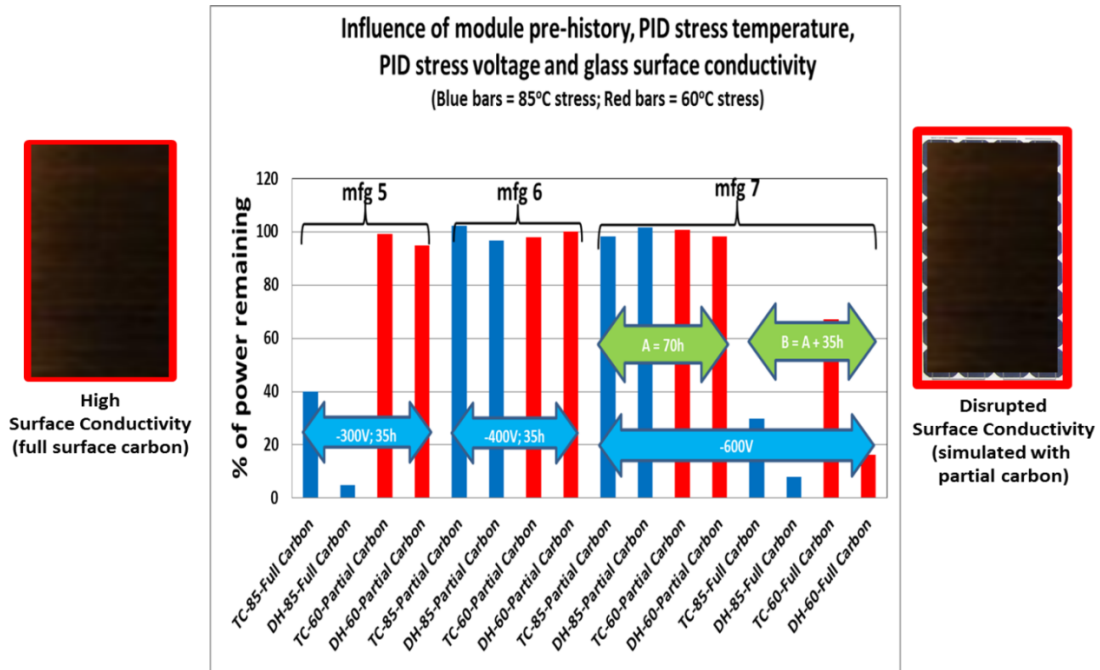
Figure 27: Avoiding PID by Disrupting the Glass Surface Conductivity near Frame
Edges (Tatapudi, 2012).

A general model for the leakage current of PID test as a function of temperature,
humidity, and voltage is given in the following equation (Hoffmann & Koehl, 2012).

$$I = I_{max}/(1 + (I_{max}/c - 1)/\exp(I_{max} \times (rf - a) \times b))$$

with

$$I_{max} = U/R_a(358 \text{ K}) \, A \cdot \exp\left[-(E_a/ \text{ R}) \cdot (1/T_{test} - 1/358 \text{ K})\right]$$

The remaining parameters a = 0.3, b = 1.5/mA, and c = 0.3 mA describe the slope
of the current increase and the offset of the sigmoidal curve shown in Figure 28.
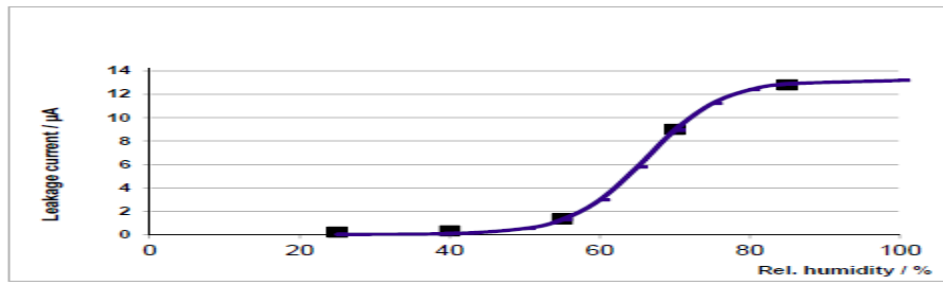
Figure 28: Sigmoidal Leakage Current Dependence on Relative Humidity.

It is possible that the primary voltage drop location is shifted from the glass surface to the bulk and cell/encapsulant interface when the RH increases to higher than 60%. The humidity on the glass surface probably forms a continuous water layer and efficiently conducts electricity when the RH exceeds 60%. Therefore, at higher humidity and lower temperature levels (for example, $60^{o}C/85\%RH$), the primary voltage drop occurs in the bulk and cell/encapsulant interface due to low ohmic resistance on the glass surface. At lower humidity and higher temperature levels as in the field ($85^{o}C/60\%RH$), the primary voltage drop occurs on the glass surface and in the glass and encapulant materials due to high ohmic resistance.

As shown in the voltage drop distribution schematic in Figure 29, the cell/interface reaction in the early morning is accelerated due to high surface humidity level (surface with dew) as compared to the daytime low/zero glass surface humidity. It may be envisioned that the shift in the location of voltage drop from surface (ohmic location) to interface (activation location) under high humidity condition may be identified by using the combination of both Arrhenius and electrochemical impedance plots obtained at different temperature and humidity levels. Because the semiconductor materials behave very differently in the presence of light and humidity in the interface, the PID tests may need to be performed in the presence of light to investigate the presence or absence of photoelectrochemical reaction at the cell/encapsulant interface (Noufi, Frank, & Nozik, 1981; Gerischer, 1977; Wrighton, 1977).
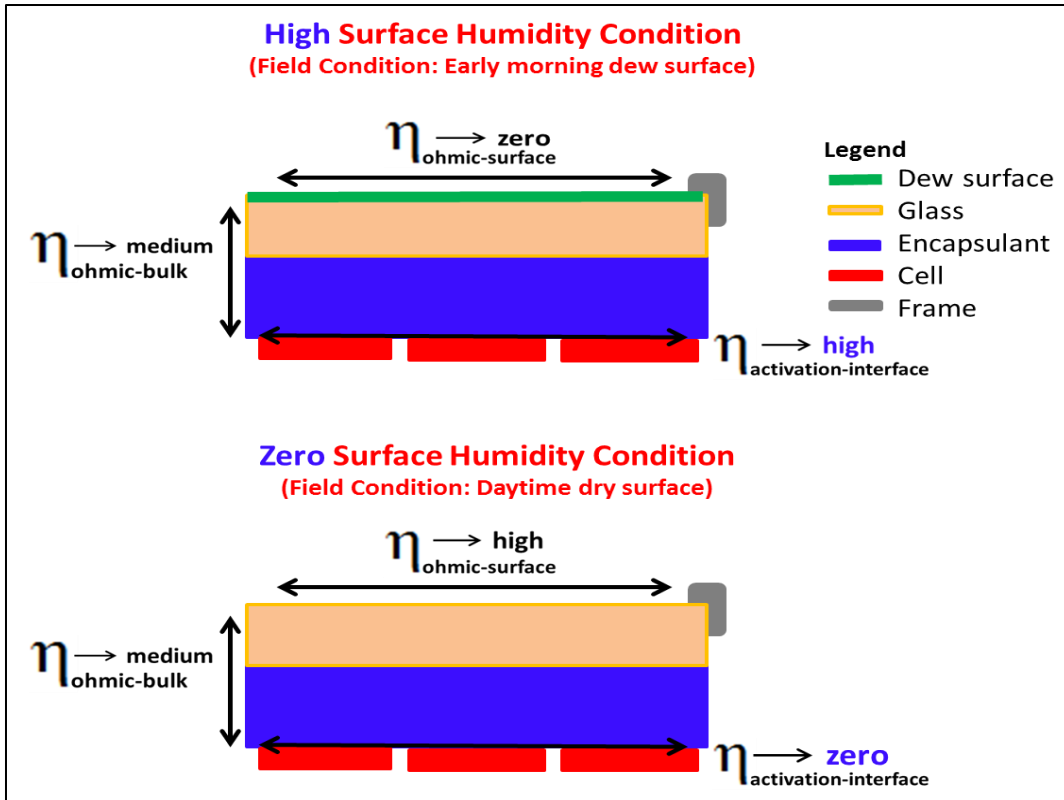
Figure 29: Voltage Drop Distribution under High and Zero/Low Glass Surface Humidity Levels.

2.3 Accelerated Aging Testing

In any AT, the general approach is to apply higher stress levels than actual use conditions over a short period of time to induce failures that would normally occur in the field. The AT can be used to induce both hard failures (reliability) and soft losses (durability or degradation).

The purpose of AT is to shorten the test time using simulated test conditions much more severe and/or faster than the actual field operating conditions while replicating actual field failure and degradation modes and mechanisms. As shown in Figure 30, the accelerated test programs for PV modules may be classified as:

- accelerated qualification testing (minimum confidence in quality),
- accelerated comparative testing (medium confidence in quality), and

- accelerated lifetime testing (maximum confidence in quality)

The first two testing programs are qualitative AT programs and the last testing program is a quantitative AT program. In qualitative AT, the manufacturer is mostly interested in identifying failures and failure modes without attempting to make any predictions as to the product's life under normal use conditions. In quantitative AT, the manufacturer is interested in predicting the life of the product (or more specifically, life characteristics such as mean-time-to-failure, failure rate over time) at the desired use conditions, from data obtained in an accelerated lifetime testing program.
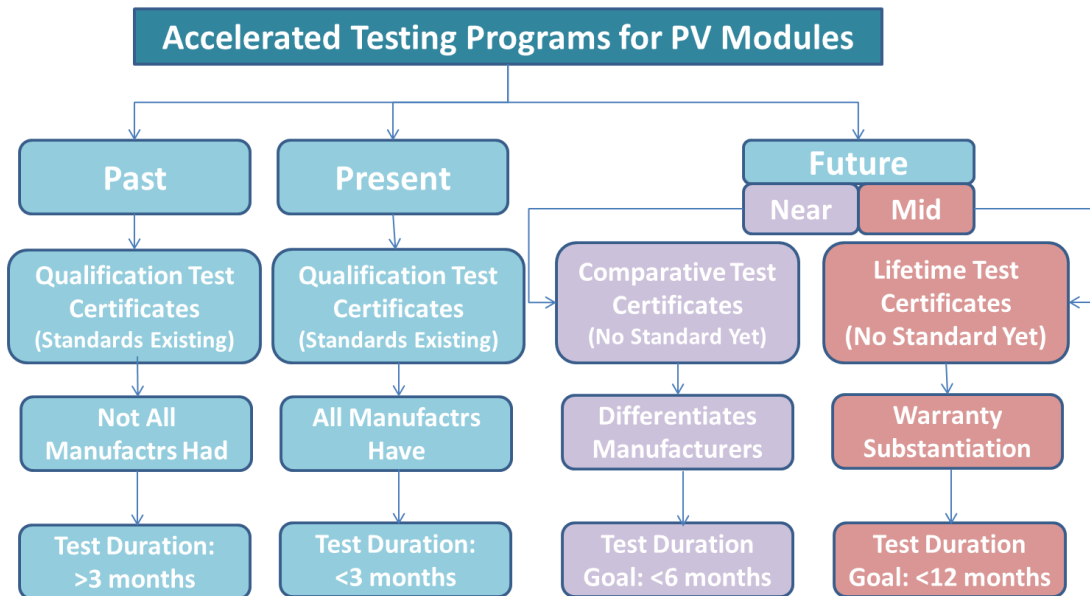
Figure 30: Past, Present, and Future Accelerated Testing Programs of PV Modules.

As indicated in the figure above, the standards for the qualification testing programs (IEC 61215 for c-Si, IEC 61646 for thin-film, and IEC 62108 for concentrated photovoltaics [CPV]) of PV modules have already been established and the standards for the comparative and lifetime test programs are yet to be developed. As an example, for ease of reading, the test sequence of IEC 61215 qualification standard is reproduced in Figure 31 (Wohlgemuth, 2011). Due to the high diffusion level of PV

62

technology in the recent past (modules installed in the last 7 years account for 96% of all the modules cumulatively installed around the world), comparative and lifetime testing programs are expected, and even demanded, by consumers and investors so the products can be differentiated. Almost all PV products now have qualification certificates.
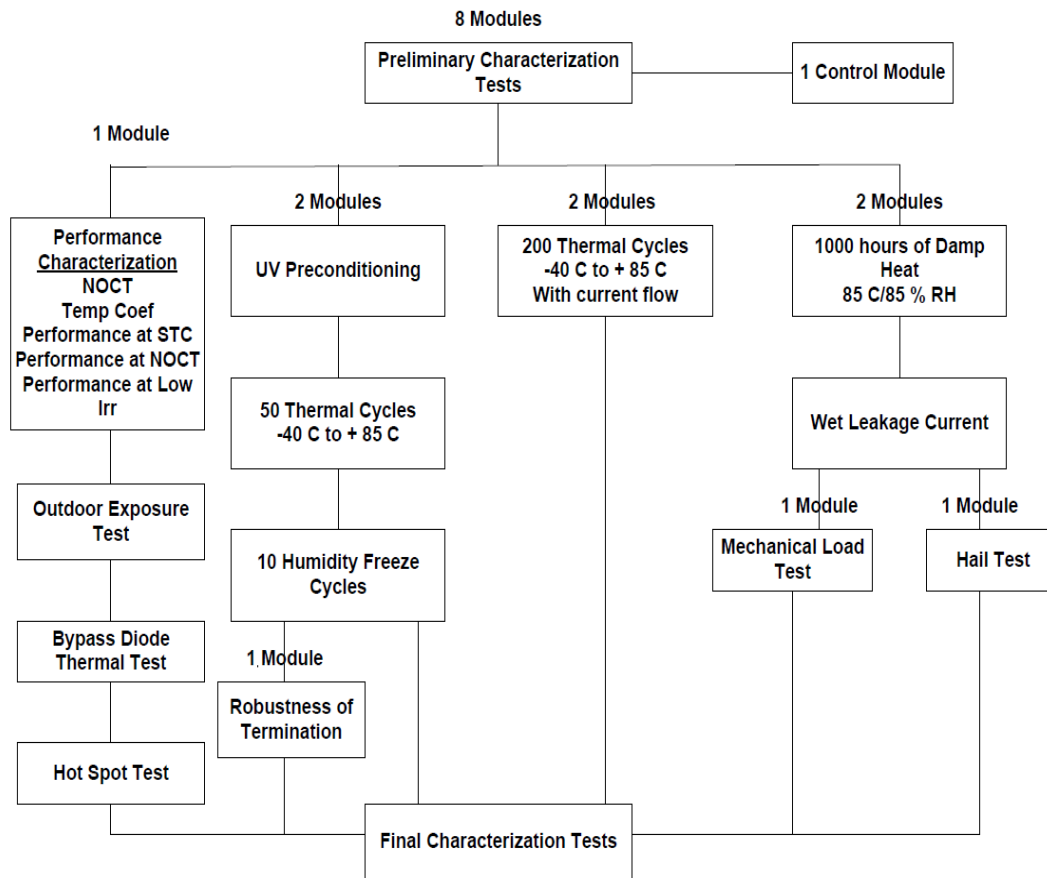
Figure 31: Test Sequences of IEC 61215 Qualification Testing (Wohlgemuth, 2011).

Accelerated Qualification Testing (AQT)

- Objective: The objective of qualification testing is to identify major failure modes during the initial stage in the field without attempting to make any predictions about the product's life under normal use conditions. The qualification testing defines minimum testing requirements to substantiate minimum durability (degradation) and reliability (failure) of a specific module

design. This program DOES NOT attempt to account for the energy penalty over a lifetime of 20 or 25 years.

- Goal: The goal from a manufacturer perspective is to introduce the product into the marketplace with minimal required quality tests. This is a test-to-pass testing program; the testing is repeated with improved design until the modules pass this test.

- Cost and time: Minimum

- Testing protocol: Standardized protocols defined by the test standards (Examples: IEC 61215 for c-Si, IEC 61646 for thin-film, or IEC 62108 for CPV).

- Test requirement: It is a pass/fail test with a maximum allowed limit of 5% power drop per test (and 8% per test sequence) after accelerated stresses. Appendix B explains how module designs have struggled, evolved, and improved between 1997 and 2011 to meet the pass requirements of the qualification standards.

- User: Used by all manufacturers and it is a market/consumer/incentive driven requirement in Europe and around the world. The qualification standards (IEC 61215 for c-Si, IEC 61646 for thin film, and IEC 62108 for CPV) are the most extensively used PV standards in the industry. A recent publication from Wohlgemuth (Wohlgemuth, 2012b) indicated the following "Whipple reported on 10 years of field results (using data from Rosenthal, Thomas, and Durand) that unqualified modules suffered from 45% field failure rate while qualified modules suffered from less than 0.1% field failure rate." Unfortunately, even this minimum qualification testing is not required in the United States, except in Florida. Solar ABCs has recently released a policy statement recommending the adoption of the qualification testing requirement in the United States.

Accelerated Comparative Testing (ACT)

- Objective: The objective of comparative testing is to identify relative failures and performance losses between different designs without attempting to make any predictions as to the product's life under normal use condition. The comparative testing protocol should define extended, combined or sequential AT requirements to compare the durability and reliability of different module designs. This program SHOULD attempt to account for the energy penalty (figure of merit) over lifetime of 20 or 25 years. For example, in the 1980s, JPL used a 10% energy/cost penalty as the figure of merit.

- Goal: The primary goal from a buyer or investor perspective is to differentiate the product designs from one manufacturer to the other in terms of their ability to survive in the field and to continue to produce power with minimal annual power loss.

- Cost and time: Medium—falls between qualification testing and lifetime testing.

- Testing protocol: Currently, several manufacturer or test laboratory defined comparative testing protocols are being used by the industry. A consensus-based uniform but climatic-specific and technology-sensitive protocol needs to be developed by a standard developing organization. Various testing laboratories, national laboratories, and manufacturers have developed several comparative testing protocols. An extended table presented in Appendix C compares these test programs. This table could serve as the basis for the development of a comparative testing standard by standard developing organization(s). The International Quality Assurance Forum (IQAF), a joint international effort from Europe, North America, and Asia, aims to develop such a high-demand protocol for the industry (see www.nrel.gov/ce/ipvmqa_task_force/ for additional details).

- Test requirement: It is a relative testing with periodic/intermittent monitoring (for failures and degradation) for a maximum allowed limit (limit the time and identify relative power loss or limit the power loss and identify relative time) defined by a standard developing organization or the consumer/investor.

- User: It could be used by the consumers or investors to compare and select appropriate climate-specific module design among various designs.

Accelerated Lifetime Testing (ALT)

- Objective: The objective of lifetime testing is to identify most, if not all, failure modes and mechanisms of the module during its entire lifetime in the field (initial, useful, and wear-out stages) with product's lifetime prediction (using statistical and physical models) under the desired field conditions. The lifetime testing protocol could define the testing requirements to predict the lifetime for any site-specific condition (and configuration). Or, the lifetime testing protocol could define the testing requirements to predict the lifetimes for the worst-case sites/climates (and configurations). This program may account for the energy penalty (figure of merit) over a lifetime of 25 years or may account for the remaining power (efficiency) through a rating system approach after 25 years of lifetime tests. For example, in the 1980s JPL used a 10% energy/cost penalty approach as the figure of merit whereas the QA Task Force of IQAF appears to lean toward the rating system approach.

- Goal: It is the ultimate failure and degradation testing to predict lifetime and/or to substantiate the warranty.

- Cost and time: Maximum

- Testing protocol: Currently, none is publicly available. A unique consensus testing protocol needs to be developed based on field failure mechanisms, failure modes, and physical/statistical models. Appropriate physical and statistical distribution models will need to be developed as well. As shown in

66

Appendix D, this testing program requires an extensive list of equipment for various standard and non-standard accelerated stress tests and pre- and post-stress/field characterizations along with physical and statistical modeling expertise. These test protocols may be developed by standard developing organization(s). As a first step, a comprehensive literature search and review needs to be conducted on the field failure and degradation modes and mechanisms, life-limiting failure modes, potential AT methods with stress/duration limits, and mathematical models. This report serves as a first step, providing a detailed literature search and review on the accelerated lifetime testing and the mathematical reliability models of PV modules. Again, the IQAF has recently instituted an all-encompassing task force to develop life testing protocols (see the website www.nrel.gov/ce/ipvmqa_task_force/ for additional details).

- Test requirement: It is a testing to determine the lifetime of the PV module design. A consensus definition for the term "lifetime" along with allowed energy penalty over lifetime will need to be developed by the standard developing organization or to be identified in the consumer-manufacturer agreement.

- User: It could be used by the individual manufacturers to determine liability for warranty returns or by consumers/investors as evidence of warranty substantiation.

2.4   Selection of Accelerated Tests for Photovoltaic Modules

A reliability test can be accelerated in multiple ways. Increasing the level of experimental variables like UV light, temperature, humidity, or voltage can accelerate the chemical processes of certain failure mechanisms such as chemical degradation of adhesive chemical bonds (resulting in eventual weakening and failure)

or of additives in the polymeric matrix (leading to discoloration). Variables like voltage and temperature cycling can both increase the rate of an electrochemical reaction (thus accelerating the aging rate). In such situations, when the effect of an accelerating variable is complicated, there may not be enough physical knowledge to provide an adequate physical model for acceleration (and extrapolation). Empirical models may or may not be useful for extrapolation to use conditions. The selected accelerated test programs must use one or more stresses simultaneously and/or sequentially to accelerate failure modes that actually occur in the real world. Module failure modes and lifetime in Miami, Florida, may be very different than in Phoenix, Arizona. One must decide which parameter(s) should be measured to best monitor the failure mode being evaluated and then define what constitutes a failure for that parameter (McMahon, 2004). The typical accelerated tests used to induce various failure modes of photovoltaic modules are listed in Table 4 (Wohlgemuth & Kurtz, 2011).

A study performed by BP Solar (Wohlgemuth, 2003) provides a good model for selecting appropriate accelerated tests and their limits specific to PV modules. In this study, BP Solar analyzed all the modules that were returned from the field from 1994-2002. During this time, nearly two million modules were in the field under warranty. The total number of returns during this nine-year period was 0.13%. About 45% of the modules were returned because of corrosion and about 41% were returned because of cell or interconnect breakage. BP Solar determined that the causes for failures were moisture ingress and thermal expansion/contraction, respectively.

Based on these field failure modes, BP Solar designed its AT program to perform thermal cycling in excess of the standard 200 cycles (IEC 61215) and the damp heat (DH) exposure in excess of the standard 1,000 hours (IEC 61215).

Table 4: Selection of Appropriate Accelerated Tests to Induce Specific Field Failure

Modes (Wohlgemuth & Kurtz, 2011)

Accelerated Stress	Failure Mode
Thermal Cycle	Broken interconnect
	Broken cell
	Solder bond failures
	Junction box adhesion
	Module connection open circuits
	Open circuits leading to arcing
Damp Heat Exposure	Corrosion
	Delamination of encapsulant
	Encapsulant loss of adhesion & elasticity
	Junction box adhesion
	Electrochemical corrosion of TCO
	Inadequate edge deletion
Humidity Freeze	Delamination of encapsulant
	Junction box adhesion
	Inadequate edge deletion
UV Test	Delamination of encapsulant
	Encapsulant loss of adhesion & elasticity
	Encapsulant discoloration
	Ground fault due to backsheet degradation
Mechanical Load	Broken interconnect
	Broken cell
	Solder bond failures
	Broken glass
	Structural failures
Dry and Wet Insulation Resistance	Delamination of encapsulant
	Ground faults
	Electrochemical corrosion of TCO
	Inadequate edge deletion
Hot Spot Test	Hot spots
	Shunts at the scribe lines
Hail Test	Broken cells
	Broken glass
Bypass Diode Thermal Test	Bypass diode failures

Note: TCO is transparent conductive oxides

The accelerated tests need to be prioritized from both reliability (failure) and durability (degradation) perspectives. It is to be noted that the lifetime of PV modules may be limited either due to hard failure issues or to degradation issues (degradation beyond warranty limits).

Prioritization from Reliability (Failure) Perspective

The prioritization of accelerated tests may be based on the initial failures in the field or the wear-out failures in the field. The qualification testing deals with the initial failures in the field and the lifetime testing deals with wear-out failures in the field. The prioritization of lifetime accelerated stress tests needs to be done based on the failure and degradation sensitiveness of the technology to a specific set of environmental conditions. The specific set of environmental conditions could be hot-dry, hot-humid, and cold-dry (temperate). There is a great need to develop a database based on the climate-specific technology-sensitive wear-out failures in the old (10 to 30 years) power plants that have similar or identical construction characteristics as that of the current generation modules. Because no such database currently exists based on the wear-out field failures, it is not possible to identify and prioritize the accelerated stress tests relevant to field-specific wear-out failures at this stage of research.

As indicated later in this report, the objective of qualification testing is to identify major failure modes during the initial stage in the field without attempting to make any predictions about the product's life under normal use condition. Because the current qualification testing programs (IEC 61215 and IEC 61646) have been developed based on the recorded initial field failures, the qualification failure databases from different test laboratories could help prioritize the accelerated stress tests, which would allow the manufacturers to successfully pass the qualification testing and to introduce the product in the marketplace. Note that the prioritization of the accelerated tests for the lifetime testing should be based on the field-specific wear-out failures, whereas the prioritization of the accelerated tests for meeting the qualification testing requirements may be based on the qualification testing failure databases of various test laboratories (TamizhMani et al., 2012). As shown in Figure 32A, crystalline silicon technology is sensitive to the following top three accelerated

tests to meet the pass criteria of the IEC 61215 qualification testing standard (based on the testing of 1,111 modules of the most recent 2009-2011 designs): humidity freeze, thermal cycling, and DH. As shown in Figure 32B, these post-stress failures were identified using visual inspection, insulation test, and wet resistance failure criteria at the completion of each accelerated test of the qualification testing programs. (Note that the failure rate in Figure 32A may be lower than the sum of failure rates shown in Figure 32B due to the application of up to three pass criteria for each stress test).
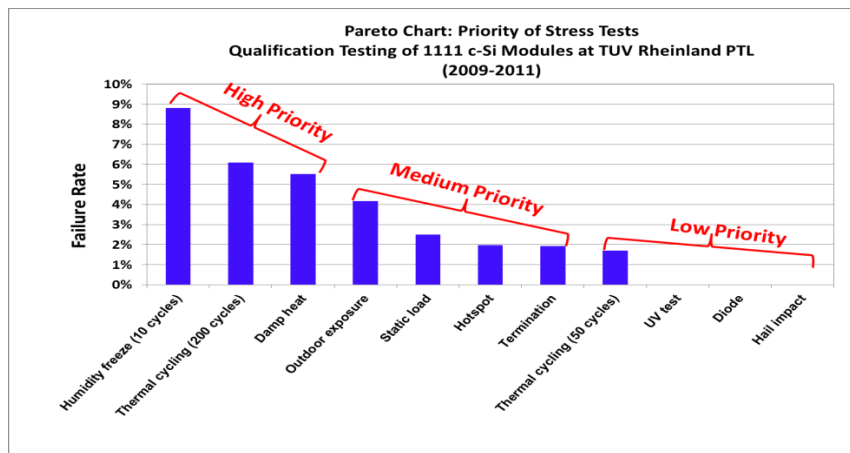
Figure 32A: Prioritization of accelerated stress tests for c-Si modules to meet the qualification testing standard of IEC 61215
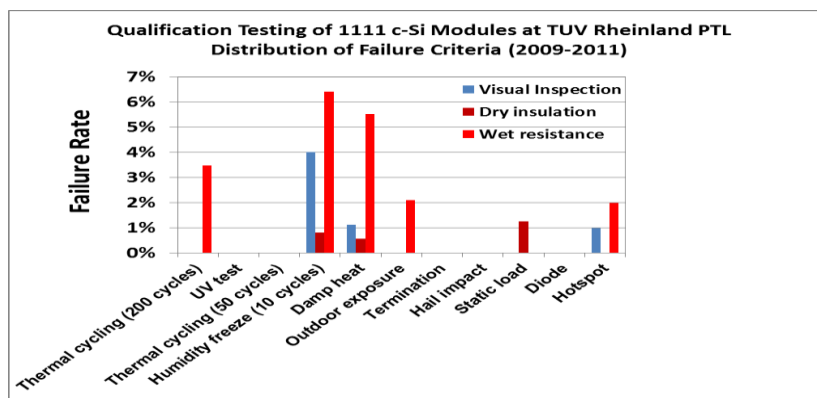
Figure 32B: Failure criteria (visual, dry, or wet) dictating the qualification failure rate for c-Si shown in Figure 32A

Figure 32: Prioritization of Accelerated Stress Tests for c-Si Modules to Meet the Qualification Testing Standard of IEC 61215 (TamizhMani et al., 2012)

As shown in Figure 33A, the thin-film technologies are sensitive to the following top

three accelerated tests to meet the pass criteria of the IEC 61646 qualification

testing standard (based on the testing of 272 modules of the most recent 2009-2011

designs): humidity freeze, DH, and light soaking. As shown in Figure 33B, these

post-stress failures were identified using visual inspection test, insulation test, and

wet resistance failure criteria at the completion of each accelerated test of the

qualification testing programs. All the other discussions presented above for the c-Si

technology apply to the thin-film technologies as well.
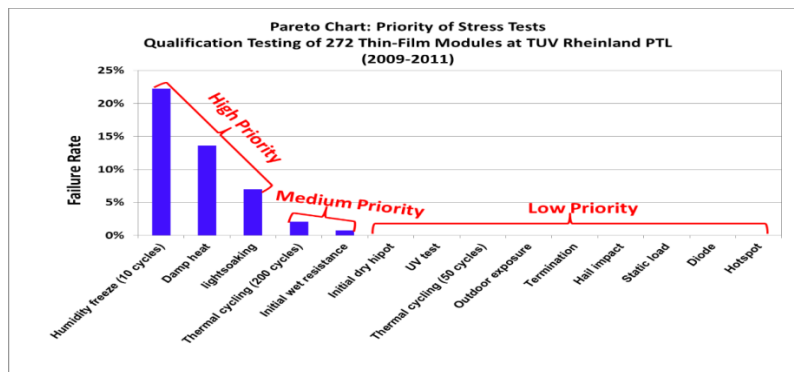
Figure 33A: Prioritization of accelerated stress tests for thin-film modules
to meet the qualification testing standard of IEC 61646
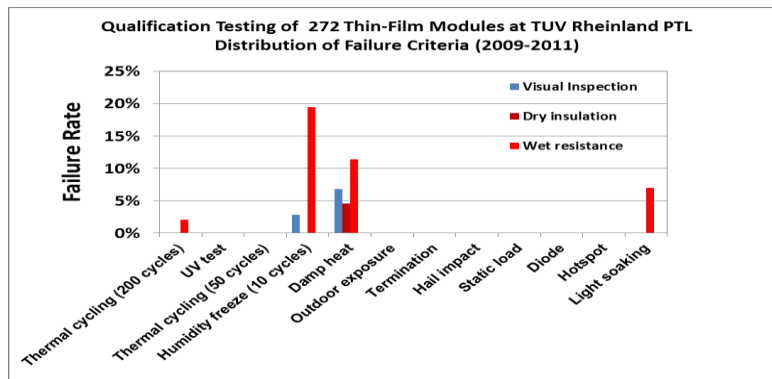
Figure 33B: Failure criteria (visual, dry, or wet) dictating the
qualification failure rate for thin-film shown in Figure 33A

Figure 33: Prioritization of Accelerated Stress Tests for Thin-Film Modules to Meet

the Qualification Testing Standard of IEC 61646 (TamizhMani et al., 2012)

Prioritization from Durability (Degradation) Perspective

As shown in Figure 34, the post-stress qualification failures rates (identified in Figure 32A above for c-Si) are dictated not only by visual inspection observations, insulation test, and wet resistance test failure criteria but also by the power degradation criteria at the completion of each accelerated test. In the qualification testing of c-Si modules, a power degradation limit of 5% from the initial measured power is used whereas in the lifetime testing, a power degradation limit of 20% may be used assuming 20%/20-year warranty limit. In the qualification testing of thin-film modules, a power degradation limit of 10% from the rated power is used, whereas in the lifetime testing, a power degradation limit may be determined based on the warranty limit. Because—at the completion of the qualification testing programs—none of the 272 thin-film modules showed less than 90% of its rated power, no plot corresponding to the qualification failure rate due to degradation limit is presented here.
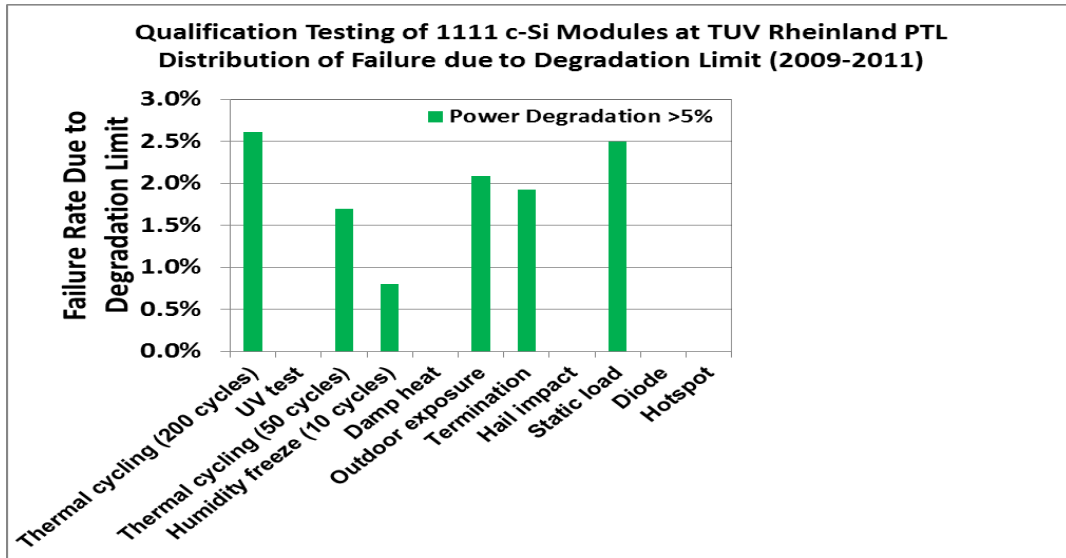
Figure 34: Degradation Limit Criterion Dictating the Qualification Failure Rate for c-Si Shown in Figure 32A (TamizhMani et al., 2012).

Pre- and Post-Characterization of Materials and Modules

The chemical, physical, thermal, and electrical properties of PV materials and devices used in a PV module dictate the overall quality, durability, and reliability, which in turn dictate the levelized cost of energy (LCOE, $/kWh). Understanding these properties before and after field installations and accelerated stress tests is very important to develop less expensive but more effective materials and devices. The materials will need to be characterized before and after HALT in environmental chambers and weathering (UV-temperature-humidity) chambers. Also, the old and existing materials will need to be evaluated before and after field installations.

As a minimum, the PV cell/module characterizations should include:

- visual inspection (see the visual inspection checklist provided in the Appendix A of this report),
- current-voltage measurements under various light conditions (it is the most important characterization for the failure and degradation evaluation and it is briefly discussed below),
- spectral response/quantum efficiency,
- electroluminescence, and
- infrared scanning.

The materials and package characterizations of PV modules may include:

- water vapor transmittance of backsheets,
- optical transmission for encapsulants and superstrates,
- bulk resistivity and dielectric withstand voltage for encapsulants and backsheets,
- compositions of polymeric and cell materials,
- phase change of polymeric materials,
- contaminations inside the materials and devices,

- UV-Vis spectrophotometric analysis of materials,

- Fourier transform infrared (FTIR) of materials,

- differential scanning calorimetry (DSC) of polymeric materials,

- thermogravimetric analysis of polymeric materials,

- chromatography of polymeric materials,

- dry and wet dielectric properties of packages,

- mechanical properties of materials using universal materials testers,

- scanning electron microscopy of materials and devices,

- optical microscopy of components and devices,

- Arrhenius analysis for activation energy determination,

- impedance analysis for activation overpotential determination,

- surface and bulk resistance testing of glass, encapsulant, and backsheet, and

- moisture ingress testing.

The current-voltage measurement is the most important characterization technique for the failure and degradation evaluation of PV modules and it is briefly discussed below. To detect various failure and degradation modes due to changes in the materials and/or cells in a PV module after the accelerated tests and field exposure, the current-voltage (I-V) curves can be analyzed in several different ways including (Wohlgemuth, 2011; TamizhMani, 2012):

- multiple shoulders in an I-V curve is an indication of cell mismatch;

- increase in slope of the horizontal part of I-V curve is an indication of decrease in shunt resistance;

- decrease in slope of the falling part of I-V curve is an indication of increase of series resistance;

- a drastic decrease in open-circuit voltage may be an indicator of activation of one or more bypass diodes in the module;

- a sharp break in the I-V curve is an indication of bypass diode activation;

- a decrease in short-circuit current may be an indicator of discoloration of encapsulant, AR coating, soiling, loss of surface passivation, loss of cell area via cracking and chipping;

- a decrease in open-circuit voltage may be an indicator of loss of cells from circuit, bypass diode shorting, cell junctions shunting, and loss of surface passivation;

- a decrease in fill factor may be an indicator of solder bond thermo-mechanical fatigue, metallization corrosion, solder bonds corrosion, interconnects corrosion, interconnect ribbons broken or partially broken, and cell junctions partially shunted; and

- a decrease in module efficiency and fill factor at low irradiance levels compared to high irradiance levels is a potential indicator of cell shunting issues, so characterizing the module at different irradiance and temperature levels as per IEC 61853-1 standard would be of great interest to identify the cell shunting issues.

The use of I-V characterization for the quality, durability, and reliability evaluation of an old array (26+ years in Phoenix, Arizona; hot-dry location) is illustratively explained in the plot shown in Figure 35 (Olakonu et al., 2014). Note that the short circuit current (I_{sc}) loss of about 30% in this figure, is primarily attributed to encapsulant browning, but this loss may also be due to a combination of other issues identified above. The I_{sc} loss due only to encapsulant discoloration or soiling can be identified and isolated by performing complementary quantum efficiency measurements.
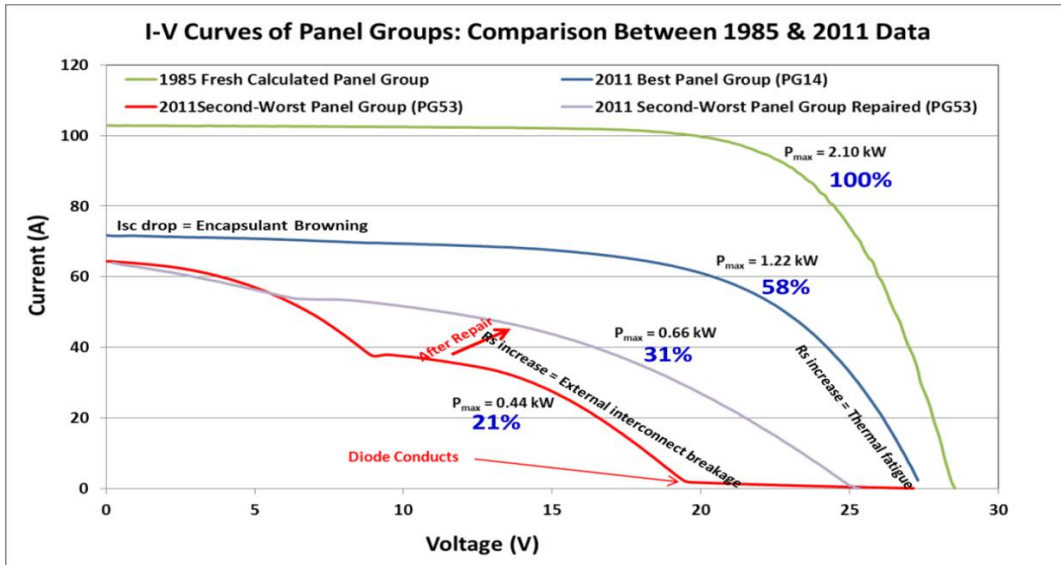
Figure 35: Use of I-V Characterization in Old PV Power Plants (Olakonu et al., 2014).

2.5   PV Reliability Prediction

The reliability of a product is defined as the ability/probability of operating or performing under certain conditions for a certain period of time. Because the degradation losses leading to failure occur in an uncertain manner during the prolonged life of PV modules, the reliability of PV modules should be framed in a dynamic and probabilistic context. Hence, the reliability of a PV module or system may be defined as the probability that the product will perform its specified function under specified (environmental) conditions throughout its specified life expectancy. AT requires extrapolation in the accelerating variable(s) and time. This implies critical importance of model choice. This section focuses on reliability modeling of PV modules. Modeling generally consists of analyzing the data to characterize the system or product, and then linking such characterization to a suitable mathematical formulation. Longrigg (1989) provides a three-step summary of photovoltaic reliability modeling, methodology, and data analysis: (1) break-down the product or system into its components and analyze the criticality of individual parts; (2) for

each system/product, subsystem, or component, collect and analyze either life test data or historical data on the failure rates; and (3) combine the results from (1) and (2) to obtain the reliability measure such as mean time between failure. Longrigg classifies the analysis as either statistical (operational reliability assessment from actual empirical data) or predictive (reliability estimation in the development stage from historical data).

Statistical analysis of PV module reliability data involves fitting the data to an empirical probability distribution, and then estimating the parameters of the distribution to derive the reliability characteristics such as failure rate, mean time to failure (MTTF), reliability function, etc. Murthy and Blishchke (2000) identify two approaches to modeling:

- In the "black-box" approach, the failure is modeled without consideration of the underlying mechanism. A product or component is either in a working or failed state. Typically, a component starts in its working state, and changes to a failed state after some time. Because the time to failure is uncertain, the appropriate mathematical formulation for modeling failure is a distribution function, such as exponential distribution, Weibull distribution, or lognormal distribution. This approach involves the empirical models (failure mechanism is unknown) to mathematically extrapolate the reliability characteristics from the accelerated condition to the actual use condition and the distribution models.

- In the "white-box" approach, the failure is characterized in terms of the underlying failure mechanism. Dasgupta and Pecht (1991) categorize failure mechanisms into (1) overstress failures (interfacial deadhesion, brittle fracture, elastic deformation, etc.) and (2) wear-out failures (corrosion, diffusion, creep, fatigue crack, etc.). They also provide an alternate categorization based on the nature of the stresses that trigger the

mechanism: mechanical failure, thermal failures, electrical failures, radiation failures, and chemical failures. Modeling of failure mechanisms involves the use of stochastic process formulations. This approach involves physical models (failure mechanism is known) to confidently extrapolate the reliability characteristics from accelerated condition to the actual use condition using physics/chemistry principles and the failure mechanism models. The types of reliability/durability data typically recorded for PV modules by the industry are degradation data; so understanding the degradation mechanisms is critical to the analysis. The "white-box" approach would be more appropriate, though difficult, for PV modules.

Accelerated Degradation Modeling

PV modules are usually highly reliable products. Reported field degradation rates for crystalline silicon modules are very small, averaging about 0.8% per year (Jordan & Kurtz, 2012). As such, Accelerated Degradation Test (ADT), which generates degradation data, rather than ALT (which generates life data), seems more appropriate. Yang (2009) describes the concept of ADT, the test method, and data analysis. Gorjian, et al. (2009) provide a good review of degradation models for reliability analysis. Three common types of stresses used in ADT include constant stress (either multiple or single constant-stress), step-stress, and cyclic stress. As noted by Yang (2009), most ADT use constant-stress test method because of the simplicity in data analysis and stress application.

PV module degradation data are usually obtained by measuring power output of n test samples each at time t_i, i=1, 2, … and presented as shown in Table 5.

Table 5: Degradation Data Recording Format

		Time tj				
		t1	t2	…	…	tm
Sample i	1	y1,1	y1,2	…	…	y1,m
	2	y2,1	y2,2	…	…	y2,m
	…	…	…	…	…	…
	…	…	…	…	…	…
	n	yn,1	yn,2	…	…	yn,m

y_{ij} represents the degradation measured on sample i at time tj. Data can be collected at any time on any sample, meaning the measurement times for samples u and v need not be equal and can be denoted as t_{uj} and t_{vk}

Vasquez and Rey-Stolle proposed a reliability-based model assuming normal distribution of module power output with the distribution parameters (mean and standard deviation) having a linear relationship with the time (Vazquez & Rey-Stolle, 2008). It is important to study the behavior of the power drop, rather than just the measured power.

As mentioned above, published studies of ADT applications for PV module reliability analysis mostly use multiple constant stresses. Xia, Wohlgemuth and Cunningham (2009) attempted to correlate the accelerated aging tests with the real field lifetime. They stressed 4-cell laminated mini-modules in UV, 85°C/85%RH, 85°C/95%RH, and 124°C/0.14MPa (20psi). The performance drops at these different aging conditions were monitored and compared. No inference was made to the used condition. Hacke, et. al (2012) use accelerated testing at three temperatures (50°, 60°, and 85°C) and 85% relative humidity to calculate the acceleration factors for crystalline silicon PV modules. Cuddihy (1986) used ADT from exposure to different levels of relative humidity and temperatures to study the lifetime predictions related to electrochemical corrosion in encapsulated PV modules.

Lee, Elmore, and Jones (2011) develop a statistical model for prediction of PV module life-time using step-stress accelerated degradation testing (SSADT). The degradation model is defined in two stages: (1) the degradation pattern is obtained from ADT; and (2) a physical model (such as Arrhenius and Eyring models) is defined.

2.6   Conclusion on Reliability Literature

Clearly, a major void in the PV industry today is a reliability protocol for predicting PV module lifetime in any environmental condition. It has been nearly 30 years since the LSA project ended, and the design/construction of PV modules has gone through a dramatic change since then. Yet no other systematic and comprehensive study on lifetime prediction of PV modules has been carried out.

A PV module lifetime prediction study would require designing accelerated tests to replicate observed field reliability issues. Although there is a pretty good confidence today that the accelerated tests to replicate known field failures have been identified, the major issue is that "we do not know how to test modules for a 25-year lifetime" (Wohlgemuth, 2011). This would require the ability to (1) objectively identify major degradation/failure mode(s) under a given climate from the multitude of field and lab observed failures; (2) determine appropriate levels of stress factors based on weather data analysis; and (3) select or design and conduct appropriate accelerated testing.

CHAPTER III

INVESTIGATION OF DOMINANT FAILURE MODE(S) FOR FIELD-AGED CRYSTALLINE

SILICON PV MODULES UNDER DESERT CLIMATIC CONDITIONS

3.1   Introduction

It has been 26 years since systematic studies on solar PV module lifetime prediction

were undertaken as part of the 11-year flat-plate solar array (FSA) project (Ross Jr.

and Smokler, 1986). This project resulted in the development of qualification testing

(Osterwald and McMahon, 2009). Since then, PV modules have gone through

significant changes in construction materials and design. Efforts (Osterwald &

McMahon, 2009; Osterwald, 2008; Kuhn & Funcell, 2005) have been made to adapt

some of the techniques developed to the current technologies, but they are too often

limited in scope and too reliant on empirical generalizations of previous results.

JPL's methodology to developing prediction model includes four major elements

(Ross Jr., 1984): Identification of key degradation mechanisms, establishment of

mechanism-specific reliability goals, quantification of mechanism parameter

dependencies, and development of degradation prediction methods. Few other

researchers have since proposed more elaborate methodologies. McMahon et al.

(2000) discusses a 5-step protocol to use accelerated environmental tests (AET) for

life-prediction: Identify and isolate all failure modes, design and perform AETs, use

appropriate statistical distributions to model specific failure rates, choose and apply

relevant acceleration models to transform failure rates, and develop a total module

failure rate as a composite of individual rates to allow service lifetime prediction for

each use condition. Quintana and Kurtz (2008) identify four elements as basis for

predictive model: field testing, failure mechanisms identification, failure analysis and

modeling, and accelerated testing.

A common element to these systematic approaches to PV module lifetime prediction

is identifying and ranking field failure modes/mechanisms. While myriad of studies

(Wohlgemuth et al., 2005; Wohlgemuth, 2003 & 2011; Wohlgemuth & Kurtz, 2011; Packard, et al., 2012; King, et al., 2000; Sandia, 1999; Sakamoto & Oshiro, 2005; Quintana et al., 2000; Meyer & Dyk, 2004) has been done and published on identifying field failure modes/mechanisms, determining the dominant mode(s) or mechanism(s) has received very little attention. JPL approach was to first identify what is perceived as the weakest link in a module construction; the anticipated failure modes for that link are then assumed dominant (Gaines, et al., 1977). The problem with such approach is its heavy reliance on engineering judgment. Another commonly used technique consists of carefully inspecting individual modules for major defects as defined in the international standards (IEC 61215, 2005; IEC 61730, 2004), and identifying the highest frequency of these defect(s). As exemplified in [9], this approach does not consider whether or not the observed "major defect" affects the performance output.

In this study, the FMEA/FMECA (failure mode and effect (criticality) analysis) technique is used in determining the dominant failure mode(s) of c-Si PV modules under the AZ hot and dry climatic condition. Conventionally, FMEA/FMECA approach is very subjective. It uses the risk priority number (RPN), which is a product of three parameters: severity of a failure (S), occurrence of the failure (O), and detection of the failure (D). The values for S, O, and D are subjectively assigned, based on qualitative analyses and engineering judgments. The main objective of this study was to move as far as possible from the traditionally subjective approach to a formal, objective, and data-driven determination of RPN.

Yang (2007) and Bowles (2003) discuss the deficiencies of RPN technique for prioritizing failure modes, which are due to that the values of RPN are not continuous and they may contain many duplicates. However, it shall be noted that these deficiencies are inherent to the RPN concept, rather than the methodology presented

in this paper. The aim of this study is to devise an approach for objectively

determining RPN, assuming it is the technique of choice to the analyst.

There are different types of FMEA/FMECA (system FMEA/FMECA, design

FMEA/FMECA, process FMEA/FMECA) that are used to address quality and reliability

aspects; including identifying, prioritizing, and eliminating potential failure causes

from system/product design or manufacturing process. This paper focuses on

prioritizing known failure modes from c-Si PV modules operating under specified

climatic conditions.

In the next section, we review the literature on FMEA/FMECA concepts, reliability of

PV modules under hot and dry climate, application of FMEA/FMECA in PV, and

decision trees in data mining concepts. The methodology used in this study is

described in section III; and the results of our investigation are presented and

discussed in section IV.

3.2   Concepts

FMEA/FMECA General Concept

The IEC 60812 standard (IEC 60812, 2006) defines the failure modes and effect

analysis (FMEA) as a systematic procedure for the analysis of a system to identify

the potential failure modes, their causes and effects on system performance. The

FMECA is an extension to the FMEA. Letter "C" indicates that the criticality (or

severity) of the various failure modes are considered and ranked. There are many

types of FMEA/FMECA, each of which may be conducted for many purposes. The

concept described here focuses on system FMEA/FMECA that would lead to a ranked

list of potential system failure modes.

The system design FMECA analysis process consists of two main steps: Preparation

of an FMECA worksheet and identification of the rating guidelines.

FMECA Worksheet

The major elements of an FMECA worksheet include:

Potential failure modes: There are many ways a component or system may fail. Identified failure modes depend on system components, environment, and past history of failures in similar systems.

Potential cause of the failure: For any given failure mode, there could be more than one cause. The cause or mechanism of a failure mode is the physical or chemical processes that cause an item to fail. The IEC standard points out that the identification and description of failure causes is not always necessary for all failure modes, rather, should be done on the basis of the failure effects and severity. The more severe the effects of failure modes, the more accurately failure causes should be identified and described.

Potential effects of the failure mode: This is the consequence of a system failure mode. A failure effect may be caused by one or more failure modes of one or more items. Warranty documents, field service data, and reliability data can be used to identify potential effects.

Current controls/fault detection: This identifies the way by which occurrence of failure is detected and the means by which the operator is made aware of the failure. It could be a procedure, test, design review, or an engineering analysis.

Rating Guidelines

There is no universal or standard rating guideline. In general, it can be qualitative or quantitative; with the numerical values from 1 to 5 or 1 to 10. The potential system deficiencies are ranked using the risk priority number (RPN), which is defined as:

$$RPN = S \times O \times D \tag{5}$$

S, O, and D are rating values respectively representing the severity of effect, occurrence, and detection.

Severity of effect (S):

This rating indicates the seriousness of the effect of the potential system failure mode. It is based on the worst effect of the failure mode. The severity is high for critical effects, and very low for non-critical effects. We reproduce in Table 6 below an example of qualitative severity classification from SEMATECH (1992):

Table 6: Severity Ranking Criteria (SEMATECH, 1992)

Rank	Description
10	Failure will cause non-system operation or non-compliance with government regulations
8 – 9	Failure will cause non-functionality of system
6 – 7	Failure will result in deterioration of part of system performance
3 – 5	Failure result in slight deterioration of part of system performance
1 – 2	No discernible effect

Occurrence (O)

This rating value corresponds to the estimated number of failures that could occur for a given cause over the operational life of the system. Failure modes are identified in terms of probability of occurrence, grouped into discrete levels. These levels establish the qualitative failure probability level. An example of frequency classification can be found in Rausand (2004). It is reproduced in Table 7 below.

Table 7: Occurrence Ranking Criteria (Rausand, 2004)

Rank	Frequency	Description
1	Very unlikely	Once per 1000 years or more seldom
2	Remote	Once per 100 years
3	Occasional	Once per 10 years

| 4 | Probable | Once per year |
| 5 | Frequent | Once per month or more often |

Detection (D)

This rating corresponds to the likelihood that the detection method or control will detect the failure before the system reaches the end-user. The detection ranking presented in Table 8 is extracted from (SEMATECH, 1992)

Table 8: Detection Ranking Criteria (SEMATECH, 1992)

Rank	Description
10	Very low (or zero) probability that the defect will be detected. Verification and/or controls will not or cannot detect the existence of a deficiency or defect.
8 – 9	Low probability that the defect will be detected. Verification and/or controls not likely to detect the existence of a deficiency or defect.
5 – 7	Moderate probability that the defect will be detected. Verification and/or controls are likely to detect the existence of a deficiency or defect.
3 – 4	High probability that the defect will be detected. Verification and/or controls have a good chance of detecting the existence of a deficiency or defect.
1 – 2	Very high probability that the defect will be detected. Verification and/or controls will almost certainly detect the existence of a deficiency or defect.

Concluding Notes on Rating Guidelines

Alternate evaluation criteria provides ranking on a 1 to 10 scale (IEC 60812, 2006; MIL-STD-1629A, 1980). As noted in IEC 60812 (2006), ratings numbers 6 and up

are usually very straightforward, whereas those below are very subjective. Also, MIL-STD-1629A standard (MIL-STD-1629A, 1980) indicates that the analysis requires an equal scale (i.e. 1 through 10 or 1 through 5) for both the severity and occurrence; otherwise, one category will hold more "weight" than the other in the criticality analysis.

Reliability of PV under Arizona Hot-Dry Climate

A crystalline silicon PV module is made by connecting individual cells. The typical construction is superstrate/encapsulant/cells/encapsulant/backsheet. Glass is the common choice for superstrate. Ethylene vinyl acetate (EVA) copolymer has been the dominant encapsulation material for crystalline silicon modules since it was introduced in the 1980s. Encapsulants are used as a mean to dissipate heat and to protect PV modules against harsh environmental conditions, including vibration, moisture, stresses, etc. Metal contacts are often attached on the top of solar cells to define a grid pattern called bus-bars. Tinned copper ribbons called tabs or interconnects are soldered to the bus bars at the front to form a series (S) or series-parallel (SP) arrangement of the cells. The cell arrangement is then sandwiched between two layers of encapsulants and laminated.

Failure and degradation mechanisms of PV modules are dictated by their design/construction and the field environment in which they operate. The design/construction of PV module has gone through significant changes since 1975 (Ross Jr., 2012). The design and components change include cell type (from mono-Si to poly-Si and mono-Si along with various thin-film technologies), superstrate (from silicone to glass), encapsulant (from silicone to EVA), substrate (from fiberglass board to polymeric backsheet), cell string (from one to multiple), interconnect between cells (from one to multiple) and bypass diode (from none to multiple).

88

The key field degradation mechanisms identified in the 70s and 80s for crystalline silicon PV modules are summarized in (Ross Jr., 1985). That paper indicates that the module encapsulation system and the circuit integrity are the area mostly susceptible to reliability issues. Issues identified related to encapsulated system include soiling, yellowing, delamination, and corrosion; and those related to circuit integrity include interconnect fatigue and solder joint failures. Cell cracking, metallization adherence, series resistance and durability of anti-reflective coatings were also identified as major issues.

The reliability issues associated with each component of the module construction were identified in the previous chapter. They are summarized in Table 9 below.

Table 9: Reliability Issues of Crystalline Silicon PV Modules

Module Component	Reliability issues
Superstrate	UV stability and light transmission of superstrate materials; Weatherability, compatibility with encapsulant, and strength of both superstrate and substrate; Thermal expansion coefficient.
Encapsulant	Photodegradation stability; Weatherablity; Sustained flexibility; Dielectric isolation; Light transmission and/or UV stability; Thermal conduction.
Cell and Interconnects	Corrosion and conductivity of cells interconnections; Ability to withstand thermal and wind loading and other environmental stresses for extended periods; Delicate attachment between interconnecting wire and the cell must withstand all environmental stresses;

	Vulnerability of PV cells to environmental hazards, including Wind, Dust, Temperature extremes, Humidity, and Oxygen.
Backsheet	Water vapor resistance; Dielectric isolation; Scratch resistance; Adherence to encapsulant.

There have been numerous recent studies on the reliability of field deployed PV modules operating under dry and hot climatic conditions. Tucker et al. (2006) evaluates EVA-based encapsulant modules deployed on a two-axis tracker in Tempe, Arizona for 9 years as part of validation experiments of photothermally-enhanced encapsulant formulations. Visual defects include encapsulant discoloration, corrosion behind junction box, backsheet discoloration, corrosion at the cell interconnects, and encapsulant delamination behind cell. The highest average Isc drop was 2.7%; and a set of 2 modules exhibiting only encapsulant discoloration showed an average power drop of 3.1%.

Tang et al. (2006) evaluated modules removed from a water-pumping array operated in the hot-desert climatic condition of Arizona for 27+ years. The most prominent visual defect found was the graying of the superstrate silicone with hair-thin cracks. No notable delamination of the superstrate and busbar corrosion was observed. A power drop from the initial manufacturer rating was found to be 1.08% per year.

Raghuraman et al. (2006) analyze the reliability 44 PV modules exposed in Mesa - Arizona for 2 to 7 years. Crystalline silicon modules showed an average performance drop of 0.45% per year; with no visual defect in 2-4 years of exposure.

Singh, Belmont, and Tamizhmani (2012) analyze the degradation of 1900 crystalline silicon modules operating in Tempe – Arizona for 12 – 18 years. They observed that

the degradation ranged from 0.6% to 2.5% per year depending on the manufacturer, with modules exhibiting hot spot defects degrading at a higher rate than others.

Berman, Biryukov, and Faiman (1995) evaluated a grid-connected photovoltaic system in the Negev desert of Israel and observed that the modules had turned yellow-brown after five years of operation.

Cronin et al. (2013) studied the degradation rates of 20 grid-tied PV systems installed in Tucson Arizona. Systems with crystalline silicon modules ranged from 2 to 5 years old. The degradation rates measured with two separate methods are ranged from -4.3 to 0.8 ±0.5-4.6%/year.

Kopp et al. (2012) evaluated grid-tied systems deployed in Tucson, Arizona for 2 to 12 years. For crystalline silicon modules, they found that 73% of the modules inspected exhibited browning, 77% showed cell discoloration, and 45% suffered delamination. No correlation could, however, be established between visual defects and performance degradation.

FMEA/FMECA Application on PV

Even though the FMEA/FMECA is the most widely used systematic reliability analysis technique across various industries such as aerospace, electromechanical, computers, semiconductor, medical device, automotive, etc., its application in the photovoltaic industry is relatively new. Catelani et al. (2011) uses the FMEA/FMECA to analyze and classify the major failure modes of PV modules. However, it follows the traditional qualitative analysis, making it extremely subjective. For instance, the failures observed on PV modules installed in a dry and hot climatic are different, in terms of modes, occurrence, and effects, to those observed, say, in a humid environment. The paper does not indicate how the listed failure modes were identified, and for which climatic condition(s) they applied. Sandia National

Laboratories use FMEA extensively during the design phase of PV systems (Collins, et al.). Clearly, their focus is on design FMEA (DFMEA).

Data Mining - Decision Trees

Data mining is becoming a matured method for information and knowledge discovery. Large and complex observational datasets, such as field failure data on thousands and thousands of PV modules, contain large amounts of hidden useful knowledge. Data mining techniques enable extraction of such knowledge. Gardner and Bieker (2000) shows how the data mining techniques can increase product yield and quality to the next higher level by quickly finding and solving tougher semiconductor manufacturing problems.

Data mining techniques are classified into four main tasks: classification, association, clustering, and sequence discovery. Classification is one of the most useful techniques. From Kantardzic (2011), classification is defined as a process of mapping data items into predefined groups or classes. It is often referred to as supervised learning because the classes are pre-determined before examining the data. Classification rules are derived based on the training data set.

Classification algorithms include decision trees-based algorithms, statistical-based algorithms such as Bayesian classification, distance-based algorithms such as K-nearest neighbors (KNN), and neural network-based algorithms. Decision Trees are the most popular and useful data mining models. They are generally very efficient and have good accuracy; however, their successful use depends on the quality of the data at hand. Areas of application include financial analysis, manufacturing and production.

A typical decision tree uses "divide and conquer" technique to construct tree in a top-down recursive manner (see Figure 36). The root (topmost node) and each internal node (non-leaf node) denote a test on an attribute. Each branch represents an

outcome of the test. Each Terminal Node (leaf node) holds a class label. Test attributes are selected based on a statistical measure. Attribute selection measures or splitting rules determine how the tuples at a given node are to be split. Three popular splitting rules are Information Gain, Gain Ratio, and Gini Index. The use of information gain is described in Appendix C (Han & Kamber, 2006). A decision tree-based algorithm reproduced from Dunham (2003) is presented in Appendix D.
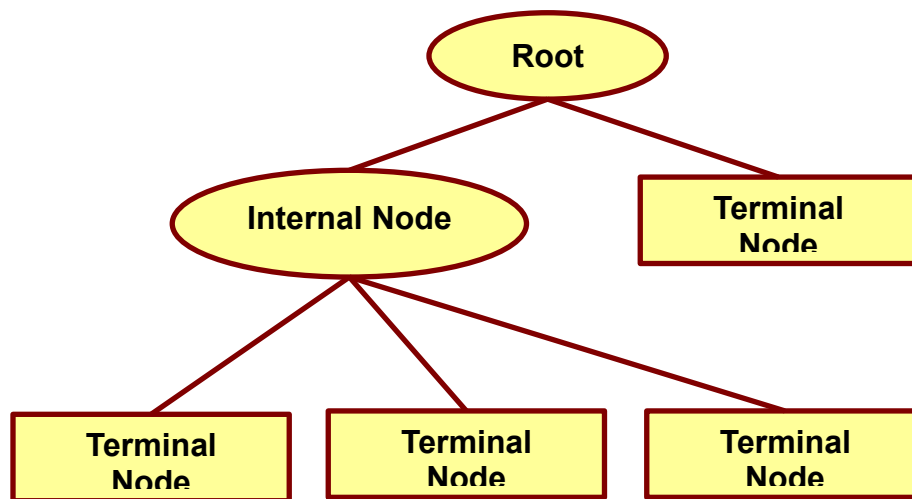
Figure 36: A Decision Tree Example

3.3   Methodology

In order to determine the dominant failure mode(s) under the targeted environment, the risk priority number (RPN) is used as the quantitative metric. As aforementioned, the RPN is defined as the product of severity S, which ranks the seriousness of the failure mode; the occurrence O, which ranks the frequency of the failure mode; and the detection D, ranking the likelihood the failure will be detected before it reaches the end-user. To minimize subjectivity, we will use a scale from 1 to 5 for all ranks. The classification found in the literature and presented in section II above is adapted as summarized in Table 10 below. The last column, "Score", indicates our ranking scales.

Table 10: Severity, Occurrence, and Detection Ratings Used in this Study

Severity (S)	Occurrence (O)	Detection (D)	Score
Defect will cause module not to work and become a safety hazard	Defect frequent: fp > 0.20	Controls will not or cannot detect the existence of a deficiency or defect: 0% chance	5
Module might be safe, but non- functional: Pmax drop > 20%	Defect probable: 0.10 < fp ≤ 0.20	Controls not likely to detect the existence of a deficiency or defect: chance < 50%	4
Module not meeting warranty requirement: Rd > 0.8% AND Pmax drop < 20%	Occasional probability of occurrence: 0.01 < fp ≤ 0.10	Controls are likely to detect the existence of a deficiency or defect: chance = 50%	3
Slight deterioration of part or system (long term concern): Rd < 0.8% AND Pmax drop < 20%	Remote probability of occurrence: 0.001 < fp ≤ 0.01	Controls have a good chance of detecting the existence of a deficiency or defect: chance > 50%	2
No effect on performance: Pmax drop ≤ 8%	A very unlikely probability of occurrence: fp ≤ 0.001	Controls will almost certainly detect the existence of a deficiency or defect: chance = 100%	1

Pmax = Maximum power output;
Rd = degradation rate;
fp = Failure mode probability per operating time;

It is necessary to explain the use of some of the classifying variables in the table above, such as Rd and Pmax drop.

Jordan and Kurtz (2012) conducted an extensive literature search on PV module degradation rates and found that for crystalline silicon modules, the average published degradation rate was 0.8% per year (see Figure 6). Since warranty period provided by manufacturers typically range from 20 to 30 years, if we assume an average of 25 years warranty, and an average of 0.8% drop from the initial power output each year, then we have 0.8*25 = 20% drop in performance throughout the warranty period. Thus, a PV module is generally considered non-functional when its maximum power output drops by more than 20% of the initial power while still under warranty.

We describe later in this section our decision trees approach to determining the effect of each defect on the performance drop, the failure mode probability (fp), and the chances for each existing control to detect individual defects.

Degradation Rate

Assuming a linear degradation, degradation rate (rd) was determined as followed:

$$degradation\ rate\ (r_d) = \frac{percentage\ of\ power\ drop\ (Pmdrop)}{years\ of\ operation\ (age)} \qquad (6)$$

The percentage of power drop is calculated was followed:

$$P_m drop = \frac{(Manufacturer\ rated\ Power - Present\ Day\ Power)}{Manufacturer\ rated\ Power} \times 100 \qquad (7)$$

As noted by Jordan and Kurtz (2012), calculating the degradation rate using the manufacturer's rated power as opposed to the baseline measurements can add significant error to the final value. This must be taken into consideration when reporting degradation rate. The approach above is deemed sufficient for the purpose of this study. Other studies related to the measurement of degradation rates include Cronin et al. (2013) and Davis et al. (2013).

Data Description

Our approach is a data-driven approach. Table 11 provides the descriptions of the PV systems evaluated. A total of 5,835 modules from 11 different PV systems installed in the Phoenix area were inspected. Performance measurements were collected on a lesser number of samples (2,538). Module ages ranged from 4 to 18 years.

Table 11: Description of Test Samples

Model Code	Technology	Fixed Tilt/Tracking	Construction	Number of Modules in the System	Exposed Years at the Time of Evaluation	Evaluation Year
A-18	mono-Si	Fixed latitude	G/P/FR	216	18	2009-2011
A-13	mono-Si	1-axis	G/P/FR	168	13	2009-2011
B	mono-Si	1-axis	G/P/FL	1153	13	2009-2011
C-12	poly-Si	1-axis	G/G/FR	177	12	2009-2011
C-4	poly-Si	1-axis	G/G/FR	39	4	2009-2011
D	poly-Si	1-axis	G/P/FR	48	12	2009-2011
E	mono-Si	1-axis	G/P/FR	50	12	2009-2011
F	mono-Si	1-axis	G/P/FR	120	12	2009-2011
G	mono-Si	1-axis	G/P/FR	2352	12	2012-2013
BRO1	mono-Si	Fixed horizontal	G/P/FL	756	16	2012-2013
BRO2	mono-Si	Fixed horizontal	G/P/FL	756	16	2012-2013
			G=Glass; P=Polymer	5835		
			FR=Framed			
			FL=Frameless			

In the next subsections, we discuss failure modes identification and our methodology to assign S, O, and D values to individual failure modes.

Failure Mode Identification

Procedures to capture failure modes/mechanisms as fully as possible on module designs have been evolving since the flat-plate solar array (FSA) project (Ross Jr., 1986). Techniques used for failure identification include careful monitoring/inspections of field application with statistically significant number of modules, observed failure data from qualification testing, and failure data from 0.5 to 2 years intermediate length tests with relevant stresses (Ross Jr., 1984). Wohlgemuth and the BP Solar reliability team published many studies on reliability issues with c-Si modules between 1994 and 2002 based on long term field installed

systems. Failure data were collected by analyzing commercial warranty returns, deploying and monitoring individual modules over long time periods, and monitoring the performance of PV systems over time (Wohlgemuth, et al., 2005; Wohlgemuth, 2003). In an analysis of nearly two millions field returns crystalline silicon modules, he identified corrosion, cell or interconnect breakage, junction box issues, output lead, and delamination as the primary field failures. From Wohlgemuth and Kurtz (2011) and Wohlgemuth (2011), the list of major failure modes associated with crystalline silicon modules includes broken interconnects, broken cells, corrosion, delamination, discoloration of encapsulant, solder bond failures, broken glass, hot spots, ground fault, junction box and module connection failures, structural failures, bypass diode failures, and arcing. These reported failures, combined to the checklist recently published by NREL (Packard, Wohlgemuth, and Kurtz, 2012), constitute our potential failure modes.

Table 12 below provides a summary of the field failure modes used as checklist in this study, the potential causes/mechanisms, the relevant qualification/safety tests for detecting the defects, and the relevant accelerated stress tests used as control before the product is shipped to the consumers.

Table 12: Checklist of Design Failure Modes and Relevant Qualification/Safety Tests (Wohlgemuth and Kurtz, 2011)

Field failures	Causes/Mechanisms	Characterization Test	Accelerated stress test per IEC61215 standard
Broken Interconnects	Thermal expansion and contraction, repeated mechanical stress	Visual inspection	200 Thermal Cycles (TC200) Mechanical load (ML)

			TC200
Broken cells	Mechanical stresses	Electroluminescence (EL)	ML
			Hail
Corrosion	Moisture induced corrosion of cell metallization	Visual inspection	1000h Damp heat (DH1000)
Delamination	Adhesive bond sensitive to UV or contamination from the material	Visual inspection	DH1000 Humidity freeze 10 cycles (HF10) Ultra-violet (UV)
Encapsulant discoloration	Heat and UV	Visual inspection	UV
Solder bond failures	Stresses induced by thermal cycling or vibration	Visual inspection	TC 200 ML
Hot spots	Operating current > Isc	Infra-red scan (IR)	Hot spot test (HS)
Bypass diode failures		OC diode inspections with handheld device	HS Diode test
Backsheet		Visual inspection	UV

Determining the Occurrence of Failure

There are three steps involved in determining the occurrence of defects:

(1) Each module is carefully inspected against a checklist of potential defects, similar

to that in (Packard, Wohlgemuth, and Kurtz, 2012). Inspections are carried out

visually, with an infrared (IR) camera, and in some cases with electroluminescence

(EL). The IR scanning enables identifying hot spots. A Fluke infrared camera was used to scan the modules. The EL was used to identify (micro)-cracks in the cells and inactive portions of the cells. Our EL setup uses CoolSamBa Camera from Sensovation. Examples of an IR scan and an EL imaging are shown in Figure 37. Solder bond failures were derived from series resistance (Rs) estimations. Key contributors to Rs include solder bonds, emitter and based regions, cell metallization, and busbars (Noel, et al., 1978; Dyk & Meyer, 2004; Meier, et al., 2006). Meier et al. (2006) shows that more than 70% of Rs is dominated by the solder bonds component. This allows us to assume that an increase in series resistance mostly reflects solder bond defects. An Rs increase of more than 1.5 times the initial value was assumed to indicate a solder bond defect. The Rs of each module was estimated from the performance data using the empirical expression from Dobos (2012):

$$R_S = C_S \frac{V_{oc} - V_{mp}}{I_{mp}} \tag{8}$$

where $C_S = 0.32$ for mono-crystalline silicon and 0.34 for poly-crystalline silicon modules.
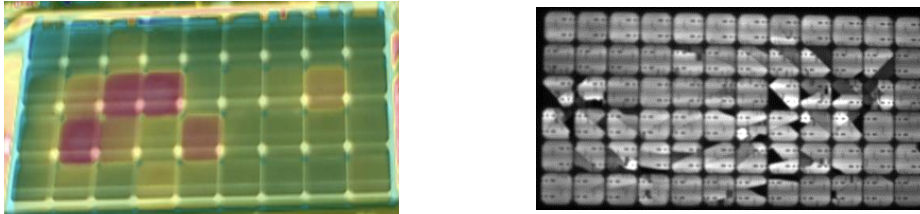
Figure 37: Examples of IR Scan (Left) and EL Image (Right)

(2) The cumulative number of component failures per 1000 (CNF/1000) over the operating time of each failure mode is then computed as followed:

$$CNF/1000 = \frac{(cumulative \ \% \ defects)/10}{cumulative \ operating \ time} = \frac{\sum_{systems}(\% \ defects)/10}{\sum_{system}(operating \ time)} \tag{9}$$

where operating time is in Years.

(3) Occurrence or frequency ratings are assigned to each failure mode based on Table 10, generated using the guidelines presented in section II of this chapter.

Potential Causes/Mechanisms of the Defects and Existing Control Mechanisms

Descriptions of destructive and non-destructive techniques to evaluate the degradation/failure mechanisms of long-term field-exposed modules can be found in (Ross Jr., 1985; Tucker et al., 2006; Tang et al., 2006; Raghuraman et al., 2006; Singh et al., 2012; and Catelani et al., 2011).

Design qualification and safety standards (IEC 61215, 2005; IEC 61730, 2004) represent the main controls for uncovering defects before new designs reach the customers. They help identify design, materials, and process flaws that are likely to lead to premature failure (infant mortality) (Wohlgemuth and Kurtz, 2011). The qualification and safety testing involves a set of well-defined accelerated stress tests (irradiation, environmental, mechanical and electrical) with strict pass/fail criteria based on extended functionality/performance, minimum safety/insulation, and detailed visual requirements. Wohlgemuth and Kurtz (2011) and Wohlgemuth (2011) discuss the accelerated stress tests designed to induce known field failure modes (see Table 12).

Determining the Likelihood of Detecting Failure Modes

Detection ratings are assigned based on the guidelines presented in section II and summarized in Table 13. Question is how do we quantify the likelihood of detection?

Table 13: Detection Assignment

Detect	Likelihood (%)	Rating
Controls cannot detect defect	0 - 5%	5
Controls not likely to detect defect	< 50%	4

Controls likely to detect defect	50 - 50	3
Controls have good chance of detecting defect	> 50%	2
Controls will almost certainly detect defect	95 - 100%	1

In his tutorial, Wohlgemuth (2011) discusses the ability of each stress test to effectively induce relevant field failure modes. His verdict is summarized in Table 14. TamizhMani et al. (2008) has been conducting a failure analyses on the design qualification testing of PV modules since 1997. Data for crystalline silicon modules is shown in Figure 38. We look at the data as a way to validate Wohlgemuth's conclusions.

It should be pointed out that most PV systems evaluated under this study are at least 10 years old, meaning the PV modules were produced before 2005. Also, the relevant stresses for the applicable climatic condition of this study are thermal cycling (heat) and ultraviolet radiation (UV). From Fig. 38, less than 5% of the modules were failing in TC200, and no failure was observed in UV test. However, field observations show a high number of encapsulant discoloration defects, which are results of heat and UV (see Table 12). This is in agreement with Wohlgemuth's verdict.
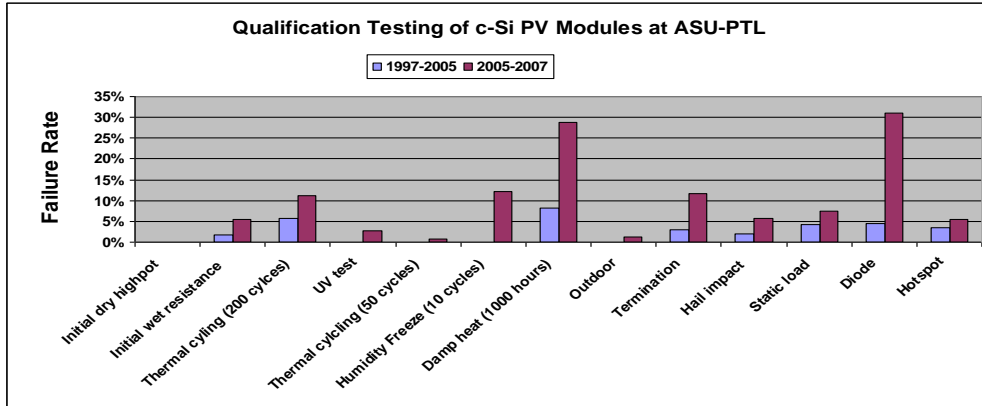
Figure 38: Failure Rate Comparison of c-Si Modules from 1997 to 2007

Table 14: The Likelihood that Stress Tests Induce Relevant Failure Modes

(Wohlgemuth, 2011)

Stress tests	Verdict	Chances of duplicating the relevant failure
TC200	No	5%
HF10	Yes	95%
DH1000	Unclear	50%
ML	No for components of circuit	5%
Hail	Yes	95%
Diode	OK for thermal stress	95%
HS	Probably	50%
UV	Absolutely NO	5%

The last column of Table 14 above shows the chances, in percentage, for the given stress test to duplicate the relevant failure mode, based on the verdict. We will assume a 5% risk level. Thus, when the stress is certain to induce the relevant failures/defects, a 95% chances is assigned; when it might, we assign 50% chance; and when it would absolutely not, 5% chance is assigned.

Denote by $P(X_i)$ the chance that a stress test i can induce a relevant failure mode.

Let $i = 1, 2, \ldots, s$ the possible stress tests that can be used to duplicate a given failure mode.

The likelihood that a failure mode can be duplicated is given by

$$P(\cup_{i=1}^{s} X_i) = 1 - \prod_{i=1}^{s}[1 - P\{X_i\}] \tag{10}$$

Determining Severity: Effects of Defects on Module Performance

Table 15 below depicts our approach to quantifying the severity. It is based on the description provided in Table 10 at the beginning of this section.

The modules evaluated were all 20 years old or less. So we consider two categories: Those in the infant stage (less than 10 years of field operation) and those that have been in the field for over 10 years.

Table 15: Severity Assignment

Degradation Rate (Rd)	% of Pmax drop	Age of Module	Severity
Rd ≤ 0.8%	Pmdrop≤ 8%	-	1
Rd ≤ 0.8%	8% < Pmdrop ≤ 20%	-	2
Rd >0.8%	Pmdrop ≤ 20%	-	3
Rd >0.8%	Pmdrop >20%	10 < age ≤ 20 years	4
Rd >0.8%	Pmdrop >20%	Age ≤ 10 years	5

Data mining techniques were used to identify defects corresponding to each severity. Specifically, a decision tree-based algorithm (Dunham, 2003) was used on a dataset containing 2,538 tuples. Each tuple represents inspection and performance data on an individual field-aged PV module. The data consists of:

Percentage of power drop (Pmdrop): This is the module's output power loss, in percentage, relative to the initial power output. This attribute is grouped into three

categories: category C1 consisting of modules with output power loss less or equal to 8%; category C2 consisting of modules with output power loss greater than 8% but less or equal to 20%; and category C3 consisting of modules with output power loss greater than 20%.

Degradation rate (Rd): Ratio of power drop (in percentage) by the age of the powerplant or PV system. This quantity is necessary for determining whether or not the module is meeting warranty requirements. Rd = 0.8% represents the warranty limit. Thus, those failing to meet warranty requirements will have Rd > 0.8. Module's age represents the length of time the module has been operating in the field, up to when the system was evaluated.

Failure modes or defects: Each failure mode has a "Y" (Yes) or "N" (No) outcome. A "Y" indicates that the associated failure mode or defect was observed on the module during the inspection. The potential failure modes are: Encapsulant discoloration, Broken or chipped cells, Solder bond failure, Delamination, Metallization discoloration, Hot spots, Backsheet warping or detaching, Cell discoloration, Broken interconnect, and Burn through backsheet.

Recall from Table 15 above that the severity assignment is based on Rd, Pmdrop, and age. Thus, these attributes were replaced by the severity attribute. The decision tree is to classify the degradation severity of a PV module based on its observed defects.

A data set is full of randomness or uncertainties due to interactions among attributes (some failure modes may lead to others), outliers, etc. The amount of information related to each attribute (failure mode) is associated with the probability of occurrence. The entropy concept, which measures the amount of uncertainty or randomness in a set of data, is used to quantify such information. The data set is then iteratively partition into subsets where all elements in each final subset belong to the same class. The basic strategy is to choose splitting attributes with the highest

info gain first; a gain being defined as the difference between how much info is needed to make a correct classification before the split versus how much info is needed after the split.

The inspection data from the 2,538 tested modules listed in Table 11 are used as the training data for building the decision tree. Using the decision tree, the effect of each defect (failure mode) on the power degradation of PV modules can be computed. In summary, the characteristics of the algorithm are as followed:

❖ Inputs:

  ▪ Data partition, D: Field inspection data on 2,560 PV modules.

  ▪ Attribute_list: Checklist of possible defects (an outcome of "Y" indicates that the defect was observed); and Severity assignment I, II, III, IV, or V (see Table 15).

  ▪ Attribute_selection_method: "Info Gain" splitting rule. This is the rule used to decide, at each node, which attribute to select.

❖ Outputs: Decision Tree

❖ Outcome: Severity values determination for a set of failure modes.

The decision tree helps partition failure modes into classes. For example, the tree in Appendix E shows that the subset (solder bond, encapsulant discoloration, delamination) belongs to severity class 4; and the subset (Backsheet warping, hot spot) belongs to severity class 3.   Severities of individual failure modes are assigned by computing the marginal effect of each failure mode.

Let M_i be a failure mode node at a particular position i in the decision tree. Denote M_i (Y) the branch with "Y" outcome and $M_j(N)$ the branch with "N" outcome. Let $n_i(Y)$ and $n_j(N)$ be the number of associated terminal nodes, and $S_i(Y)$ and $S_j(N)$ be the sum of associated severity values. The marginal effect of failure mode M, denoted by ΔM, is obtained as:

$$\Delta M = \frac{\sum_i S_i(Y)}{\sum_i n_i(Y)} - \frac{\sum_j S_j(N)}{\sum_j n_j(N)} \qquad\qquad (11)$$

Then, the severity of individual failure mode is determined from their marginal effect as followed:

If Marginal effect, assign severity value

ΔM   of

ΔM > 1   5

0.75 < ΔM ≤ 1   4

0.50 < ΔM ≤ 0.75 3

0.25 < ΔM ≤ 0.50 2

ΔM ≤ 0.25   1

3.4 Results and Discussions

The results for occurrence, detection, and severity ratings are shown in Table 16, Table 17, and Table 18 respectively. Weka 3.6.8 software (1999-2012) was used to build the decision tree. The decision tree output for ID3 is shown in Appendix C. The ID3 technique is the basic divide-and-conquer decision tree algorithm that uses information gain as splitting criteria. It was chosen because it does not apply any pruning procedure. While pruning might improve the performance of the tree, it might result in a loss of needed information. For example, a subtree classifying the failure mode "hot spot" could end up being removed to achieve better performance for the overall tree.

Because of the size of the dataset, the created tree may overfit. So the accuracy of the classification was evaluated by cross-validation (see Appendix F). The percentage of tuples placed in the correct class was determined to be 73%, and nearly 27% of tuples were incorrectly classified out of the 2538 tuples. Severity level 3 turns out to have the highest true positive (TP) and false positive (FP) rates of 0.96 and 0.58,

respectively. A tuple ti is said to be TP if it is correctly predicted to be in a certain class, while a FP indicates an incorrect class prediction.

Table 19 summarizes the SOD values and computes the RPN. Figure 39 provides a graphical representation of the defects ranked by their RPN values. It can be observed that solder bond failures and encapsulant discoloration are dominant modes under the hot and dry desert climatic condition. Backsheet warping or detaching seems to be significant as well. However, this was mostly observed at only one site where the modules were all frameless.

It shall be noted that the diode failure was not considered in the severity rating for two reasons: (1) Modules with open-circuited diodes were removed from the severity analysis as the power output could not be obtained; and (2) OC diode failures were not seen as a cause for intrinsic PV degradation.

The solder bond failures discussed in this paper reflects the relative increases of series resistance. According to King et al. (2000, 1999), gradual increase in the series resistance may result in system power drop in the order of 0.5%/year. Solder bond failure or series resistance increase is typically caused by mechanical influences of daily thermal cycling. Thermal expansion and contraction cause the solder bond to become more brittle and dissociate into large grains of tin and lead (King et al., 2000; Sandia, 1999). Thus, the mechanism related to this mode is a thermo-mechanical fatigue.

The exposed surface (superstrate) of modules with encapsulant discoloration show light yellow, yellow brown, or dark brown color. The Ethylene vinyl acetate (EVA) copolymer is the most widely used encapsulant material in crystalline silicon PV modules since mid-1980s. All the modules evaluated under this study were EVA-based modules. The primary purpose of the encapsulant is to provide structural support, electrical and physical isolation, and high optical transmittance for the solar cell circuits.

There is a rich literature on discoloration of EVA, its causes and mechanisms. One school of thoughts, led by Pern and Czanderna (Pern and Czanderna, 1992; Pern, 1997), advocates that the main cause for discoloration of EVA of field-weathered modules is the reduction of ultraviolet absorber (UVA) concentration, the increase of gel content, and the formation of acetic acid. Holley et al. (1994), Agro et al. (1994), Holley and Agro (1998), and Klemchuk et al. (1997) countered that the fundamental mechanisms leading to yellowing of earlier EVA encapsulants was due to interaction between the additives in the encapsulant formulation, rather than degradation of the polymeric EVA molecules.

Whatever the cause of EVA discoloration, the photothermal degradation mechanism involves two primary factors: UV exposure and heating. This indicates that encapsulant discoloration is expected to prevail in hot dry climates like Phoenix – Arizona with high solar UV insolation and elevated temperature.

The discoloration of EVA (and other concomitant reactions from the degradation products) reduces the optical transmission, power output, and service life of PV modules. As reported in (Tang et al., 2006; Raghuraman et al., 2006; Singh et al., 2012), the degradation rate of PV modules installed in Phoenix - Arizona varies from 0.6%/year to 2.5%/year; however, it is unknown how much can be attributed to EVA discoloration. Peike et al. (2011) points out that the aging process of EVA degradation under the influence of heat, humidity, and UV is still not fully understood.

Table 16: Occurrence Values of Failure Modes

MODEL ID	No. of Modules	Years Fielded	Percent of Defects (%)								
			Broken Cells	Encapsulant delamination	Encapsulant discoloration	Backsheet Warping or Detaching	Burn through Backsheet	Metallization or Busbar discoloration	Solder failure	HotSpots	Diode failure
A-13	168	13.3			100.000				87.3333333	1.190	
A-18	216	18		1.38888889	100.000				80.7291667		
B	1155	13.3		0.173	99.827	54.545			7.606	0.606	
D	48	11.7			77.083				2.564	6.250	
E	50	11.7				66.000					
F	120	11.7				1.667	1.6666667	18.333333	81.25	3.333	
AF	2352	12		9.226	4.039	0.510	1.616	29.337	23.5880399	1.913	8.638
C12	216	11.7	23.61111111	33.796	0.463	0.463		0.926	1.031	11.111	
Cumulative	4325	103.4	23.61111111	44.5845358	381.412252	123.1853	3.2823129	48.595994	284.101834	24.40424655	8.637874
CNF/1000			2.361111111	4.45845358	38.1412252	12.31853	0.3282313	4.8595994	28.4101834	2.440424655	0.863787
CNF/1000 per op. time			2.28E-02	4.31E-02	3.69E-01	1.19E-01	3.17E-03	4.70E-02	2.75E-01	2.36E-02	3.66E-02
Occurrence Score			*3*	*3*	*5*	*4*	*2*	*3*	*5*	*3*	*2*

Table 17: Detection Values of Failure Modes

	Broken Cells			Encapsulant delamination			Encapsulant discoloration	Backsheet Warping or Detaching	Burn through Backsheet	Metallization or Busbar discoloration	Solder failure		HotSpots	Diode Failure	
Controls	TC	ML	Hail	DH	HF	UV	UV	UV	HS	DH	TC	ML	HS	HS	Diode
P(Xi)	0.05	0.05	0.95	0.50	0.95	0.05	0.05	0.05	0.50	0.50	0.05	0.05	0.50	0.50	0.95
1-P(Xi)	0.95	0.95	0.05	0.50	0.05	0.95	0.95	0.95	0.50	0.50	0.95	0.95	0.50	0.50	0.05
Π[1-P(Xi)]	0.045125			0.02375			0.95	0.95	0.50	0.50	0.9025		0.50	0.025	
Likelihood of detection (%)	95			97.6			5	5	50	50	9.8		50	97.5	
Detection	*1*			*1*			*5*	*5*	*3*	*3*	*4*		*3*	*1*	

Table 18: Severity Values of Failure Modes

	Broken Cells	Encapsulant delamination	Encapsulant discoloration	Backsheet Warping or Detaching	Burn through Backsheet	Metallization or Busbar discoloration	Solder failure	HotSpots	Diode Failure
Marginal effect	-0.857	-0.373	0.6667	0.5294	0	0.7273	1.25	0.2857	-
Severity Rating	1	1	3	3	1	3	5	2	1

Table 19: RPN Values

	Broken Cells	Encapsulant delamination	Encapsulant discoloration	Backsheet Warping or Detaching	Burn through Backsheet	Metallization or Busbar discoloration	Solder bond failure	HotSpots	Diode Failure
Occurrence Rating	3	3	5	4	2	3	5	3	2
Detection Rating	1	1	5	5	3	3	4	3	1
Severity Rating	1	1	3	3	1	3	5	2	1
RPN	3	3	75	60	6	27	100	18	2
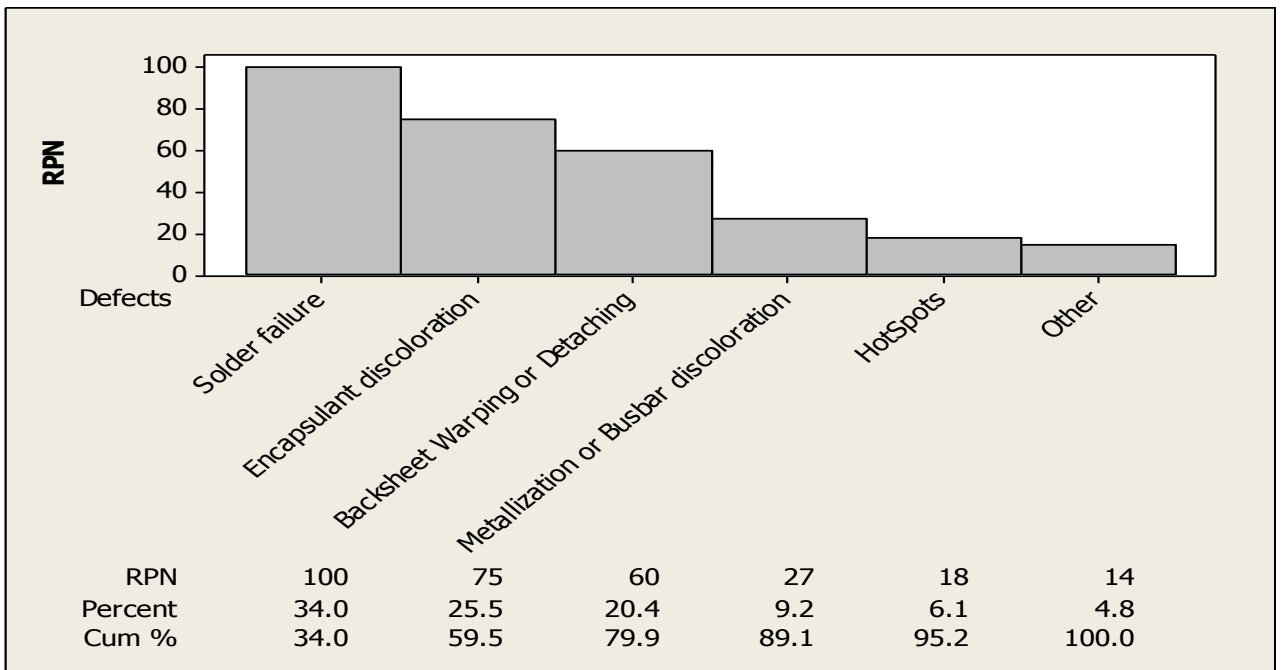
Figure 39: RPN vs. Failure Modes

3.5   Conclusions

We have developed a procedure for prioritizing failure modes using FMEA/FMECA and data mining (decision trees) techniques. Conventionally, FMEA/FMECA approach would heavily rely on engineering judgment, making values assigned to parameters very subjective. The approach presented in this paper relies on quantitative measures and sizable datasets. It is determined that solder bonds failures and encapsulant discoloration are dominant modes under the hot and dry desert climatic condition of Phoenix, Arizona.

CHAPTER IV

INVESTIGATION OF ENVIRONMENTAL FACTORS AFFECTING THE PV MODULE

DEGRADATION

4.1   Introduction

The Flat-Plate Solar Array (FSA) project (1975-1986), funded by the US Department

of Energy and managed by the Jet Propulsion Laboratory (JPL), laid the foundation

for Photovoltaic Reliability Research (PRR). That work outlined a closed-loop

development process approach that encompasses developing design requirements,

module laboratory testing, module production, application experiments, failure data

acquisition, and failure analysis. Three key environmental factors were identified:

temperature, humidity and UV intensity. A discrete environmental cell approach has

been proposed to integrate the environmental impact into the lifetime prediction of

solar modules (Kolyer et al., 2008). More recently, Chen and Meeker (2008)

discussed the time series modeling of degradation due to outdoor weathering. They

used the fitted model of the time series to estimate the future distribution of

cumulative degradation over a period of time and to compute reliability measures

such as the probability of failure. Monroe and Pan (2009) made the connection of the

stochastic weathering condition to an acceleration factor on annual basis, so the

lifetime prediction can be made on an annual scale. More interestingly, they showed

that the outdoor acceleration factors at various global locations are dramatically

different; therefore, products designed to target a local market should take a close

consideration of its local climate condition.

Motivation

There are two general motivations behind this study. First, for outdoor products

environmental factors are the important sources of variability to degradation data;

thus adding the information of environmental factors into the degradation model will

provide more accurate inferences or predictions of the degradation process. Second, when accelerated life testing is designed for either product qualification or product reliability prediction, it is expected that the test can produce the same failure modes as happened in the field; thus, the testing condition is better to mimic the field use condition with proper acceleration factors.

Outline of our Approach

In this chapter, we will investigate a practical approach to weather modeling and its usage in PV module degradation analysis. We have analyzed the performance data of one PV module collected over a long time of period (approximately 11 years). These data will be used to demonstrate the methodology to be developed in this study. Our approach includes the following steps:

- Time series modeling of outdoor temperature;
- The regression analysis of PV power output degradation over 11 years with a covariate of maximum ambient temperature ;
- Model-based lifetime prediction of outdoor solar panel systems;
- Validation by real data;

4.2   Model Development

Data and Notations

The data were collected from PV modules installed outdoor in Mesa, Arizona since 1998. They are mounted open-rack, open-circuit, and latitude tilted as shown on Figure 40. A reference cell is mounted on the same plane to obtain global irradiance. A temperature sensor attached on the back of the module provides the backskin temperature. The maximum power output of a module is derived from an electrical performance test. The measurements were supposed to be carried out every quarter, but often some measurements were missed. The performance data are translated

from actual conditions to standard test conditions (STC) using linear regression. STC refers to 1000 W/m^2 irradiance, 25°C cell temperature, and AM1.5G spectrum.

Figure 40: PV Panels in the Field Test

In general, the data can be denoted by $\{t, \mathbf{x}(t), k, y(k)\}$, where t and k are observation times for environmental factors (inputs) and performance measure (output), respectively. The inputs, $\mathbf{x}(t)$, are multivariate time series; while the response is denoted by $y(k)$, which is the degradation measure. In this study, we use ambient temperature only as the input variable and the degradation measure is the percentage of power output as its initial measurement. Note that the time indices for input and output are different, because environmental factors and product performance are in general measured at different frequency. For example, in our dataset we have monthly temperature data, but quarterly degradation data.

Degradation Model

In Based on the JPL's recommendation, the parametric model of PV panel power output degradation is given by

$$ln\left(\frac{100}{R}\right) = bt^a \tag{12}$$

where R is the power output percentage comparing to the initial output; parameter a is associated with the material's natural lifetime; parameter b can be regarded as an

acceleration factor that expand or compress the product's life span due to environmental stresses. Therefore, parameter b is a function of stress factors. When the stress is a stochastic process, $b(s(t))$ is the instantaneous acceleration factor at the time t and the instantaneous degradation becomes

$$d \ln\left(\frac{100}{R}\right)/dt = b(s(t))at^{a-1} \tag{13}$$

The cumulative degradation over the time period k is, thus,

$$\ln\left(\frac{100}{R}\right) = \int_0^k b(s(t))at^{a-1}dt \tag{14}$$

In general, the function $b(s)$ is determined by the physical or chemical kinetic model of specific degradation mechanism and the stochastic stress process $s(t)$ can be modeled by a time series. The integration is difficult to solve. Instead, we may approximate it using an average acceleration factor. Let k be the time of degradation measurement, then,

$$\ln\left(\frac{100}{R(k)}\right) = \bar{b}k^a \tag{15}$$

And

$$\bar{b} = \frac{1}{k}\int_0^k b(s(t))dt \tag{16}$$

Log-linear function is often used to model acceleration factor. For example, Arrhenius function is common for modeling the effect of static temperature and this function can be transformed to a log-linear function on the inverse of absolute temperature (in degree Kelvin), i.e.,

$$\ln(b) = c_0 + c_1 s(t) \tag{17}$$

where $s(t) = \frac{1}{T(t)}$ is the natural temperature stress level and it is a function of time. Combining Equations (15)-(17), we have

$$\ln\left(-\ln\frac{R(k)}{100}\right) = \ln\bar{b} + a\ln k = c_0 + c_1\frac{1}{k}\int_0^k s(t)dt + a\ln k = c_0 + c_1\bar{s}(k) + a\ln k \tag{18}$$

We can apply the least square method to obtain the values of parameters a, c_0 and c_1.

4.3   Data Analysis

Time Series Model of Temperature Data

The temperature data were collected on the site of the solar panel testing field. We treat the maximum ambient temperature in each month as an environmental stress factor. The reason of selecting this environmental factor will be elaborated later. Figure 41 plots the monthly maximum temperature. One can see that cycling pattern over years, as well as a slightly increasing trend. Therefore, a Holt-Winters model with additive seasonality is selected to model this time series.
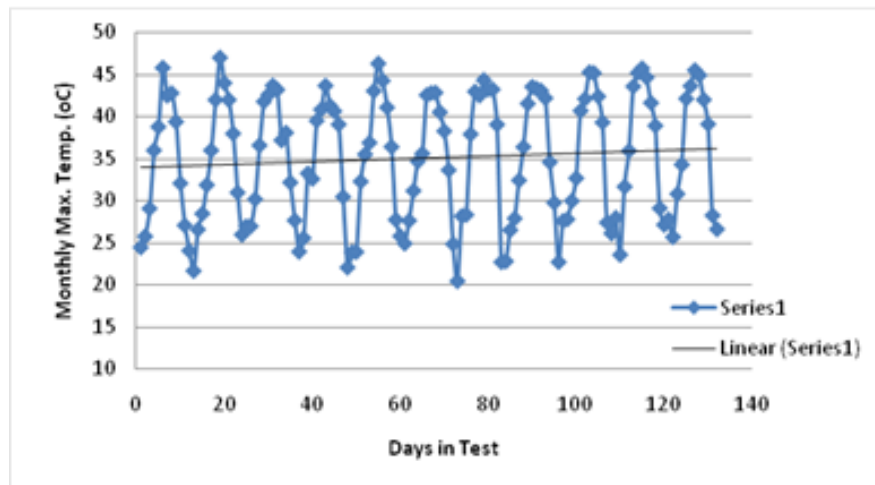
Figure 41: Plot of Ambient Temperature Data

The Holt-Winters model is a type of classical time series models for data exhibiting both trend and cycle. It has three components – level, trend and seasonality, and each component is modeled by an exponential smoothing function. After fitting the Holt-Winters model to our temperature series, it is found that the series is best described by the following equations:

$$Temp(t) = Level(t) + t \times Trend(t) + Season(t) \tag{19}$$

$$Level(t) = \alpha(Temp(t) - Season(t-p)) + (1-\alpha)(Level(t) + Trend(t-1)) \tag{20}$$

$$Trend(t) = \beta(Level(t) - Level(t-1)) + (1-\beta)Level(t-1)$$
$$Season(t) = \gamma(Temp(t) - Level(t)) + (1-\gamma)Season(t-p)$$

(21)

where α, β and γ are exponential smoothing parameters and their values are 0.05, 0 and 0.275, respectively. The parameter p is 12, the period of a year's cycle. The initial values of the three components are

$$Level(0) = 36.74 \qquad Trend(0) = 0.0348$$

$$Season(1) = -9.409 \qquad Season(2) = -9.599$$

$$Season(3) = -4.865 \qquad Season(4) = -0.920$$

$$Season(5) = 5.370 \qquad Season(6) = 7.458$$

$$Season(7) = 8.990 \qquad Season(8) = 8.277$$

$$Season(9) = 5.802 \qquad Season(10) = 2.171$$

$$Season(11) = -7.469 \qquad Season(12) = -10.33$$
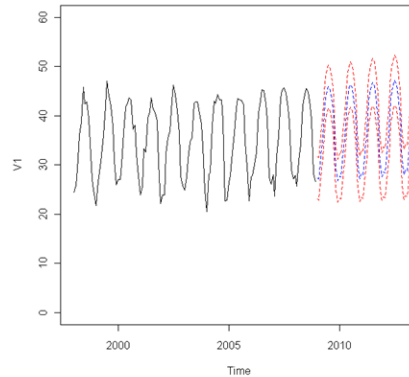
Figure 42: Time Series Prediction of Ambient Temperature in Next Five Years

Using this time series model, we predict the temperature for the next five year. The predicted values and the 95% confidence intervals are depicted below.

To simplify our analysis, we will use only temperature factor in this paper. As it is well-known in the PV field that at least temperature, UV and humidity will have

impacts on PV panel degradation, the result presented in this paper is incomplete; instead, our main purpose is to demonstrate a practical approach of integrating auxiliary weather information into product's reliability analysis. There are two main degradation mechanisms that temperature may involve: 1) Temperature cycling through daytime and nighttime will cause thermal expansion and contraction of interconnects and solder bonds, thus increase in series resistance and cause power drop; 2) higher and extended daytime static temperature will weaken solder bonds in PV cells (interconnect/cell) and interconnects (ribbon/ribbon). From our testing experience, very few modules have experienced power losses after 200 thermal cycles from -40°C to 85°C. In fact, an analysis conducted by PTL (TamizhMani et al., 2010) indicated that 1220 modules went through 200 thermal cycling, with about 10% experiencing power loss, all of which were predominantly due to the failure of bypass diode, not due to thermal cycling stress. Therefore, in this paper, we will focus on the second degradation mechanism aforementioned and use maximum temperature as the environmental factor.

Parameter Estimation

The regression model used in the data analysis has a subtle difference from Equation (18). We chose to use

$$ln(-ln R(k)/110) = c_0 + c_1 \bar{s}(k) + a \ln k \tag{22}$$

to avoid the possibility of "not a number" on the left hand side when the real values of R (they could be larger than 100) are used. This is equivalent to adding a constant term to the exponential function for $\ln(100/R)$.

To validate the approach that we proposed, we first use the degradation and temperature data of the first 9 years to build the degradation model, then use the

data of the last two year to validate the model. Table 20 below shows a summary of regression result:

Table 20: Coefficients of Linear Regression & Analysis of Variance

Table 20A: Coefficients of linear regression

	Estimate	Std. Error	t value	Pr(>|t|)
(Intercept)	1.654e+01	9.055e+00	1.827	0.08194
temp	-5.875e+03	2.763e+03	-2.127	0.04547
log(day)	7.081e-02	2.266e-02	3.125	0.00512

Table 20B: Analysis of Variance (ANOVA) of linear regression

	Df	Sum Sq	Mean Sq	F value	Pr(>F)
temp	1	0.103834	0.103834	13.2450	0.001534
log(day)	1	0.076574	0.076574	9.7678	0.005115
Residuals	21	0.164630	0.007840		

From the ANOVA table (Table 20B), one can see that both temperature and time (log(day)) are significant on the 0.05 confidence level. The regression coefficients estimated are significant too. We use this model to predict the degradation in the next two years (2007-2008), and compare them with the measured degradation values. As shown in Figure 43, the measured degradation values in 2007 and 2008 fall into the 95% prediction interval of the model.

Using all available data from 1998 to 2008, we fit the linear regression function of Equation (8). The coefficient table and ANOVA table are given below in Table 21A and Table 21B. Again, both temperature and time are statistically significant factors. The coefficient of time term is significant, and the coefficient of temperature is marginally significant. The residual plot (Figure 44) does not show any particular pattern and the quantile-quantile plot fall on the diagonal line. Therefore, we regard this model being adequate.
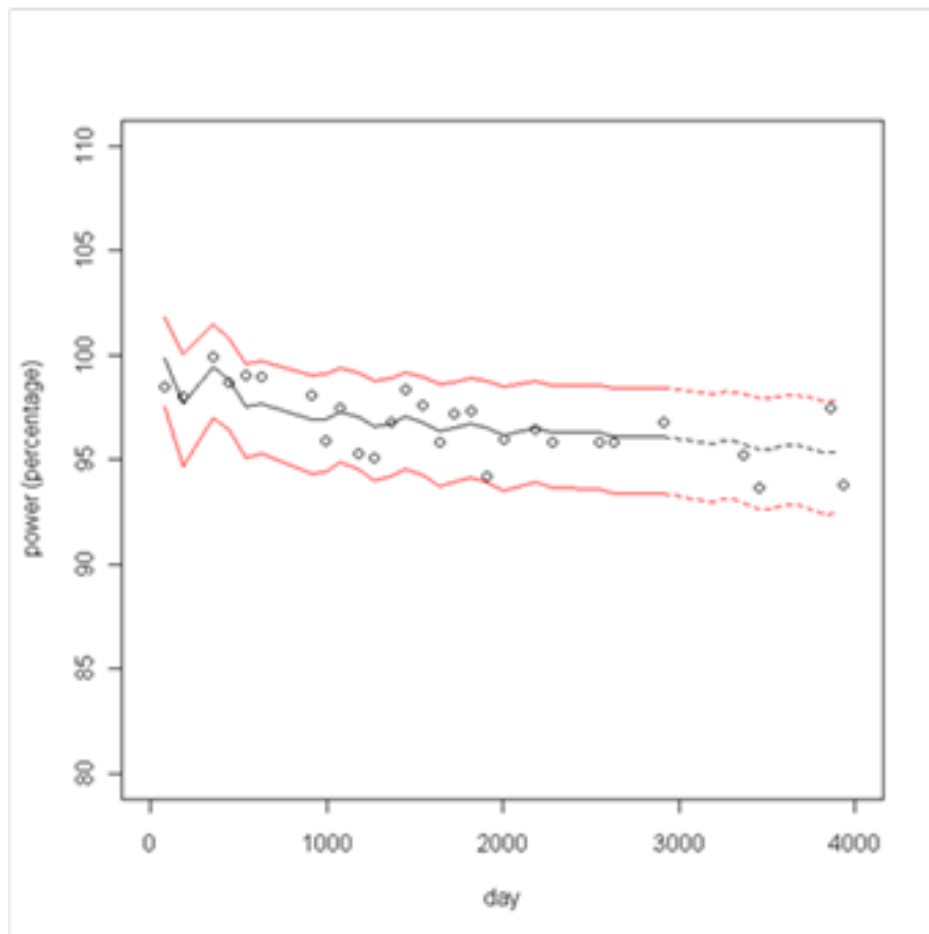
Figure 43: Prediction of Degradation of the Last Two Years

Table 21: Coefficients of Linear Regression & ANOVA Using All Available Data from

1998 to 2008

Table 21A: Coefficients of linear regression

	Estimate	Std. Error	t value	Pr(>|t|)
(Intercept)	1.654e+01	9.533e+00	1.735	0.09497
temp	-5.884e+03	2.905e+03	-2.025	0.05363
log(day)	7.552e-02	2.251e-02	3.355	0.00253

Table 21B: Analysis of Variance (ANOVA) of linear regression

	Df	Sum Sq	Mean Sq	F value	Pr(>F)
temp	1	0.15648	0.156476	17.526	0.0003065
log(day)	1	0.10050	0.100504	11.257	0.0025342
Residuals	25	0.22320	0.008928		
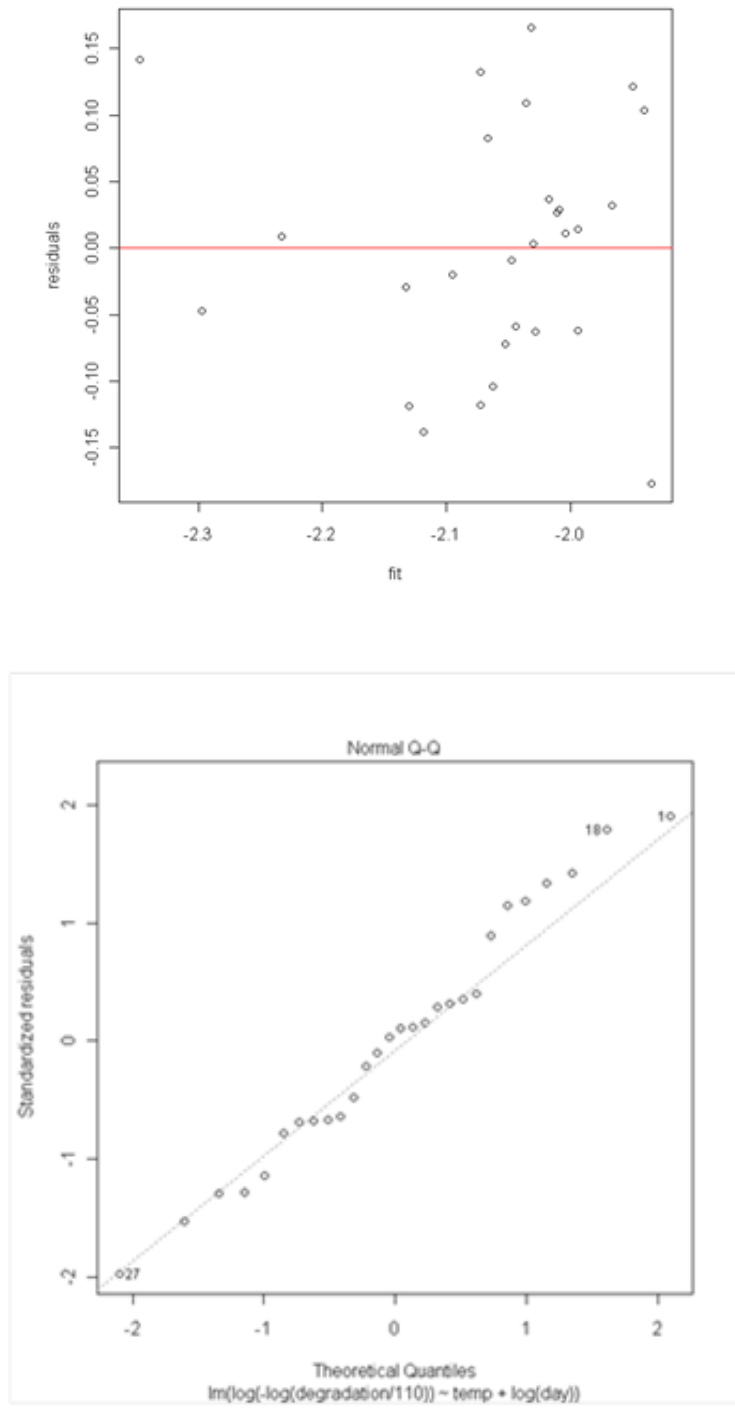
Figure 44: Plot of Residuals vs. Fitted Value (Top) and Normal Quantile-Quantile Plot
(Bottom)

Prediction

We make a prediction of the solar power degradation by using the degradation model and the time series model of temperature that were established in the previous sections. The prediction period is set to be 5 years. With the nominal temperature prediction, the power degradation and its 95% confidence intervals are plotted in Figure 45 below.
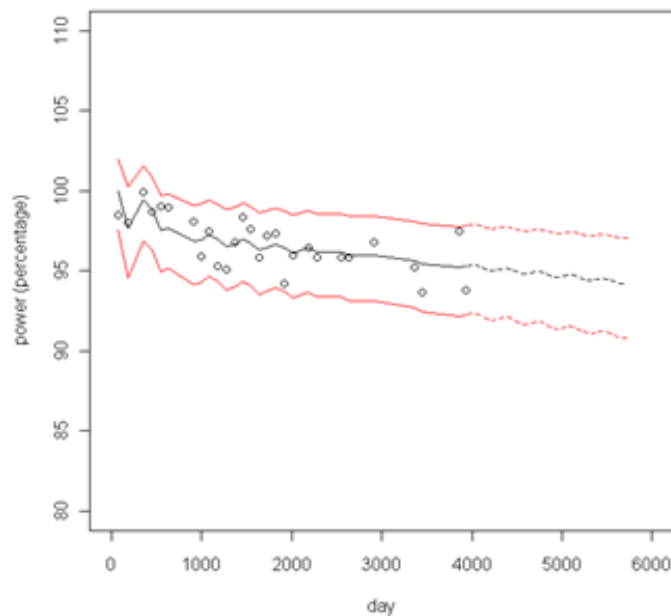
Figure 45: Degradation Prediction of Next Five Years

In Figure 46, we provide the predicted values and the prediction bounds at 95% confidence level of power percentage. One can see that at the end of the next five year, the lower bound of power percentage will be larger than 90% of its initial value. However, this plot does not include the uncertainty in temperature prediction. We may want to investigate a worst-case scenario, where the temperature series will go on its upper prediction bound (i.e., extreme hot weather in years ahead). In this case, the power reduction will accelerate quickly (see Figure 46), and its 95% prediction lower bound will be well below 90% at the end of the next five years. As

the variation of degradation measurements is caused by both measurement error and the variation in stochastic weather time series, it would lead to overly optimistic reliability prediction if the temperature prediction error is ignored. However, we are against to making any specific conclusion on the degradation prediction based on this set of field test data. As mentioned before, not all possible environmental stress factors and degradation mechanisms are included in our data analysis. The purpose of this paper is rather to demonstrate a practical approach to integrating the information of environmental factor into degradation model and to illustrate the effect of stochastic environmental factor.
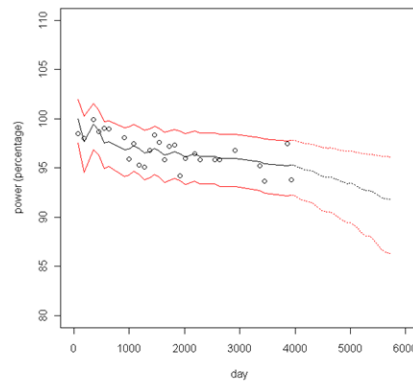
Figure 46: Degradation Prediction of Next Five Years when the Temperature Prediction is at its Prediction Upper Bound

4.4   Summary

In this chapter we propose a practical approach to integrating stochastic outdoor weather information to PV degradation analysis. We apply our approach on a dataset of solar panel power output measurements of over eleven years obtained from a field test yard in Mesa, AZ. The data analysis shows that the daytime static temperature is a significant factor to PV degradation. Also, it shows that the effect of the variation in stochastic weather data on degradation prediction should not be ignored.

CHAPTER V

ACCELERATED AGING TEST FOR LIFETIME PREDICTION

5.1   Introduction and Background

A typical module construction is

superstrate/encapsulant/cells/encapsulant/backsheet (see Figure 47). Glass is the

common choice for superstrate. Ethylene vinyl acetate (EVA) copolymer has been the

dominant encapsulation material for crystalline silicon modules since it was

introduced in the 1980s. Metal contacts are often attached on the top of solar cells to

define a grid pattern with bus-bars. Tinned copper ribbons called tabs or

interconnects are soldered to the bus bars on the front of one cell and the back of an

adjacent cell to form a series (S) arrangement of the cells. The cell arrangement is

then sandwiched between two layers of encapsulant and laminated.
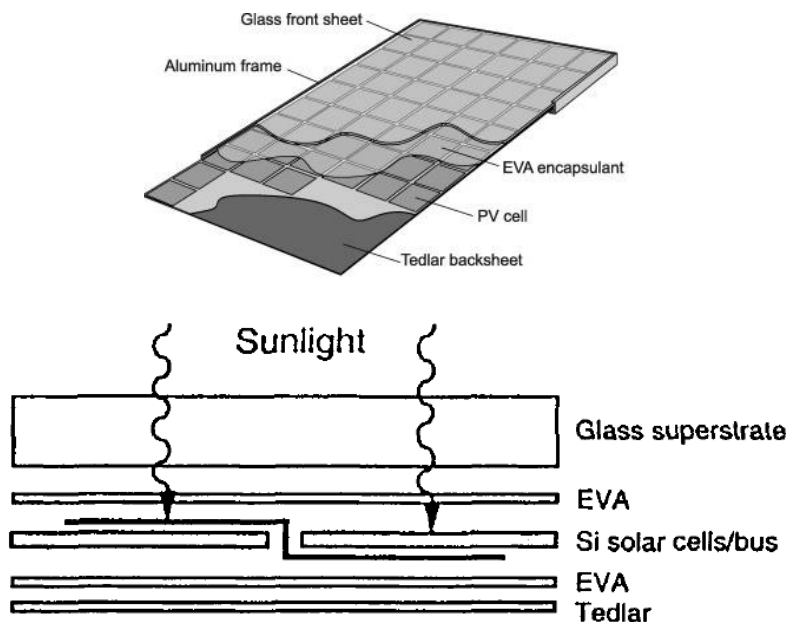
Figure 47: A Typical Module Construction (Top) and a Simplified Diagram (Bottom)

Showing the Configuration Commonly Featured in Monoctystalline and Polycrystalline

Si PV Modules (Pern, 1997)

A key to achieving 20-25 years lifetime for PV modules is an understanding of the degradation mechanisms related to natural degradation of materials in field environments, including the ability to predict long-term effects of exposure to extreme environmental stress factors such as high intensity UV light, humidity, and high temperature and/or temperature cycling.

A PV module lifetime prediction study requires the use of accelerated aging tests to duplicate observed field failure modes and mechanisms. The basic premise is based on the hypothesis that the products will behave the same way in the short period of time under the right levels of increased stress as they do in a longer period of time when used at normal stress. Accelerated aging tests are widely used in the PV industry to obtain timely life characteristics of PV modules, systems, or components. A comprehensive literature review was provided in chapter 3.

The purpose of accelerated aging tests (AAT) for photovoltaic (PV) modules is to shorten the test time by using simulated test conditions, which are more severe than the actual field operating conditions, to replicate actual field failure modes and mechanisms; and then extrapolate the test data through appropriate physical acceleration model for reliability estimate at the desired field conditions. Thus, the primary task for any PV module lifetime prediction study should start with identifying and ranking field failure modes/mechanisms.

In chapter 2, the failure modes, effects, and criticality analysis (FMEA/FMECA) technique was used to determine the dominant failure mode(s) of c-Si PV modules under the Arizona hot and dry climatic condition. Using an approach that relies on quantitative measures and sizable datasets, it was determined that solder bonds (including interconnect) failures and encapsulant discoloration are dominant modes under the hot and dry desert climatic condition of Phoenix, Arizona.

The purpose of the study in this chapter is to design and perform accelerated aging test (AAT) susceptible to replicate solder bonds and encapsulant discoloration degradations/failures under hot and dry desert climate.

Accelerated Tests for Solder Bonds

Metallic interconnects are ribbons connecting and providing electrical continuity between PV cells (see Figure 48). Failures related to the collection of current in crystalline silicon modules have been reported since the earliest days of PV deployment. This was one of the first observed field failures because most early PV modules had only 1 interconnect ribbon between cells and only one solder bond on the front and one on the back of each cell. A single failure of the solder bond, interconnect ribbon or a crack in the solar cell resulted in complete power loss of the whole module (Dumas and Shumka, 1982; Ross Jr., 1982). JPL research (Ross, Jr., 1986) led to the use of multiple interconnects with methods for selecting optimal levels of interconnect redundancy based on minimizing life-cycle energy costs. Mechanisms associated with solder bonds or interconnect failures or degradations are described in (Quintana et al., 2002; Meydbray et al., 2007).

The thermal cycle test in the IEC 61215 qualification test sequence was designed to evaluate these failure modes (Hoffman et al., 1982). The test requires that modules be subjected to 200 cycles of -40°C to 85°C. Modules that experience greater than 5% relative output power loss during post-test fail the test. Recent data has shown that the 200 thermal cycles is not sufficient to ensure a 20-25 year lifetime; but several reports in the literature indicate modules that have survived 1500 to 2000 thermal cycles (Wohlgemuth and Kurtz, Feb 2011, Jun 2011).

Measurable effects of solder bonds and interconnect failures on PV module's maximum power output include increased series resistance in the electrical circuit and/or loss of fill factor. Other characteristics include increased heating in the

127

module, and localized hot spots causing burns at the solder-joints, the polymer backsheet, and in the encapsulant (Quintana et al., 2002). Fill factor can be obtained from light IV characteristics, while dark current-voltage (dark IV) measurement is very effective for quantifying the increase in series resistance. Thermal infrared (IR) imaging is commonly used for identifying localized hot spots.

Accelerated Tests for Encapsulant Discoloration

The encapsulation material (e.g. EVA) is a critical component of a PV module. Encapsulants are polymeric materials used as a mean to hold the cells in place facing the sun, couple light into the cells, dissipate heat and protect the modules against harsh environmental conditions, including wind load, vibration, moisture ingress and other stresses. In addition, they provide electrical isolation, and good adhesion to other module materials such as cells, interconnect ribbons and glass. They must also be able to accommodate stresses induced by the significant differences in thermal expansion coefficients between the polymeric materials, silicon solar cells, and metallic interconnects without over-stressing these materials (See Figure 48).
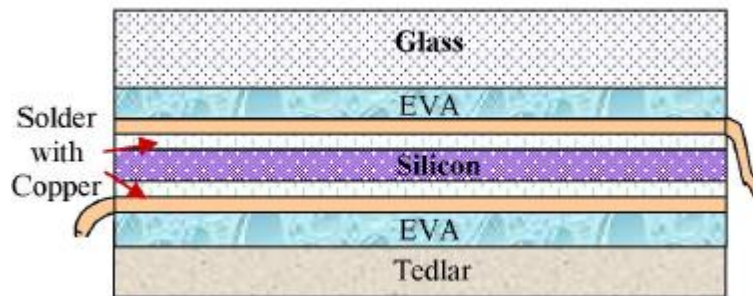
Figure 48: Layered View of a Typical PV Module Showing Solder and EVA

Discoloration of EVA based photovoltaic encapsulants during field aging of solar modules is a chronic issue that has been prevalent in the PV industry since this was first observed in late 1980's. A good qualitative and quantitative review of EVA discoloration for early modules can be found in (Czanderna and Pern, 1996). Two

major observations are reported: (1) EVA discoloration ranged from light yellow to dark brown, with the latter correlated to the greatest performance losses; and (2) EVA discoloration mostly take place in high operating temperatures and high solar insolations, and can occur after exposure periods ranging from 4 to 10 years. Furthermore, the loss in optical transmittance, the drop in output power, the acidic corrosion of metallic elements and metalizations, and the reduced lifetime of PV modules are seen as effects of EVA discoloration.

Improvements to EVA encapsulant formulations were implemented starting in 1998. As a result, encapsulant manufacturers claim that many of the new materials have not exhibited any yellowing during approximately 15 years of outdoor aging.

King et al. (2000) identify three major changes in material properties resulting from environmental aging of the encapsulant material, the first of which is optical losses (yellowing). At the module level, primary optical losses with direct measurable effects on PV module's maximum power output include loss in short-circuit current (Isc). Parretta et al. (2005) analyzes the optical degradation of ~15 years old field deployed modules and observed a drop in output current of 9-14%, leading to a power loss in the range 11-22%. Moderate Pmax losses (~<=20%) can generally be attributed to optical properties degradation or Isc losses (Sample, 2011).

As previously noted, encapsulant exhibits yellowing (and eventually browning) under the influence of both heat and UV exposure. According to Holley and Agro (1998), discoloration can be expected for temperatures above 85-90°C, UV radiation above 1-sun, and EVA-based sample exposed for extended periods of time. The "UV Preconditioning Test" in the IEC 61215 design qualification test standard was designed to induce this phenomenon (Wohlgemuth and Kurtz, 2011). It consists of subjecting the module to 15 kWh/m^2 between 280 nm and 385 nm with at least 5 kWh/m^2 between 280 nm and 320 nm; with the module temperature maintained at

60 ºC ± 5 ºC. Tamizhmani et al. (2012) discuss a survey in which no degradation was observed on any of the 1000+ modules subjected to UV Preconditioning Test.

PV Life Prediction Efforts with AAT

As discussed in Chapter 2, accelerated aging tests are widely used in the PV industry to obtain timely life characteristics of PV modules, systems, or components. Conventionally, accelerated life test (ALT) is used to estimate product's reliability characteristics. The approach is to apply higher stress levels than actual use conditions on test units or groups of test units, obtain failure times for individual units, and then extrapolate the test data through appropriate physical acceleration model for reliability estimate at the desired field conditions. However, PV modules are designed to operate without significant failure or degradation for many years (20 – 30 years). Meaning very few units would degrade significantly in a field test of, say, 6 months to 1 year. For such highly reliable products, testing at some stress levels would often yield few or no failures within the allocated time constraint. This situation makes it impossible to analyze the life data and make meaningful inferences about product reliability. A viable alternative would be to collect degradation data via accelerated degradation testing (ADT). Meeker et al. (1998) list two practical advantages of ADT over ALT: (1) Substantially greater reliability information, and (2) The reliability estimates are more credible and precise. The basic concept of ADT, including comparisons with ALT, is described in Yang (2009). Cuddalorepatta et al. (2006) use thermal cycling test to assess the durability of pb-free solder interconnect and compare to the pb solder laminates. Test samples were single-cell laminates. Test profile consisted of up to 1000 cycles; with cycling temperature of -40°C to 80°C, dwell time of 20 minutes, heating rate of 3°C/min, and cooling rate of 6°C/min. Interconnect damage was measured in terms of the increase in series resistance.

Meydbray et al. (2007) conducted Thermal Cycling test to investigate the interconnect degradation in back contact high efficiency solar cells. Test samples consist of 3-cell minimodules; the test profiles include high temperature profile of -40°C to 125°C; and the series resistance was recorded to evaluate the damage in solder joints.

Park et al. (2014) study the thermal fatigue life of pb solder for degradation rate prediction. Three cycling profiles include a temperature profile of -50°C to 100°C, -35°C to 85°C, and -20°C to 70°C. The dwell time for each profile was 10min.

Kempe (2008, 2010) discusses method for quickly evaluating encapsulants. Single-cell laminate samples were subjected to 60ºC/60% RH and 2.5 UV suns in an Atlas Ci4000 Weather-Ometer with a light intensity of 114 W/m^2 between 300 and 400 nm; with the black panel standard temperature maintained at 100ºC ± 7ºC resulting in a temperature of 70ºC to 80ºC for the transparent glass lap shear samples.

Shioda (2011) studies the discoloration of EVA under accelerated UV test condition. The yellowness index (YI) is analyzed with respect to the black panel temperature (BPT) and UV intensity. It is concluded that ~ 1.3 SUN at BPT=110°C seems to be fastest accelerated condition for long term EVA reliability study in UV chamber.

Gambogi (2011) discusses the color change of encapsulant with UV exposure in glass/EVA/backsheet laminate. Samples are subjected to 0.55 W/m^2 at 340nm in a UV chamber with BPT=64°C and 50% RH.

Klemchuck et al. (1997) subject samples to 0.55 W/m^2 and 100^{0}C BPT at 340 nm until significant discoloration had occurred.

Pern and Glick (2000) study the photothermal stability of EVA samples exposed under 6.5 SUN, 65°C BPT at 300-400nm.

Xia et al. (2009) suggest that 25 years of field operation can be achieved with an accelerated condition with an Atlas Ci4000 Xenon weather-ometer chamber set to 0.7 W/m^2 and BPT=90^{0}C.

Gu (2011) study the degradation mechanism of encapsulant under simultaneous multiple stresses, such as temperature, moisture, and UV; as an important step for service life prediction.

Dever et al. (1992) study the synergistic effects of UV radiation and thermal cycling on PV material for space station.

The above studies provide good references on how to set up the experimentation, how to select the range of stress variables with respect to targeted failure mode(s) or mechanism(s). In Phoenix, Arizona (for example), flat plate PV arrays experience an average of 6.5 daily sun hours solar insolation at latitude tilt and many temperature cycles at a very narrow range (near static temperature) of 60-90^{0}C depending on the installation type (open rack or rooftop). We want to have a designed experiment with multiple stress variables so that both main factor effects and interactions may be studied.

This paper extends the synergistic effects idea of Dever et al. (1992) to the flat plate PV module. It uses a statistical factorial design to analyze the effects of simultaneous factors on the degradation of c-Si PV modules under the dry and hot climatic condition. The factors of interest are the maximum temperature, the dwell time, and the UV radiation. Test samples will be inspected at predefined times to measure the dark and light performance characteristics. Degradation data obtained will be analyzed with the aim of developing a service life model.

5.2   Experimental Approach

Experimental Design

Testing was conducted in an Atlas Ci4000 Xenon Weather-Ometer. Test samples were one-cell coupons built similar to commercial PV modules with EVA encapsulant and TPE backsheet. The glass is 3.2 mm thick; the EVA curing temperature is about

145$^{\text{o}}$C, the tabbing wire size is 0.2mm x 1.6mm (thickness x width), solder thickness is 0.05 ± 0.01mm, and solder type is 60/40 (Sn/Pb).

Studying the synergistic effect of UV radiation and thermal cycling on PV module requires both tests to run simultaneously. The primary factors affecting the durability of encapsulant (browning) and solder bond (degradation) in a UV test and static heat test include: level of UV radiation, exposure time, and constant/static temperature. In a thermal cycling test, the primary factors (or stress variables) are: ramp and cooling rates, and minimum and maximum temperatures.

Ramp and cooling rates and minimum temperature were dictated by the chamber. Observing that the dwell times and exposure times are identical factors, the following factors were of interest:

- Factor A: dwell time at maximum static temperature

- Factor B: Black Panel temperature (BPT), which is related to the sample temperature.

- Factor C: UV radiation level

The high and low levels of each factor are to be investigated. Table 22 below lists the levels selected for each factor, and Figure 49 shows the test profile for each run. The wavelength for the UV radiation was set to 340 nm. The low and high ranges for the UV correspond to the chamber irradiance settings of 0.35 W/m^2 and 0.7 W/m^2 respectively. The module temperatures were not directly monitored; but it is dictated by the black panel temperature (BPT). The low and high BPT ranges are estimated to correspond to module temperature ranges of 60$^{\text{o}}$C – 75$^{\text{o}}$C and 95$^{\text{o}}$C – 100$^{\text{o}}$C, respectively.

Table 22: High and Low Levels of Test Factors

	A: UV @ 340 nm	B: BPT	C: Dwell @ max Temp
Low	0.35 (1 - 1.5 sun)	80 ºC	31 min
High	0.7 (2 - 2.5 sun)	120 ºC	180 min
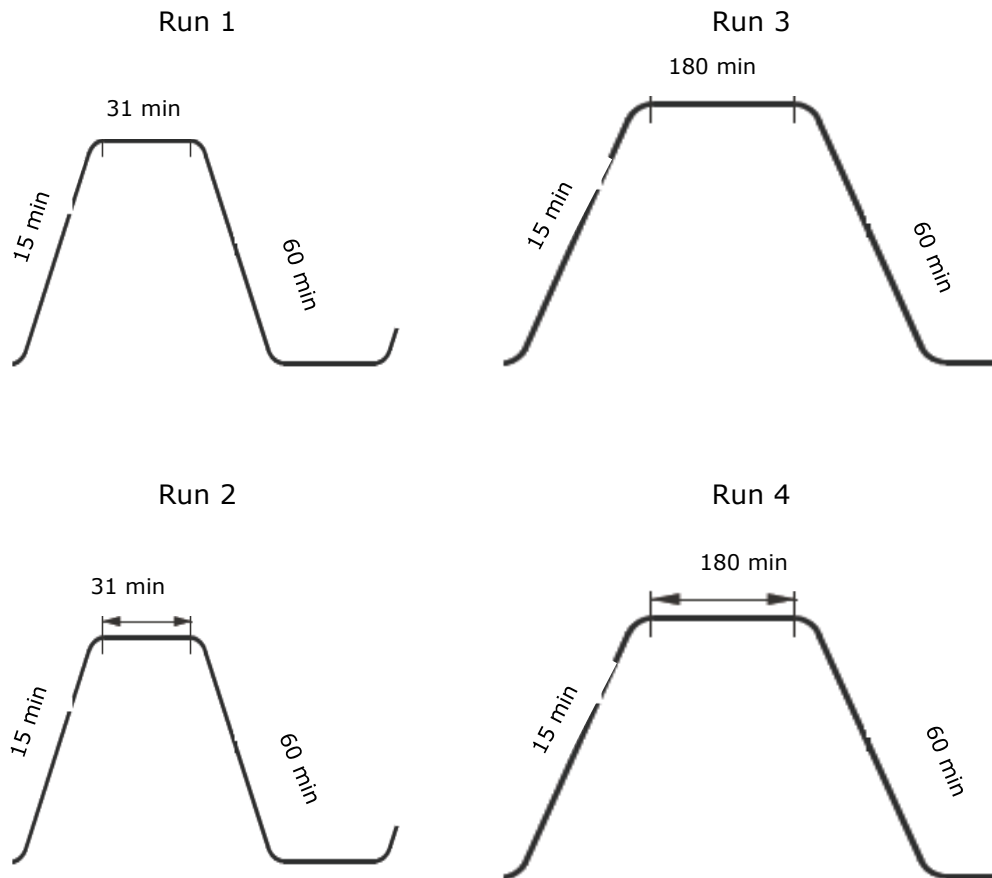
Figure 49: Test Profiles

The test design in Table 22 above would require 8 runs. That is a 2^3 factorial design.

Due to resources and time constraint, a one-half fraction of the 2^3 design (2^{3-1}),

called resolution III design (2_{III}^{3-1}), was adopted. The design matrix is shown in Table

23 below using the geometric notation, where the "+" and "−" signs represent the high and low levels respectively of the factors.

Table 23: 2_{III}^{3-1} Fractional Factorial Design Matrix

	Factors		
Run	A (UV)	B (BPT)	C (Dwell)
1	+	+	-
2	-	-	-
3	+	-	+
4	-	+	+

Two test samples were used for each run, for a total of 8 samples. One sample was used as control sample for performance measurements (IV) at inspection times. The control sample is used for measurement repeatability assurance. Practically, performance measurements of control sample should be repeatable (within 1%) at each inspection time as it is not subjected to stress test.

Data Collection and Processing

The properties of interest are obtained from performance measurements. At each inspection time, current-voltage (IV) measurements were conducted either indoor or outdoor. Indoor measurements were done using the TriSol solar simulator setup. A sample output from the simulator is shown in Figure 50. As it can be observed, both series resistance (Rseries Dark) and short-circuit current (Isc) are measured, as both light and dark measurements can be taken in the same setup.
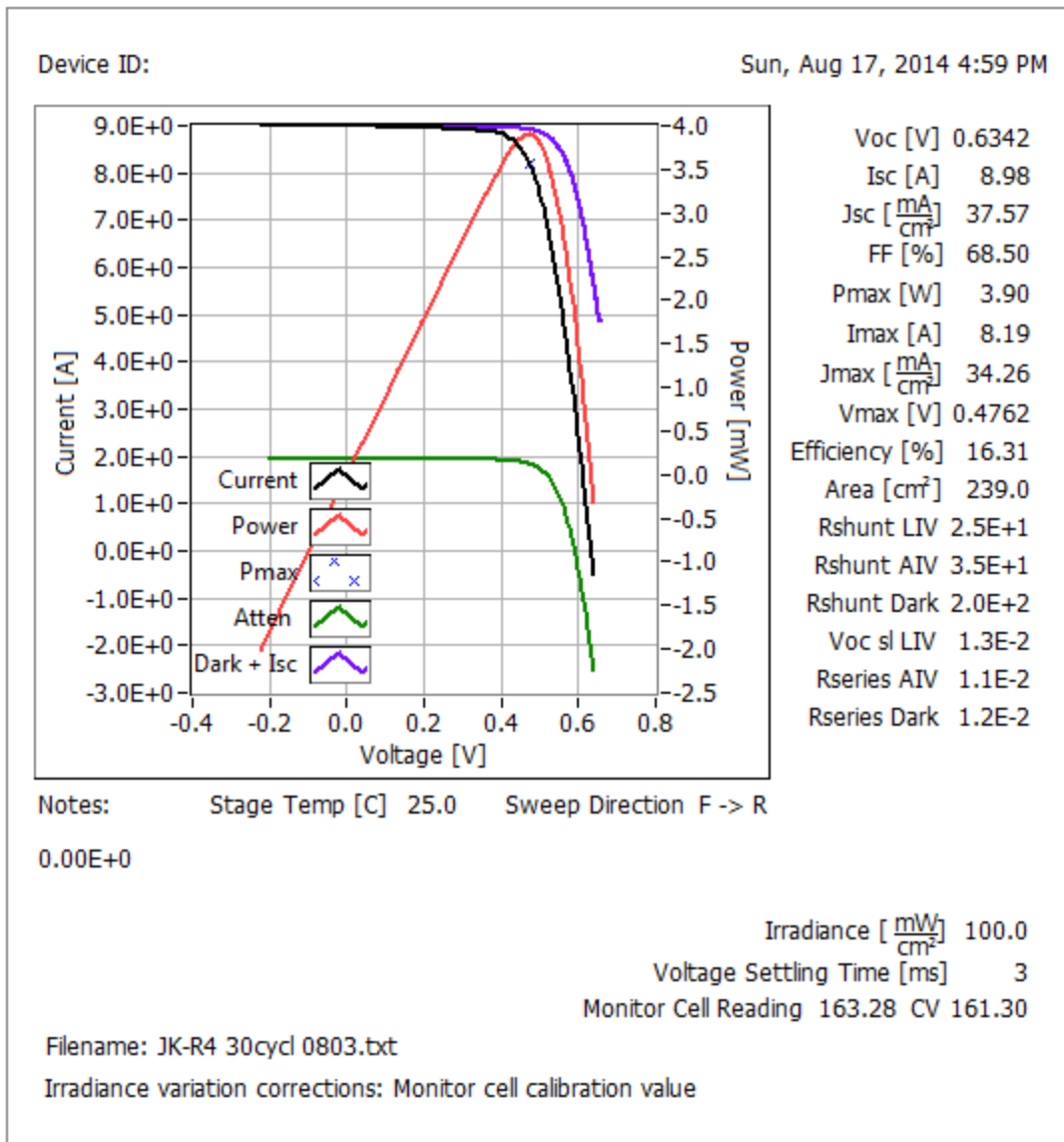
Figure 50: Sample Indoor Performance Measurements (IV) Output Curve

Outdoor measurements were done using a DayStar IV curve tracer, under natural sunlight on clear days. A sample outdoor IV output is shown in Figure 51. Only the short-circuit current is directly obtained. The series resistance (Rs) is obtained using the empirical expression from Dobos (2012) presented in Chapter 3.
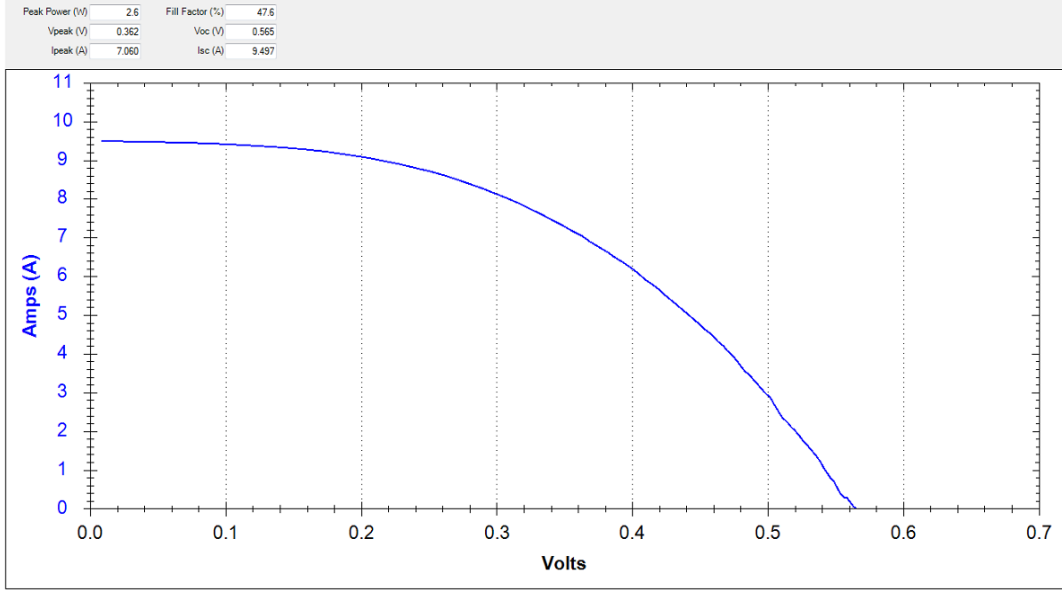
Figure 51: Sample Outdoor Performance Measurements (IV) Output Curve

We now describe how property degradations were derived from performance data.

Let P_{ij} be the property characteristic of sample i at a given inspection time t_j (j = 0, 1, …); and P_{0j} the property characteristic of the control sample at t_j.

At the initial time $t_j = 0$, the property characteristic for the control sample is P_{00}, and that of sample i is Pi0. Let's N_{ij} be the normalized quantities with respect to the control.

$$N_{i0} = P_{i0}/P_{00} \quad \text{and} \quad N_{ij} = P_{ij}/P_{0j} \tag{23}$$

The fraction (or percent) of remaining life is given by:

$$R_{ij} = 100 * N_{ij}/N_{i0} \tag{24}$$

Because this quantity could be higher than 100, it was multiplied by an adjustment coefficient AC=100/110. The percent degradation D_{ij} of sample i of the property of interest at a given time t_j is thus given by:

$$D_{ij} = 100 - R_{ij}^{adjusted} \tag{25}$$

Assuming equal inspection times for each run, the percent of performance drop for a given property can be summarized as shown in Table 24 below, where D_{ij} represents the average percent degradation of run i at time t_j. The processed data from our experiment is shown in Table 25.

Table 24: Degradation Data Recording Format for a Given Performance Characteristic.

		Time tj				
		t1	t2	...	...	tm
Run i	1	D1,1	D1,2	...	...	D1,m
	2	D2,1	D2,2	...	...	D2,m
	...	...	...	...	...	...
	...	...	...	...	...	...
	n	Dn,1	Dn,2	...	...	Dn,m

Table 25: Degradation Data from our Experiment

Run	Inspection Time (hours)	Isc	Rs
R1	189.7	9.091638	13.72881
	284.55	9.287188	13.72881
	379.4	9.240475	14.67655
	474.25	9.492232	15.59244
R2	21.5	8.250145	12.87374
	109.8	9.050788	13.9795
	198.1	8.587485	14.67494
	286.4	8.838917	13.9434
	365.9	7.554031	27.35848
	454.2	7.652413	25.48386

	127.5	9.192852	14.29627
R3	255	9.068009	31.5608
	348.45	7.362371	31.83234
	429.2	5.689136	47.291
	127.5	7.030903	17.42053
R4	263.5	5.839446	30.17448
	386.75	5.310293	40.15922

5.3 Degradation Data Analysis

Before tackling the effects of stress variables, an intuitive question is whether the observed degradations are truly significant and, similarly, how they differ from one intermittent inspection time to another, and from one test run to another. In the first subsection, we attempt to answer these questions with ANOVA (Analysis of Variance). The second subsection is devoted to modeling the degradation data.

Analysis of Variance (ANOVA)

The data presented in Table 24 above can be thought of as from a single-factor experiment with repeated measures described in (Montgomery, 2005), where each treatment represent a test run, and the repeated measures are inspection time measures. The statistical model used for such design is

$$D_{ij} = \mu + \tau_i + \beta_j + \epsilon_{ij} \tag{26}$$

where μ is an overall mean, τ_i is the effect of the ith run and β_j a parameter associated with the jth inspection time. Assuming random inspection times and fixed test runs, we have:

$$\sum_{i=1}^{n} \tau_i = 0$$

$$\beta_j \sim NID(0, \sigma_\beta^2).$$

We are interested in testing the hypothesis of no test run effect:

$$H_0: \tau_1 = \tau_2 = \cdots = \tau_n = 0$$

$$H_1: At\ least\ one\ \tau_i \neq 0$$

We reproduce below the computing formulas for the analysis of variance from (Montgomery, 2005):

Let $\quad D_{i\cdot} = \sum_{j=1}^{m} D_{ij} \equiv$ sum of all observations taken under run I,

$\quad D_{\cdot j} = \sum_{i=1}^{n} D_{ij} \equiv$ sum of all observations in during inspection time t_j

$\quad D_{\cdot\cdot} = \sum_{i=1}^{n} \sum_{j=1}^{m} D_{ij} \equiv$ grand sum of all observations

$\quad N = nm \equiv$ total number of observations

We have:

$\quad \overline{D_{i\cdot}} = \frac{D_{i\cdot}}{m} \equiv$ average of the observations taken under test run i

$\quad \overline{D_{\cdot j}} = \frac{D_{\cdot j}}{n} \equiv$ average of the observations in inspection time t_j

$\quad \overline{D_{\cdot\cdot}} = \frac{D_{\cdot\cdot}}{N} \equiv$ grand average of all the observations

The total sum of squares can be expressed as:

$$SS_T = \sum_{i=1}^{n} \sum_{j=1}^{m} (D_{ij} - \overline{D_{\cdot\cdot}})^2 = n \sum_{j=1}^{m} (\overline{D_{\cdot j}} - \overline{D_{\cdot\cdot}})^2 + \sum_{i=1}^{n} \sum_{j=1}^{m} (D_{ij} - \overline{D_{\cdot j}})^2 \tag{27}$$

$$SS_T = SS_{Between\ inspection\ times} + SS_{Within\ inspection\ times} \tag{28}$$

The sum of squares $SS_{Between\ inspection\ times}$ and $SS_{Within\ inspection\ times}$ are statistically independent, with degree of freedom (df)

$$nm - 1 = (m - 1) + m(n - 1) \tag{29}$$

where

$$df(SS_{Between\ inspection\ times}) = m - 1 \tag{30}$$

$$df(SS_{Within\ inspection\ times}) = m(n - 1) \tag{31}$$

The differences with inspection times depend on both the test run effects and the experimental error. So the $SS_{Within\ inspection\ times}$ can be decomposed:

$$SS_{Within\ inspection\ times} = m \sum_{i=1}^{n} (\overline{D_{i\cdot}} - \overline{D_{\cdot\cdot}})^2 + \sum_{i=1}^{n} \sum_{j=1}^{m} (D_{ij} - \overline{D_{i\cdot}} - \overline{D_{\cdot j}} + \overline{D_{\cdot\cdot}})^2 \tag{32}$$

The first term on the RHS measures the contribution of the difference between test run means to $SS_{Within\ inspection\ times}$, and the second term is the residual variation due to error; so:

$$SS_{Within\ inspection\ times} = SS_{Runs} + SS_E \tag{33}$$

Both components are independent, and their degree of freedom is given by:

$$m(n-1) = (n-1) + (m-1)(n-1) \tag{34}$$

where

$$df(SS_{Runs}) = n-1 \tag{35}$$

$$df(SS_E) = (m-1)(n-1) \tag{36}$$

To test the hypothesis, we use the ratio:

$$F_0 = \frac{SS_{Run}/(n-1)}{SS_E/(n-1)(m-1)} = \frac{MS_{Runs}}{MS_E} \tag{37}$$

The null hypothesis would be rejected if $F_0 > F_{\alpha,n-1,(n-1)(m-1)}$

ANOVA for our Experimental Data

The average degradations of series resistance (Rs) and short-circuit current (Isc) are shown in Table 26. Inspection times were not identical for each run, so analysis times of 200h, 300h, 400h, and 500h were chosen so that the property drop values are equal to the drop observed at the inspection point closest to and before the analysis time.

Table 26: Percent of Isc Drop (Left) and Rs Drop (Right) on/or Before Given Times.

Isc	Virtual inspection times (blocks)				Rs	Virtual inspection times (blocks)			
	200h	300h	400h	500h		200h	300h	400h	500h
Run1	9.1	9.3	9.2	9.5	Run1	15.2	14.7	13.7	15.1
Run2	8.6	8.9	7.5	7.7	Run2	14.7	13.9	27.4	25.5
Run3	9.2	9.1	7.4	5.7	Run3	14.3	31.6	31.8	47.3
Run4	7.0	5.8	5.3	7.4	Run4	17.4	30.2	40.2	17.0

The analysis of variance is equivalent to that of a randomized complete block design (RCBD), with the inspection times considered as blocks and the experimental runs considered as treatments. The outputs from Design-Expert 9.0.3 software are shown in Tables 27A for the series resistance (Rs), Tables 27B and 27C for and the short-circuit current (Isc), using $\alpha = 0.05$.

Table 27: Software Output for Series Resistance (Rs) and Short-Circuit Current (Isc)

Table 27A: Design-Expert output for Rs

Response: Rs

Analysis of variance table [Classical sum of squares - Type II]

Source	Sum of Squares	df	Mean Square	F Value	p-value Prob > F	
Block	384.34	3	128.11			
Model	617.75	3	205.92	2.70	0.1084	not significant
A-Rs	617.75	3	205.92	2.70	0.1084	
Residual	686.23	9	76.25			
Cor Total	1688.31	15				

Std. Dev.	8.73	R-Squared	0.4737	
Mean	23.13	Adj R-Squared	0.2983	
C.V. %	37.76	Pred R-Squared	-0.663	
PRESS	2168.83	Adeq Precision	5.099	

Treatment Means (Adjusted, If Necessary)

	Estimated Mean	Standard Error
1-R1	14.67	4.37
2-R2	20.37	4.37
3-R3	31.25	4.37

Treatment	Mean Difference	df	Standard Error	t for H₀ Coeff=0	Prob > |t|
4-R4	26.20		4.37		
1 vs 2	-5.70	9	6.17	-0.92	0.3800
1 vs 3	-16.57	9	6.17	-2.68	0.0250
1 vs 4	-11.53	9	6.17	-1.87	0.0948
2 vs 3	-10.88	9	6.17	-1.76	0.1120
2 vs 4	-5.83	9	6.17	-0.94	0.3701
3 vs 4	5.05	9	6.17	0.82	0.4345

Table 27B: Design-Expert output for Isc

Analysis of variance table [Classical sum of squares - Type II]

Source	Sum of Squares	df	Mean Square	F Value	p-value Prob > F	
Block	3.51	3	1.17			
Model	17.17	3	5.72	5.66	0.0185	significant
A-Isc	17.17	3	5.72	5.66	0.0185	
Residual	9.10	9	1.01			
Cor Total	29.78	15				

Std. Dev.	1.01	R-Squared	0.654
Mean	7.92	Adj R-Squared	0.538
C.V. %	12.70	Pred R-Squared	-0.095
PRESS	28.76	Adeq Precision	6.051

Treatment Means (Adjusted, If Necessary)

	Estimated Mean	Standard Error
1-R1	9.27	0.50
2-R2	8.17	0.50

3-R3	7.85		0.50		
4-R4	6.37		0.50		

Treatment	Mean Difference	df	Standard Error	t for H_0 Coeff=0	Prob > |t|
1 vs 2	1.10	9	0.71	1.55	0.1563
1 vs 3	1.42	9	0.71	2.00	0.0761
1 vs 4	2.90	9	0.71	4.08	0.0028
2 vs 3	0.32	9	0.71	0.46	0.6585
2 vs 4	1.80	9	0.71	2.53	0.0322
3 vs 4	1.48	9	0.71	2.07	0.0679

Table 27C: ANOVA Output from Design-Expert for the 2^{3-1} Design

Analysis of variance table [Partial sum of squares - Type III]

Source	Sum of Squares	df	Mean Square	F Value	p-value Prob > F	
Block	3.51	3	1.17			
Model	17.17	3	5.72	5.66	0.0185	significant
A-UV	6.63	1	6.63	6.56	0.0307	
B-BPT	0.14	1	0.14	0.14	0.7178	
C-dwell	10.40	1	10.40	10.29	0.0107	
Residual	9.10	9	1.01			
Cor Total	29.78	15				

Because the P-value in Table 27A is greater than 0.05, we fail to reject the null hypothesis and conclude that the experimental runs do not affect the increase in series resistance. However, the mean square for blocks is 128.11; which is quite large relative to the mean square for error of 76.25; indicating that the Rs increase is significant over time.

An increase in Rs, which in turn results in a corresponding decrease in fill factor and hence the module performance, can be caused by several factors. The key elements are the front- and back-surface contact metallization of the solar cells, the interconnects, and the connection points where the interconnects are attached to the cell metallization. The experimental findings indicate that the different experimental runs considered equally affect the solder joints and interconnects life, and that these materials could degrade significantly over time.

Table 27B shows that the model is significant; meaning we reject the null hypothesis and conclude that the experimental runs affect the drop in short-circuit current. However, from Tables 27B and 27C, the mean square block is 1.17 and the mean square error is 1.01; giving a very small ratio between the two. This is an indication that the drop in short-circuit current is not a significant contributor to the performance drop over the experimental period.

A decrease in short-circuit current can be attributed to transmittance losses. A lower percentage of Isc loss would typically be due to encapsulant discoloration (chemical changes in UV stabilizers). However, higher Isc losses could have a different mechanism or a combination of different mechanisms including extensive metallization corrosion leading to increase in series resistance. The findings from our experiment, which shows insignificant drop in Isc over the experimental period but significant variations between experimental runs, indicate that the main cause of Isc drop is encapsulant discoloration, and it is driven by one or more of the experimental factors.

To study the effect of each factor, the ANOVA output for the 2^{3-1} fractional factorial was obtained for Isc. It is shown in Table 27C. The output reveals that factor B (BPT) appears to be insignificant; meaning the UV and static temperature (dwell time at high temperature) are the main contributors to Isc drop.

5.4 Degradation Data Modeling

Degradation data are usually obtained by measuring performance characteristics; such as power output (Pmax), short-circuit current (Isc), open-circuit voltage (Voc), fill-factor (FF), or series resistance (Rs) of n test samples each at time t_i, i=1, 2, … Let $y_{i,j}$ represents the performance characteristic drop measured on sample i at time t_j. The degradation data can be presented as shown in Table 28 below.

Table 28: Degradation Data Recording Format

		Time tj				
		t1	t2	…	…	tm
Sample i	1	y1,1	y1,2	…	…	y1,m
	2	y2,1	y2,2	…	…	y2,m
	…	…	…	…	…	…
	…	…	…	…	…	…
	n	yn,1	yn,2	…	…	yn,m

Data can be collected at any time on any sample, meaning the measurement times for samples u & v need not be equal and can be denoted as t_{uj} and t_{vk}.

Let D be the acceptable level of degradation. The reliability of the product is given by:

$$R(t) = P_r\{Y(t) \leq D\}$$

Zuo, et al. (1999) discuss three approaches for modeling degradation: Stochastic process models, general path models, and linear regression model.

Random or Stochastic Process Models

An approach to model random process degradation data using s-normal distribution was proposed by Yang and Xue (1996) and extended to general distribution by Zuo,

Renyan, and Yam (1999). The degradation analysis for the data format in Table 1 involves the following steps:

(1) Assume a distribution (normal, Weibull, gamma, etc.) that can adequately represent the degradation data at each inspection time ti

(2) Estimate the parameters of the selected distribution at each inspection time ti

(3) Fit each distribution parameter into a mathematical function based on the knowledge of the degradation process

(4) Derive the reliability estimate R(t) of the product.

A major problem with this approach is the need for multiple degradation data for meaningful estimate of the distribution parameters at each inspection time. Crack growth modelling and cumulative damage models are widely known approaches to stochastic degradation models. The literature mostly uses a Wiener process, a gamma process, or their variants to model the degradation or damage level. A brief overview of these stochastic degradation models can be found in (Pan and Crispin, 2010).

Yu and Tseng (2002) describe the use of Wiener process in an optimal design of experiment for highly reliable products. Charki, Laronde, and Bigaud (2013) discuss the use of Wiener process in conjunction with physical model: For a degradation path y_{ij} of the jth inspection on unit i; let x_i be the stress level on unit i

$$y_{ij} = D\big[r(x_i, \gamma)t_{ij}, \theta\big] + e_{ij}, \quad e_{ij} \sim N(0, \sigma^2) \tag{38}$$

Where r(.) is the transfer function, found with the ratio between the mean lifetime determined for one stress level and the mean lifetime corresponding to the reference condition; and Y are the unknown parameter of the transfer function.

Degradation Path Models

The general path model approach is described in Lu and Meeker (1993); Nelson (1990); Meeker and Escobar (1998); Meeker, Escobar, and Lu (1998); and Bagdonavicius et al. (2005).

$$y_{ij} = g(t_{ij}; \beta_{1i}, \beta_{2i}, \ldots, \beta_{pi}) + e_{ij} \tag{39}$$

where $g_i(.)$ is the degradation path of unit i at time t_{ij};

e_{ij} is the error term;

$\beta_{1i}, \ldots, \beta_{pi}$ are unknown parameters; some could be random (i.e. vary from unit to unit), and others common to all units. This flexibility of incorporating both fixed and random effects into the degradation path makes this approach appealing for analyzing ADT data. The parameters can be estimated by least square method or maximum likelihood method.

For n test samples, we can plot a set of path curves as in Figure 52 based on the data in the form of Table 1. At this stage, Zuo, et al. (1999) distinguishes two categories of degradation processes:

Category 1: There is no intersection between any two path curves. In its simplest form, each $g_i(.)$ can be described in this case with the simple constant rate model (Nelson, 1990, p. 527):

$$g(t_{ij}; \beta_i) = \alpha + \beta_i t_{ij} \tag{40}$$

Where β_i is a function of stress variable(s) that can be determined from the knowledge of the physical process (e.g. Arrhenius model); and α is a fixed constant representing the common amount of degradation of all samples at the beginning of the test.

Category 2: There are intersections among the path curves. Zuo, et al. (1999) suggested the linear regression model approach described next. Lu and Meeker (1993) proposes a two-stage method to estimate the parameters. Pan and Crispin

(2010) used the function below for analyzing the degradation of light-emitting diodes:

$$g(t) = (1 + \gamma_0 t^{\gamma_1})^{-1}, \ \gamma_0, \gamma_1 > 0 \tag{41}$$
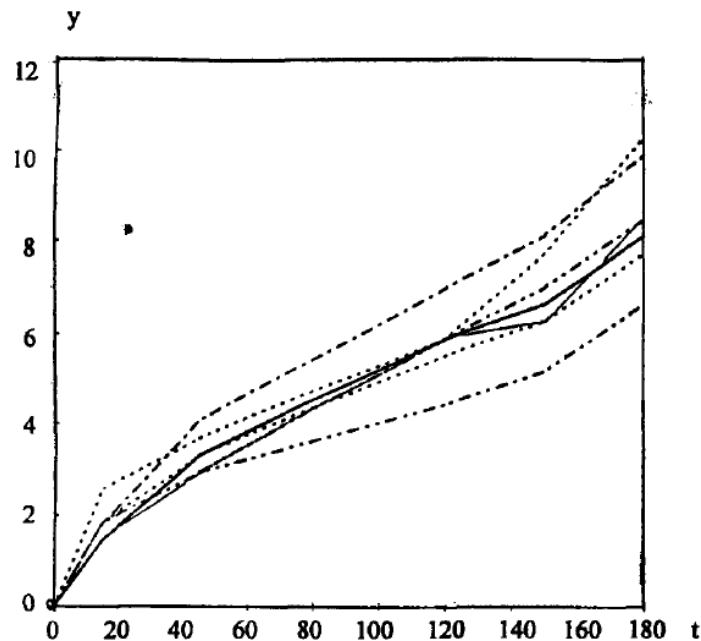
Figure 52: Sample Path Curves for Degradation Data (Zuo, et al., 1999)

Linear Regression Models

According to Zuo, et al. (1999), this approach eliminates the need for multiple data points at each inspection time. However, Nelson (1990, p.533) warns that these models may provide no physical insight and may extrapolate badly. The procedure is as followed:

(1) Collect degradation data for k test samples. For each sample i, there are n_i observations. Note that each observation can be obtained at different time point.

(2) Obtain a set of path curves by plotting y_i vs t for each unit i

(3) For a given time tj, draw a vertical line t=tj that intersects the k path curves to obtain $y_{1j}, y_{2j}, ..., y_{kj}$ and rank them in ascending order.

149

(4) Assume a distribution function

(5) Use multivariate linear regression to estimate the parameters of the distribution

5.5 Analysis of the Data

We use a slight variation of the linear regression procedure described above to analyze the data. First, steps 1-3 allow to obtain degradation values at equal inspection times k for each run; and then steps 4 & 5 was applied using a variant of Equation (22).

$$ln(-ln\, D(k)) = c_0 + c_1 \bar{s}(k) + a\, ln\, k \tag{42}$$

where D(k) represents the dimensionless degradation quantity. For example, D(k) would be 0.12 for 12% degradation.

Data are obtained by measuring performance characteristics; such as power output (Pmax), short-circuit current (Isc), open-circuit voltage (Voc), fill-factor (FF), or series resistance (Rs). The degradation D(k) at time k for a property of interest (for example, Isc) is computed using Equation (25).

For temperature-voltage, temperature-current density, and temperature-humidity acceleration, Meeker & Escobar (1998) show that the mean stress variable could be expressed as a multivariate linear regression function, where the regressors are the natural temperature 1/T and the logX, (X being the voltage, current density, or relative humidity). So for each run i, the mean stress function $\bar{s}_i$ in the equation above can be expressed as:

$$\bar{s}_i(k) = \beta_0 + \beta_1 x_{1i}(k) + \beta_2 x_{2i}(k) + \beta_3 x_{3i}(k) \tag{43}$$

where

$$x_1 = {}^1\!/_T; \quad x_2 = ln(UV); \quad x_3 = ln(dwell)$$

Combining Equations (42) and (43) yields:

$$ln(-ln\, D_i(k)) = \beta_0 + \beta_1 x_{1i}(k) + \beta_2 x_{2i}(k) + \beta_3 x_{3i}(k) + a\, ln\, k \tag{44}$$

The linear fits of the average series resistance increase for each run are shown in Figure 53 below. The equations shown were used to determine $y(k) = \ln(-\ln D_i(k))$ at chosen times k=50, 100, 200, and 300 hours. The analysis of the ensuing data is provided in Table 29, where the predictor x4 is lnk. It can be observed that both x1 and x2 (i.e. the temperature and UV) are insignificant at 0.05 confidence level. This is consistent with the observations from section 5.3. The analysis was conducted using Minitab 17 software package. Figure 54 shows the normal probability plot and the plot of residuals versus predicted values. This plot shows a curve pattern of residuals versus fitted response variable values, which indicates that the linear model, as specified in (44), is not sufficient for modeling the relationship of series resistance, Rs and regressors; and that some transformation of the left hand-side of Equation (44) is necessary. The pattern was removed using Minitab's Box Cox optimal lambda transformation as shown in Figure 55. However, the ANOVA of the transformed data (Table 30) shows that only the time (x_4) and the intercept (constant) are significant.

This latter observation was in fact expected as we observed in section 5.3 that the increase in series resistance Rs (leading to eventual failure) results from continual thermal cycling over time rather than the effects of elevated temperature or higher dwell time at elevated temperature.
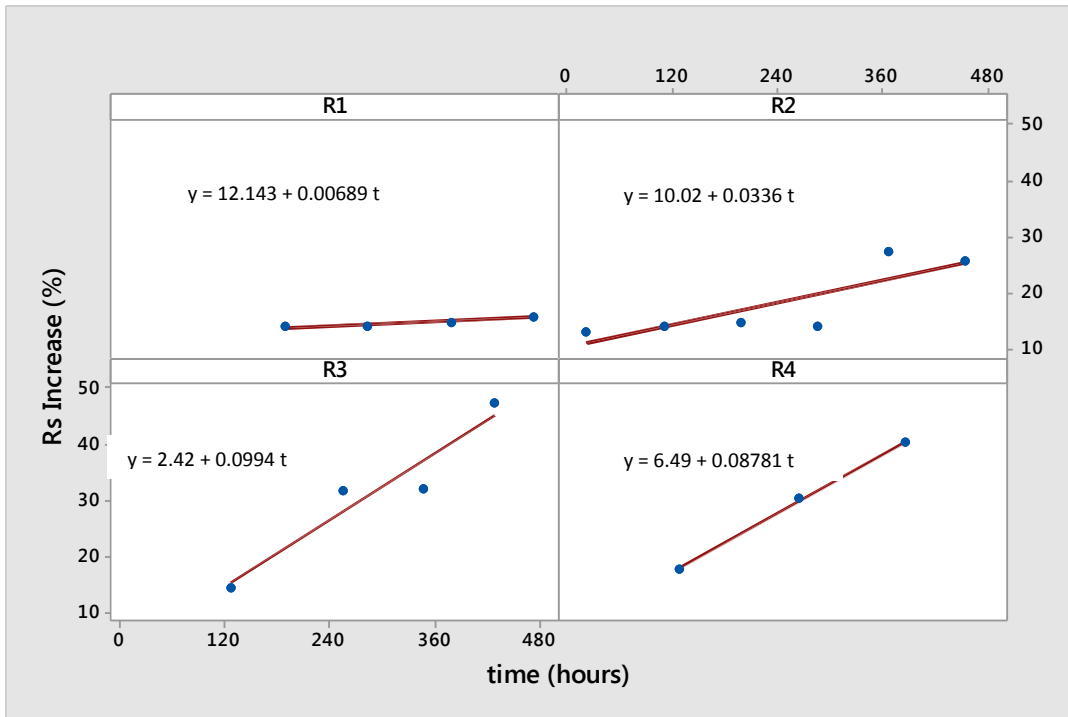
Figure 53: Linear Fits of the Average Increase in Rs for each Run Ri.

Table 29: Minitab Output for the Regression Model

Analysis of Variance

Source	DF	Adj SS	Adj MS	F-Value	P-Value
Regression	4	0.615656	0.153914	7.22	0.004
x1	1	0.000086	0.000086	0.00	0.951
x2	1	0.025094	0.025094	1.18	0.301
x3	1	0.092366	0.092366	4.33	0.062
x4	1	0.498111	0.498111	23.36	0.001
Error	11	0.234555	0.021323		
Total	15	0.850211			

Model Summary

S	R-sq	R-sq(adj)	R-sq(pred)
0.146025	72.41%	62.38%	35.70%

Coefficients

Term	Coef	SE Coef	T-Value	P-Value	VIF

Constant	0.5902	0.0365	16.17	0.000	
x1	0.0024	0.0377	0.06	0.951	1.00
x2	0.0409	0.0377	1.08	0.301	1.00
x3	-0.0785	0.0377	-2.08	0.062	1.00
x4	-0.1822	0.0377	-4.83	0.001	1.00

Regression Equation

y = 0.5902 + 0.0024 x1 + 0.0409 x2 - 0.0785 x3 - 0.1822 x4
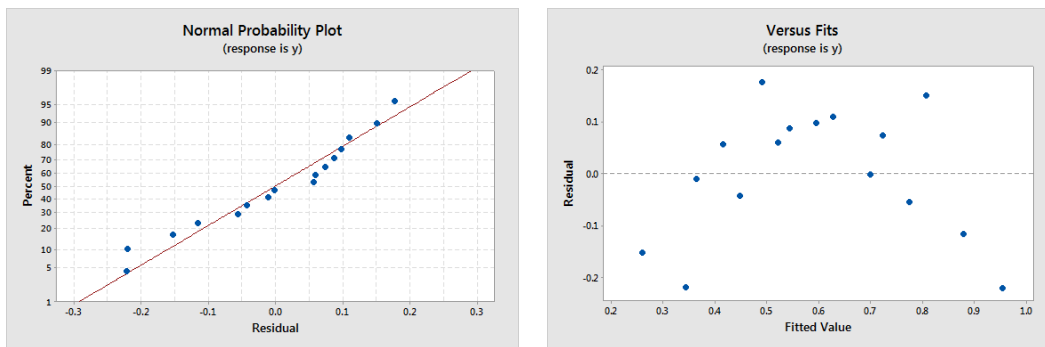
Figure 54: Linear Model Adequacy
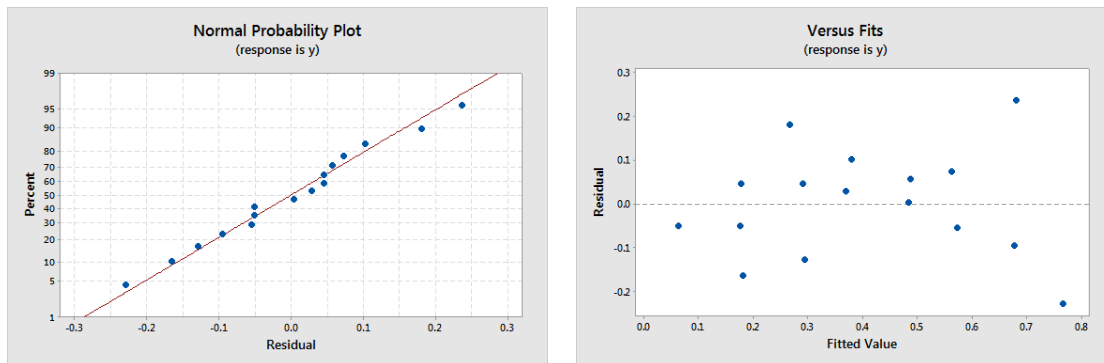
Figure 55: Adequacy Check of the Transformed Linear Model

Table 30: Minitab Output for the Transformed Regression Model

Analysis of Variance for Transformed Response

Source	DF	Adj SS	Adj MS	F-Value	P-Value
Regression	4	0.663813	0.165953	8.07	0.003
x1	1	0.000912	0.000912	0.04	0.837

153

x2	1	0.042147	0.042147	2.05	0.180
x3	1	0.040371	0.040371	1.96	0.189
x4	1	0.580384	0.580384	28.24	0.000
Error	11	0.226071	0.020552		
Total	15	0.889883			

Model Summary for Transformed Response

S	R-sq	R-sq(adj)	R-sq(pred)
0.143359	74.60%	65.36%	39.74%

Coefficients for Transformed Response

Term	Coef	SE Coef	T-Value	P-Value	VIF
Constant	0.4015	0.0358	11.20	0.000	
x1	0.0078	0.0370	0.21	0.837	1.00
x2	0.0530	0.0370	1.43	0.180	1.00
x3	-0.0519	0.0370	-1.40	0.189	1.00
x4	-0.1967	0.0370	-5.31	0.000	1.00

Regression Equation

$y^2 = 0.4015 + 0.0078\ x1 + 0.0530\ x2 - 0.0519\ x3 - 0.1967\ x4$

5.6   Conclusion

The findings of our experiments confirm that transmittance losses in crystalline

silicon PV modules are affected by UV and static temperature (dwell time at high

temperature). However, these losses did not contribute significantly to the

performance degradation of the test coupons over the length of the experiment. This

was primarily influenced by the increase in series resistance (Rs). This increase was

found to be affected by the dwell time at high temperature, i.e. static temperature;

which was established in the previous chapter.

CHAPTER VI

CONCLUSION AND FUTURE WORK

6.1   Conclusion

The objective of this research was to develop an approach to PV module lifetime

prediction. We focused on crystalline silicon PV modules operating under the dry and

hot climatic condition. Our study was carried out in three phases:

Phase I: Using field failure and performance data from PV systems installed in

Phoenix, Arizona, we developed a quantitative method for prioritizing failure modes

or mechanisms based on failure modes, effects, and criticality analysis (FMECA). This

quantitative FMECA is a new approach for the PV industry in the sense FMECA is

conventionally qualitative (thus subjective) in nature.

Phase II: Using field performance and weather data from a system installed in

Phoenix – AZ and monitored over nearly 11 years, we proposed a time series

approach to model environmental stress factors. Such model is crucial for designing

accelerated aging testing necessary for life prediction modeling. To develop and

validate our approach, we focused on a single stress factor of maximum

temperature.

Phase III: A two-step approach for lifetime prediction model was proposed based on

the findings from phases 1 & 2. First, we designed an (accelerated aging) experiment

intended to replicate the dominant failure modes or mechanisms identified in Phase

1. The experimental factors, as well as their levels, would normally be identified from

Phase 2. Our findings from that phase were used for temperature stress factor, and

existing literature was used for UV stress factor. The second step dealt with

conducting the actual experiment and analyzing the data.

For our case study, the increase in series resistance was found to be the major

contributor to module performance drop over the experimental period. Static

temperature seems to significantly affect the series resistance increase.

6.2   Significant Contributions

Key accomplishments resulting from this research study include the following:

(1) Developed technique for objectively prioritize failure modes or mechanisms as a function of field data and industry standardized practices

(2) Developed analytical tool to estimate environmental stress levels necessary for designing accelerated aging test for reliability prediction

(3) Developed analytical tools and design data for characterizing the factors involved in transmission decrease and series resistance increase of c-si module operating in a given climatic condition

(4) Developed analytical tools and design data for the prediction of series resistance increase or fill factor losses of c-si modules in hot and dry climatic conditions, major contributor to PV module performance degradation

6.3   Future Work

It is our hope that this study be a stepping stone for a bigger undertaking in the area. The approach proposed needs to be scaled to other climatic conditions, such as hot and humid, or temperate environments. Moreover, our study in phase 2 was more of an experimental study. It now needs to be expanded to include multiple stress factors. Such would require the application of multivariate time series concepts. Finally, the accelerated degradation experiment must be conducted over an extended time period with larger sample size. Due to the high reliability nature of PV modules, it is believed that a minimum of six (6) months experiment is required to obtain substantial drop of certain performance characteristics such as the short-circuit current (Isc), which was not affected during our experimental period. Moreover, the equipment limitations (for example, we could not cycle from below 25°C) greatly impacted the stress levels used, and thus the experimental data.

REFERENCES

Al-Radaideh, Q. A., and Al Nagi, E., "Using Data Mining Techniques to Build a Classification Model for Predicting Employees Performance", (IJACSA) International Journal of Advanced Computer Science and Applications, Vol. 3, No. 2, 2012

Agro, S., Galica, J., Holley, W. H., and Yorgensen, R.S., Case histories of EVA encapsulant discoloration in field modules, in: R. Noufi and H. Ullal (Eds.), 12th NREL Photovoltaics Program Review, AIP Conf. Proc. 306 (Am. Inst. Physics, Woodbury, NY, 1994), pp. 586-596

Aoki, Y., Okamoto, M., Masuda, A., & Doi, T. (2010). Module performance degradation with rapid thermal-cycling. Proceedings of Renewable Energy.

Atcitty, S., Granata J. E.,, Quintana, M. A., and Tasca, C. A., "Utility-Scale Grid-Tied PV Inverter Reliability Workshop Summary Report", Sandia Report SAND2011-4778, July 2011

Bagdonavicius, V., Haghighi, F., and Nikulin, M., "Statistical Analysis of General Degradation Path Model and Failure Time Data with Multiple Failure Modes", Communications in Statistics - Theory and Methods, 34: 1771-179, 2005

Berman, D., Biryukov, S., and Faiman, D., "EVA laminate browning after 5 years in a grid-connected, mirror-assisted, photovoltaic system in the Negev desert: effect on module efficiency", Solar Energy Materials and Solar Cells, 36 (1995) 421-432

Bowles, J. B., "An assessment of RPN prioritization in failure modes effects and criticality analysis", PROCEEDINGS Annual RELI ABILITY AND MAINTAINABILITY Symposium, 2003

Burgess, R. (2012, April 27). Sophisticated monitoring can increase value and extend the life of an array. Retrieved May 27, 2012, from http://www.renewableenergyworld.com/rea/news/article/2012/04/your-new-solar-array-actual-performancemay-vary

Burgess, R., "BOS Series: Your New Solar Array (Actual Performance May Vary)", Web Article, Renewable Energy World, http://www.renewableenergyworld.com/rea/news/article/2012/04/your-new-solar-array-actual-performance-may-vary, April 2012

Catelani, M., Ciani, L., Cristaldi, L., Faifer, M., Lazzaroni, M., and Rinaldi, P., "FMECA Technique on Photovoltaic Module", IEEE, 2011

Charki, A., Laronde, R., and Bigaud, D. (2013), "Accelerated degradation testing of a photovoltaic module", Journal of Photonic for Energy, Vol. 3, 2013

Chen, V., and Meeker, W. Q., (2008). Time series modeling of degradation due to outdoor weathering. Communications in Statistics—Theory and Methods, vol. 37, pp. 408-424.

Collins, E., Dvorack, M., Mahn, J., Mundt, M., and Quintana, M., "Reliability and availability analysis of a fielded photovoltaic system

Collins, E., Miller, S., Mundt, M., Stein, J., Sorensen, R., Granata, J., et al. (2009). A reliability and availability sensitivity study of a large photovoltaic system. IEEE Photovoltaic Specialists Conference (PVSC).

Credit Suisse. (February 2012). Equity Research—Solar Energy.

Cronin, A., Pulver, S., Cormode, D., Jordan, D., Kurtz, S., and Smith, R., "Measuring degradation rates of PV systems without irradiance data", Progress in Photovoltaics, Prog. Photovolt: Res. Appl. (2013)

Cuddalorepatta, G., Dasgupta, A., Sealing, S., Moyer, J., Tolliver, T., and Loman, J. (2006), "Durability of Pb-Free Solder Connection between Copper Interconnect Wire and Crystalline Silicon Solar Cells - Experimental Approach", IEEE CPMT APM Conference, Georgia Tech, Atlanta, March 2006

Cuddalorepatta, G., Dasgupta, A., Sealing, S., Moyer, J., Tolliver, T., Loman, J., "Durability of Pb-free Solder Connection between Copper Interconnect Wire and Crystalline Silicon Solar Cells - Experimental and Modeling Approach", ITHERM Conference, San Diego, CA, 2006

Cuddihy, E. F. (1986), "The Aging Correlation - Relative Humidity and Temperature", Flat-Plate Solar Array Project, DOE/JPL-1012-121, January 1986

Czanderna, A. W.; Pern, F. J. (1996) "Encapsulation of PV modules using Ethylene vinyl acetate copolymer as a pottant: a critical review." Solar Energy Materials and Solar Cells, 1996; 43: 101-181

Darling, S. B., You, F., Veselka, T., and Velosa, A., "Assumptions and the Levelized Cost of Energy for Photovoltaics", Energy & Environmental Science, Issue 9, 2011

Dasgupta, A. & Pecht, M. (1991). Material failure mechanisms and damage models. IEEE Transactions on Reliability, Vol. 40. No. 5.

Davis, K. O., Kurtz, S. R., Jordan, D. C., Wohlgemuth, J. H., and Hickman, N. S., "Multi-pronged analysis of degradation rates of photovoltaic modules and arrays deployed in Florida", Progress in Photovoltaics, Vol. 21, Issue 4, June 2013, P 702–712

Desombre, A. (1980). Methodology for a reliability study on photovoltaic modules. Proceedings of the 3rd European Commission PV Solar Energy Conference. Cannes, France. 741–745.

Dhere, N. (2005). Reliability of PV modules and balance-of-system components. IEEE Photovoltaic Specialists Conference (PVSC).

Dhere, N., Pethe, S., & Kaul, A. (2010). Photovoltaic module reliability studies at the Florida Solar Energy Center. IEEE International Reliability Physics Symposium.

Dobos, A. P., "An improved coefficient calculator for the California energy commission 6 parameter photovoltaic module model", Journal of Solar Energy Engineering, vol. 134, 2012

DOE/JPL 955720-80/1, "Low cost solar array project, engineering area", Quarterly report, October 1980

DOE/JPL/954328-7, "Measurement Techniques and instrumentations suitable for life-prediction testing of photovoltaic arrays", Interim Report, January 1978

Dumas, L. N. and Shumka, A., "Photovoltaic Module Reliability Improvement through Application Testing and Failure Analysis", IEEE TRANSACTIONS ON RELIABILITY, VOL. R-31, No. 3, AUGUST 1982

Dumbleton, D., and Haillant, O., Environmental Durability of PV Modules - A Model for Accelerated Testing", 37th IEEE Photovoltaic Specialists Conference PVSC 37, Seattle, Washington, June 2011

Dunham, M. H.,"Data Mining: Introductory and Advanced Topics", Pearson Education , 2003

Eguchi, Y. (2011). Evaluation and analysis of 15 years exposure PV module. Photovoltaic Module Reliability Workshop.

Emery, K., "Nondestructive Performance Characterization Technique for Module Reliabillity ", National Center for Photovoltaics and Solar Program Review Meeting, NREL/CP-520-33573, Denver, Colorado, March 2003

European Photovoltaic Industry Association (EPIA). (May 2012). Global market outlook for photovoltaics until 2016.

Gaines, G. B., Thomas, R. E., Derringer, G. C., Kistler, C. W., Bigg, D M., and Carmichael, D. C., "Methodology for designing accelerated aging tests for predicting life of PV Arrays", Flat-Plate Solar Array Project, ERDA/JPL-954328-77/1, February 1977

Gardner, M., and Bieker, J., "Data Mining Solves Tough Semiconductor Manufacturing Problems", KDD 2000, Boston, MA

Gerischer, H. (1977). On the stability of semiconductor electrodes against photodecomposition. Journal of Electroanalytical Chemistry, 82:133.

Gonzalez, C., Liang, R., & Ross, R. (1985). Predicting field performance of photovoltaic modules from accelerated thermal and ultraviolet aging data. Proceedings of the International Solar Energy Society Meeting. Montreal, Canada.

Gonzalez, C. C., Liang, R., and Ross Jr., R. G. (1985), "Predicting Field Performance of Photovoltaic Modules from Accelerated Thermal and Ultra-violet Aging Data", Flat-Plate Solar Array Project, Jet Propulsion Laboratory, 1985

Gorjian, N., Ma, L., Mittinty, M., Yarlagadda, P., and Sun, Y., "A Review on Degradation Models in Reliability Analysis", Proceedings of the 4th World Congress on Engineering Asset Management, Athens, Greece, September 2009

Granata, J., Boyson, W., Kratochvil, J., & Quintana, M. (2009). Long-term performance and reliability assessment of 8 PV arrays. IEEE Photovoltaic Specialists Conference.

Greene, M. G. (1986). Corrosion Engineering. New York: McGraw Hill.

Green, A. M. , "Solar Cells: Operating Principles, Technology and System Applications," Technical Report, University of New South Wales, Kensington, NSW, 1998.

Gu, X. (2011), "Effects of key environmental factors on degradation of PV polymeric materials", Atlas/NIST workshop on Photovoltaic Materials durability, Gaithersburg, MD, October 27-28, 2011

Hacke, P. (2012). PID—Considerations for a standardized test for potential induced degradation of crystalline silicon PV modules. Photovoltaic Module Reliability Workshop. Golden, CO. Presentation available at www.nrel.gov/docs/fy12osti/54581.pdf

Hacke, P., Terwilliger, K., Smith, R., Glick, S., Pankow, J., Kempe, M., et al. (2011). System voltage potential-induced degradation mechanisms in PV modules and methods for test. IEEE Photovoltaic Specialists Conference.

Hacke, P., Terwilliger, K., Glick, S., Trudell, D., Bosco, N., Johnston, S., and Kurtz, S. (2010), "Test-to-failure of crystalline silicon modules", IEEE, 2010

Hacke, P., Smith, R., Terwilliger, K., Glick, S., Jordan, D., Johnston, S., Kempe, M., and Kurtz, S. (2012), "Testing and Analysis for Lifetime Prediction of Crystalline Silicon PV Modules Undergoing Degradation by System Voltage Stress", IEEE Photovoltaic Specialists Conference, Austin, Texas, June 2012

Han, J., and Kamber, M., "Data Mining: Concepts and Techniques", 2nd ed., Morgan Kaufmann, 2006

Herrmann, W., Bogdanski, N., Reil, F., Kohl, M., Weiss, K., Assmus, M., et al. (2010). PV module degradation caused by thermo-mechanical stress: Real impacts of outdoor weathering versus accelerated testing in the laboratory. SPIE.

Hoffman, A. & Ross, R. (June 1978). Environmental qualification testing of terrestrial solar cell modules. IEEE Photovoltaic Specialists Conference.

Hoffmann, S. & Koehl, M. (2012). Effect of humidity and temperature on the potential-induced degradation. Progress in Photovoltaics: Research and Applications.

Hoffman, A. R., Griffith, J. S., and Ross Jr., R. G., "Qualification Testing of Flat-Plate Photovoltaic Modules", IEEE TRANSACTIONS ON RELIABILITY, VOL. R-31, NO. 3, AUGUST 1982

Holley, W. H., Agro, S., Galica, J. P., Thoma, L. A., Yorgensen, R. S., "Investigation into the causes of browning in EVA encapsulated flat plate PV modules", 24th IEEE PVSC, 1994, pp. 893-896.

Holley, W., Agro, S. Galica, J., & Yorgensen, R. (1996). UV stability and module testing of non-browning experimental PV encapsulant. IEEE Photovoltaic Specialists Conference.

Holley, W.W. and Agro, S.C., "Advanced EVA-Based Encapsulants, "Final Report January 1993-June 1997", September 1998, NREL/SR-520-25296 (US Dept of Energy contract No. DE-AC36-83CH10093)

IEA-PVPS-TASK2. (December 2007). Cost and performance trends in grid-connected PV systems. International Energy Agency Photovoltaic Power Systems Programme.

IEA (2014). Technology Roadmap. Solar Photovoltaic Energy. International Energy Agency 1974-2014

IEC 61215, "Crystalline silicon terrestrial photovoltaic (PV) modules – Design qualification and type approval", International Standard, second edition, 2005

IEC 61730, "Photovoltaic (PV) module safety qualification", International Standard, 2004-10

IEC 61646, "Thin-film terrestrial photovoltaic (PV) modules – Design qualification and type approval", International Standard, second edition, 2008

IEC 60812, "Analysis techniques for system reliability – Procedure for failure mode and effects analysis (FMEA)", 2nd ed., 2006-01

IEC 61853-1. (2011). Photovoltaic (PV) module performance testing and energy rating - Part 1: irradiance and temperature performance measurements and power rating.

IEC 68153-2. (Draft). Photovoltaic (PV) module performance testing and energy rating - Part 2: Spectral response, incidence angle and module operating temperature measurements.

Ishii, T., Takashima, T., & Otani, K. (2011). Long-Term Performance Degradation of Various Kinds of Photovoltaic Modules Under Moderate Climatic Conditions. Progress in Photovoltaics: Research and Applications, 19:170.

Jet Propulsion Laboratory (JPL). (1986). Flat-Plate Solar Array Project, Volume VI, Final Report.

Jordan, D. and Kurtz, S. (October 2011). Photovoltaic Degradation Rates - An Analytical Review. Progress in Photovoltaics: Research and Applications.

Jordan, D. C., and Kurtz, S. R., "PV Degradation Rates – An Analytical Review", NREL/JA-5200-51664, June 2012

Jorgensen, G., Terwilliger, K., DelCueto, J., Glick, S., Kempe, M., Pankow, J., et al. (2006). Moisture transport, adhesion, and corrosion protection of PV module packaging materials. Solar Energy Material & Solar Cells, 90:2739.

Kempe, M. D., "Accelerated UV Test Methods for Encapsulants of Photovoltaic Modules", 33rd IEEE Photovoltaic Specialists Conference, San Diego, CA, May 2008

Kempe, M. (2008). Accelerated UV test methods and selection criteria for encapsulants of photovoltaic modules. IEEE Photovoltaic Specialists Conference.

Kempe, M. D., "Ultraviolet light test and evaluation methods for encapsulants of photovoltaic modules", Solar Energy Materials & Solar Cells 94 (2010) 246–253

Kenny, R. P., Dunlop, E. D., Ossenbrink, H. A., and Mullejans, H., " A practical method for the energy rating of c-Si photovoltaic modules based on standard tests", Prog. Photovolt: Res. Appl. 2006; 14:155–166

King, D., Boyson, W., & Kratochvil, J. (2002). Analysis of factors influencing the annual energy production of photovoltaic systems. IEEE Photovoltaic Specialists Conference.

King, D. L., Boyson, W. E., and Kratochvil, J. A., "Photovoltaic Array Performance Model", Sandia National Laboratories, SAND2004-3535, August 2004

King, D. L.; Quintana, A. M.; Kratochvil, A. J.; Ellibee, E. D.; Hansen, R. B. (2000). "Photovoltaic Module Performance and Durability Following Long-term Field Exposure", Progress in Photovoltaics: Research and Applications. Prog. Photovolt: Res. Appl. 2000; 8:241–256.

Klemchuk, P., Ezrin, M., Lavigne, G., Holley, W., Galica, J., and Argo, S., "Investigation of the degradation and stabilization of EVA-based encapsulant in field-aged solar energy modules," Polymer Degradation and Stability, Vol 55, pp 347-365 (1997).

Kohl, M. (2011). From climate data to accelerated test conditions. Photovoltaic Module Reliability Workshop.

Köhl, M. (2011), "Is it possible to design accelerated service life tests for PV modules?", EMPA Workshop Durability of Thin Film Solar Cells, April 2011

Kohl, M. (2009). Progress towards service life assessment of PV modules. ATCAE.

Kolyer, J. M., and Mann, N. R., "Interim Report on Accelerated/Abbreviated Test Methods", Flat-Plate Solar Array Project, ERDA/JPL/954458-77/7, October 1977

Kolyer, J. M., Mann, N. R., and Farrar, J., (1978). Final report on accelerated/abbreviated test methods for predicting life of solar cell encapsulants to Jet Propulsion Laboratory. DOE/JPL/954458-10

Kopp, E. S., Lonij, V. P., Brooks, A. E., Hidalgo-Gonzalez, P. L., and Cronin, A. D., "I–V curves and visual inspection of 250 PV modules deployed over 2 years in Tucson", 38th IEEE Photovoltaic Specialists Conference PVSC, Austin, Texas, June 2012

Kuitche, J. M., Pan, R., and TamizhMani, G., "Investigation of Dominant Failure Mode(s) for Field-Aged Crystalline Silicon PV Modules Under Desert Climatic Conditions", IEEE Journal of Photovoltaics, vol. 4, No. 3, May 2014

Kuitche, J., Pan, R., and Tamizhmani, G., (2009). Some reliability and reliability testing issues in photovoltaic energy industry: a review. The 15th ISSAT

International Conference on Reliability and Quality in Design, San Francisco, CA.

Kuitche, J., TamizhMani, G., and Pan, R. (2011). Failure modes effects and criticality analysis (FMECA) approach to the crystalline silicon photovoltaic module reliability assessment. SPIE.

Kuitche, J. M., TamizhMani, G., and Pan, R., "Statistical Analysis of 10+ years Field Exposed c-Si Modules Performance Degradation", SPIE, 2012

Kuhn, H., and Funcell, A., "The Thresher Test Crystalline silicon terrestrial photovoltaic (PV) modules long term reliability and degradation," second edition, 2005-04

Kurtz, S. & Granata, J. (2009). Photovoltaic reliability R&D toward a solar-powered world. SPIE.

Kuznetsova, V., Gaston, R., Bury, S., & Strand, S. (2009). Photovoltaic reliability model development and validation. IEEE Photovoltaic Specialists Conference.

Laronde, R., Charki, A., & Bigaud, D. (April 2010). Reliability of photovoltaic modules based on climatic measurement data. International Journal of Metrology and Quality Engineering.

Lee, J., Elmore, R., and Jones, W., "Statistical Modeling of Photovoltaic Reliability Using Accelerated Degradation Techniques", PV Module Reliability Workshop, Golden, Colorado, February 2011

Longrigg, P. (1989). Reliability analysis of photovoltaic modules. Solar Cells, 26:241.

Lu, C. Joseph and Meeker, William Q. (1993), "Using Degradation Measures to Estimate a Time-to-Failure Distribution", Technometrics, Vol. 35, No. 2, May, 1993

McIntosh, K. R., Powell, N. E., Norris, A. W., Cotsell, J. N., and Ketola, B. M., "The effect of damp-heat and UV aging tests on the optical properties of silicone and EVA encapsulants", Prog. Photovolt: Res. Appl. 2011; 19:294–300

McMahon, T. J., "Accelerated Testing and Failure of Thin-film PV Modules", Progress in Photovoltaics: Research and Applications. 2004; 12:235–248 (DOI: 10.1002/pip.526)

McMahon, T., Jorgensen, G., Hulstrom, a. R., King, D., & Quintana, M. (April 2000). Module 30 year life: What does it mean and is it predictable/achievable? National Center for Photovoltaics Program Review Meeting. Denver, CO, April 2000.

Meeker, W. Q. and Escobar, L. A. (1998), "Statistical Methods for Reliability Data", John Wiley & Sons.

Meeker, W. Q., Escobar, L. A., and Lu, C. J. (1998), "Accelerated Degradation Tests: Modeling and Analysis", Technometrics, May 1998, Vol. 40, No. 2, pp. 89-99

Mehmed Kantardzic, Data Ming: Concepts, Models, Methods, and Algorithms, 2nd ed., 2011

Meier, D. L., Good, E. A., Garcia, R. A., Bingham, B. L., Yamanaka, S., Chandrasekaran, V., and Bucher, C., "Determining components of series resistance from measurements on a finished cell", IEEE, 2006

Meydbray, Y., Wilson, K., Brambila, E., Terao, A., and Daroczi, S., 2007, "Solder Joint Degradation in High Efficiency All Back Contact Solar Cells," Proceedings of the 22th European Photovoltaic Solar Energy Conference, Milan, Italy, September 3–7.

Meydbray, Y., Wilson, K., Brambila, E., Terao, A., & Daroczi, S. (2008). Solder joint degradation in high efficiency all back contact solar cells. IEEE Photovoltaic Specialists Conference.

Meyer, L. E., and Van Dyk, E. E., "Assessing the Reliability and Degradation of Photovoltaic Module Performance Parameters," IEEE Transaction on Reliability, Vol. 53, No. 1, March 2004.

MIL-STD-1629A, "Procedures for Performing a Failure Mode, Effects and Criticality Analysis, Military Standard, November 1980

Monroe, E., and Pan, R., (2009). Knowledge-based reliability assessments for time-varying climates. Quality and Reliability Engineering International, vol. 25, no. 1, pp. 111-124.

Murthy, D., & Blishchke, W. (2000). Reliability modeling, prediction, and optimization. John Wiley & Sons.

Noel, G. T., Sliemers, F. A., Deringer, G. C., Wood, V. E., Wilkes, K. E., Gaines, G. B., and Carmichael, D. C., (1978) "Measurement techniques and instruments suitable for life-prediction testing of photovoltaic Arrays", Interim report, DOE/JPL/954328-7, January 1978

Noufi, R., Frank, A., & Nozik, A. (1981). Stabilization of n-type silicon photoelectrodes to surface oxidation in aqueous electrolyte solution and mediation of oxidation reaction by surface-attached organic conducting polymer. Journal of the American Chemical Society, 103:1849.

NREL. (2012). Proposed test protocols - IEC 61215 on steroids. Photovoltaic Module Reliability Workshop.

Olakonu, K., Belmont, J., Tatapudi, S., Kuitche, J., TamizhMani, G. (2014). Degradation and Failure Modes of 26-Year-Old 200 kW Power Plant in a Hot-Dry Desert Climate . 40th IEEE Photovoltaic Specialist Conference (PVSC40)

Oreski, G. and Wallner, G.M., "Evaluation of the aging behavior of ethylene copolymer films for solar applications under accelerated weathering conditions", Solar Energy 83 (2009) 1040–1047

Osterwald, C. R. (2008), "Terrestrial Photovoltaic Module Accelerated Test-to-Failure Protocol", Technical Report, NREL/TP-520-42893, March 2008

C.R. Osterwald, C. R., and T.J. McMahon, T. J., "History of Accelerated and Qualification Testing of Terrestrial Photovoltaic Modules: A Literature Review," Progress in Photovoltaics, vol. 17, no. 11-33, Oct. 2008.

Osterwald, C. & McMahon, T. (2009). History of accelerated and qualification testing of terrestrial photovoltaic modules: A literature review. Progress in Photovoltaics: Research and Applications, 17:11-33.

Otth, D. H. and Ross Jr., R. G. (1983), "Assessing photovoltaic module degradation and lifetime from long term environmental tests", Proceedings Institute of Environmental Sciences, 1983, pp. 121-126

Otth, D. & Ross, R. (April 1983). Assessing photovoltaic module degradation and lifetime from long-term environmental tests. Proceedings of the Institute of Environmental Sciences 29th Annual Meeting. Los Angeles, CA.

Packard, C. E., Wohlgemuth, J. H., and Kurtz, S. R., "Development of a Visual Inspection Data Collection Tool for Evaluation of Fielded PV Module Condition", National Renewable Energy Laboratory (Technical Report: NREL/TP-5200-56154), August 2012

Pan, R. and Crispin, T. (2010), "A hierarchical modeling approach to accelerated degradation testing data analysis: A case study", Quality and Reliability Engineering International, 2010

Pan, R., Kuitche, J. M., and TamizhMani, G., "Degradation Analysis of Solar Photovoltaic Modules: Influence of Environmental Factor", RAMS, 2011

Park, N., Jeong, J., and Han C. (2014), "Estimation of the degradation rate of multi-crystalline silicon photovoltaic module under thermal cycling stress", Microelectronics Reliability, Article in press, 2014

Parretta, A., Bombace, M., Graditia, G., and Schioppo, R., "Optical degradation of long-term, field-aged c-Si photovoltaic modules", Solar Energy Materials & Solar Cells 86 (2005) 349–364

Peike, C., Kaltenbach, T., Weib, K. A., Koehl, M., "Non-destructive degradation analysis of encapsulants in PV modules by Raman Spectroscopy," Solar Energy Materials & Solar Cells 95 (2011) 1686 – 1693

Pern, F.J., "A Comparative Study of Solar Cell Performance Under Thermal and Photothermal Tests," Proc. PV Performance and Reliability Workshop, L. Mrig, ed., NREL/CP-411-5148, Golden, CO: National Renewable Energy Laboratory, Sept. 1992, pp. 327-344.

Pern, F.J., "Ethylene-vinyl acetate (EVA) encapsulants for photovoltaic modules: Degradation and discoloration mechanisms and formulation modifications for improved photostability", Die Angewandte Makromolekulare Chemie, 252 (1997), pp. 195–216

Pern, F.J., and Czanderna, A. W., "Characterization of ethylene vinyl acetate (EVA) encapsulant: Effects of thermal processing and weathering degradation on its discoloration," Solar Energy Materials and Solar Cells 25 (1992) pp. 3-23

Pern, F.J., and A. W. Czanderna, A.
W., "EVA degradation mechanisms simulating those in PV modules," American Institute of Physics, Proc. 268, pp. 445–452, (1992)

Petersen, R. C. and Wohlgemuth, J. H., "STABILITY OF EVA MODULES", IEEE, 1991

Photovoltaic Systems Divisions, "Module durability research at Sandia", Highlights of Sandia's Photovoltaic Program, Sandia National Laboratories, vol. 3, 1999

Pingel, S., Frank, O., Winkler, M., Daryan, S., Geipel, T., Hoehne, H., et al. (2010). Potential induced degradation of solar cells and panels. IEEE Photovoltaic Specialists Conference.

Polverini, D., Field, M., Dunlop, E., and Zaaiman, W.," Polycrystalline silicon PV modules performance and degradation over 20 years", Progress in Photovoltaics: Research And Applications, Prog. Photovolt: Res. Appl. (2012)

Quintana, M. A., King, D. L., Hosking, F. M., Kratochvil, J. A., Johnson, R. W., and Hansen, B. R., "Diagnostic Analysis of Silicon Photovoltaic Modules after 20-Year Field Exposure", IEEE, 2000

Quintana, M. A., King, D. L., McMahon, T. J., and Osterwald, C. R., 2002, "Commonly Observed Degradation in Field-Aged Photovoltaic Modules," Conference Record of the 29th IEEE Photovoltaic Specialists Conference, New Orleans, LA, May 19–24, pp. 1436–1439.

Quintana, M. A., and S. R. Kurtz, S. R., "Reliability R&D - DOE program review", Austin – Texas, April 2008
Raghuraman, B., Lakshman, V., Kuitche, J., Shisler, W., TamizhMani, G., and Kapoor, H., "An overview of smud's outdoor photovoltaic test program at arizona state university", IEEE 4th World Conference on Photovoltaic Energy Conversion (WCPEC4), Hawaii, May 2006

Rausand, M., "System Reliability Theory", 2nd ed., 2004

Reliawiki.Com. (n.d.). Introduction to accelerated life testing. Retrieved from http://reliawiki.com/index.php/Introduction_to_Accelerated_Life_Testing

Revie, R. W. (2000). Uhlig's corrosion handbook. New York: John Wiley & Sons.

Ross Jr., R. G. (1982), "Photovoltaic Array Reliability Optimization", IEEE TRANSACTIONS ON RELIABILITY, VOL. R-31, NO. 3, AUGUST 1982

Ross, R. (December, 1982). Proceedings of the Flat-Plate Solar Array Project Research Forum on Quantifying Degradation. Jet Propulsion Laboratory (Document 5101-231; DOE/JPL-1012-89).

Ross Jr., R. G. (1983), "Time-Integration of Environmental Loads and Stresses for Correlating Field Exposure and Accelerated Testing", Flat-Plate Solar Array Project, Jet Propulsion Laboratory, 1983

Ross Jr., R. G. (November 1984). "Reliability research toward 30-year-life photovoltaic modules", Proceedings of the 1st International Photovoltaic Science and Engineering Conference. Kobe, Japan.

Ross Jr., R. G., "Crystalline-silicon reliability lessons for thin-film modules", Jet Propulsion Laboratory, Pasadena, California, 1985

Ross Jr., R. G. "FSA Engineering & Reliability Development Methods — Can They be Applied Today?", InterSolar meeting, San Francisco, California, July 2012

Ross Jr., R. G. and Smokler, M. I. (1986) "Flat-plate solar array project, final report", DOE/JPL-1012-125, vol. VI: Engineering Sciences and Reliability, 11 years of Progress, October 1986

Sakamoto, S., and Oshiro, T., "Dominant degradation modes of crystalline silicon photovoltaic modules manufactured in 1990's", 20th European Photovoltaic Solar Energy Conference, Barcelona, Spain, June 2005

Sample Tony, "Failure modes and degradation rates from field-aged crystalline silicon modules", NREL Reliability Workshop, 2011

Sample, T. (2011). Failure modes and degradation rates from field-aged crystalline silicon modules. Photovoltaic Module Reliability Workshop.

SEMATECH, "Failure Mode and Effects Analysis (FMEA): A Guide for Continuous Improvement for the Semiconductor Equipment Industry", Technology Transfer #92020963B-ENG, September 1992

Shioda, T., "UV accelerated test based on analysis of field exposed PV modules", Proceedings of SPIE Vol. 8112 81120I-1, 2011

Shigekuni, T., & Kumano, M. (1997). Yellowing reaction in encapsulant of photovoltaic modules. IEEE Photovoltaic Specialists Conference.

Silverman, T., Bosco, N., & Kurtz, S. (2012). Relative lifetime prediction for CPV die-attach layers. IEEE Photovoltaic Specialists Conference.

Singh, J., "Investigation of 1,900 Individual Field Aged Photovoltaic Modules for Potential Induced Degradation (PID) in a Positive Biased Power Plant", Master Thesis, ASU, December 2011

Singh, J., Belmont, J., and TamizhMani, G., "Degradation Analysis of 1900 PV modules in a Hot-Dry Climate: Results after 12 to 18 years of field exposure", IEEE, 2012

Standard & Poor's. (November 2009). Methodology and assumptions on risks for utility-scale solar photovoltaic projects.

TamizhMani, G. and Kuitche, J. (2013). "Accelerated lifetime testing of photovoltaic modules", Solar America Board for Codes and Standards, www.solarabcs.org, July 2013

TamizhMani, G., and Kuitche, J. M., "Reliability, Standards and Certification of Photovoltaic Modules", Tutorial, 34th IEEE Photovoltaic Specialists Conference PVSC 34, Philadelphia, Pennsylvania, June 2009

TamizhMani, G., Li, B., Arends, T., Kuitche, J., Raghuraman, B., Shisler, W., Farnsworth, K., Gonzales, J., Voropayev, A., Symanski, P., "Failure Analysis of Design Qualification Testing: 2007 vs. 2005", Proceedings of the 33rd IEEE Photovoltaic Specialists Conference, San Diego, CA – USA, 2008

TamizhMani, G., Li, B., Arends, T., Kuitche, J., Raghuraman, B., Shisler, W., Farnsworth, K., and Voropayev, A., (2010). Failure analysis of module design qualification testing – III: 1997-2005 vs. 2005-2007 vs. 2007-2009 (extended abstract). The 35th IEEE Photovoltaic Specialists Conference, June 20-25, 2010, Waikiki, Hawaii.

TamizhMani, G., Li, B., Arends, T., Shisler, W., Voropayev, A., Parker, D., et al. (2012). Failure rate analysis of module design qualification testing - IV: 1997-2005 vs. 2005-2007 vs. 2007-2009 vs. 2009-2011. IEEE Photovoltaic Specialists Conference.

TamizhMani, G. (February 2012). 12-18-year-old PV power plants in Arizona: Potential induced degradation analysis of 1900 individual modules. Photovoltaic Module Reliability Workshop.

Tang, Y., Raghuraman, B., Kuitche, J., TamizhMani, G., Backus, C. E., and Osterwald, C., "An evaluation of 27+ years old photovoltaic modules operated in a hot-desert climatic condition", IEEE 4th Energy Conversion (WCPEC4), Hawaii, May 2006

Tatapudi, S. (December 2012). Potential induced degradation (PID) of pre-stressed photovoltaic modules: Effect of glass surface conductivity disruption. MS Thesis, Arizona State University.

Tseng, S. T., Hamada, M. S., and Chiao, C. H. (1995), "Using degradation data from a fractional factorial experiment to improve fluorescent lamp reliability", Journal of Quality Technology 27, 363-369.

Tseng, S. T., Tang, J. and Ku, I. H. (2003), "Determination of burn-in parameters and residuals life of highly reliable products", Naval Research Logistics 50, 1-14

Tucker, R. T., Kuitche, J. M., Arends, T., Tamizh-Mani, G., and Hammond, R., "Nine (9)-year review of field performance of EVA-based encapsulants", 21st European Photovoltaic Solar Energy Conference, Dresden - Germany, September 2006

U.S. Department of Energy. (February 2012). Chapter 4: Photovoltaics: Technologies, Cost and Performance. SunShot Vision Study, pp. 68-96. Retrieved from www1.eere.energy.gov/solar/pdfs/47927_chapter4.pdf Degradation Studies. Progress in Photovoltaics, 16:419

Van Dyk, E. E., and Meyer, E. L., "Analysis of the effect of parasitic resistances on the performance of photovoltaic modules", Renewable Energy 29 (2004) 333–344

Vazquez, M., and Rey-Stolle,I., "Photovoltaic Module Reliability Model Based on Field Degradation Studies," Progress in Photovoltaics: Research and Applications Prog. Photovolt: Res. Appl. 2008; 16:419–433.

Veldman, D., Bennett, I. J., Brockholz, B., and De Jong, P. C., "Non-destructive testing of crystalline silicon photovoltaic back-contact modules", IEEE, 2011

Wang, X., Kurdgelashvilib, L., Byrneb, J., and Barnetta, A., "The value of module efficiency in lowering the levelized cost of energy of photovoltaic systems", Renewable and Sustainable Energy Reviews, RSER-1531, 2011

Web article http://energy.sandia.gov/?page_id=11833

Weka software, "Waikato Environment for Knowledge Analysis," Version 3.6.8, The University of Waikato, Hamilton – New Zealand, 1999-2012

Wohlgemuth, J. (1993). Testing for module warranties. Photovoltaic Performance and Reliability Workshop. Golden, CO.

Wohlgemuth, J. (2003). Long-term photovoltaic module reliability. NCPV and Solar Program Review Meeting 2003. NREL/CD-520-33586. 179-183.[9]. (NREL/CD-520-33586).

Wohlgemuth, J. (2008). Reliability of PV systems. SPIE. San Diego, CA.

Wohlgemuth, J. (2011). Tutorial/short course on reliability: PV cells, modules, and systems. IEEE Photovoltaic Specialists Conference. Seattle, WA.

Wohlgemuth, J., "How Standards Control Module Design for Better or Worse," in NREL 2011 PV Module Reliability Workshop, Golden, Feb. 2011.

Wohlgemuth, J. H., "Reliability: PV cells, modules, and systems", Tutorial, 37th IEEE Photovoltaic Specialists Conference PVSC 37, Seattle, Washington, June 2011

Wohlgemuth, J. H., "Use of field survey result to identify failure modes", Atlas/NIST Workshop on Photovoltaic Material Durability, Gaithersburg, Maryland, October 2011

Wohlgemuth, J. (2012a). IEC 61215: What it is and isn't. Photovoltaic Module Reliability Workshop (PVMRW).

Wohlgemuth, J. (September 2012b). Standards for PV modules and components - Recent developments and challenges. 27th European Photovoltaic Solar Energy Conference and Exhibition (EU PVSEC). (2012). Frankfurt, Germany: September 24-28, 2012. NREL Report number: NREL/CP-5200-56531.

Wohlgemuth, J., Cunningham, D., Amin, D., Shaner, J., Xia, Z., & Miller, J. (2008). Using accelerated tests and field data to predict module reliability and lifetime. Proceedings of EUPVSEC.

Wohlgemuth, J., Cunningham, D., Monus, P., Miller, J., & Nguyen, A. (2006). Long term reliability of photovoltaic modules. Proceedings of the 4th World Conference on Photovoltaics.

Wohlgemuth, J. H., Cunningham, D. W., Nguyen, A. M., Miller, J., "Long Term Reliability of PV Modules," Proceedings of the 20th European Photovoltaic Solar Energy Conference, Barcelona, Spain, 2005

Wohlgemuth, J. H. and Kurtz S., "Using Accelerated Testing to Predict Module Reliability", 37th IEEE Photovoltaic Specialists Conference PVSC 37, Seattle, Washington, June 2011

Wohlgemuth, J. H., and Kurtz, S., "Reliability testing beyond qualification as a key component in photovoltaic's progress toward grid parity", IEEE International Reliability Physics Symposium proceedings, January 2011, pp. 5E.3.1-5E.3.6

Wohlgemuth, J. H. and Kurtz S., "Reliability Testing beyond Qualification as a Key Component in Photovoltaic's Progress toward Grid Parity," IEEE International Reliability Physics Symposium, Feb. 2011.

Wohlgemuth, J. & Kurtz, S. (April 2011). Reliability testing beyond qualification as a key component in photovoltaic's progress toward grid parity. IEEE International Reliability Physics Symposium. Monterey, CA.

Wrighton, A. J. (1977). Thermodynamic potential for the anodic dissolution of n-type semiconductors. Journal of the Electrochemical Society, 124:1706.

Xia, Z., Wohlgemuth, J., and Cunningham, D. (2009), "A Lifetime Prediction of PV Encapsulant and Backsheet via Time Temperature Superposition Principle", IEEE Photovoltaic Specialists Conference.

Yang, G., Life Cycle Reliability Engineering, John Willey & Sons, 2007, pp 208-210

Yang, G. (2009), "Accelerated Degradation Testing and Analysis", Tutorial, Annual Reliability and Maintainability Symposium, 2009

Yang, K. and Xue, J. (1996), "Continuous state reliability analysis", Proc. Annual Reliability and Maintainability Symp, 1996, pp 251 – 257

Yu, H. F. and Tseng, S. T. (2002), "Designing a screening experiment for highly reliable products", Naval Research Logistics 49, 514-526.

Zuo, M.J.; Renyan Jiang; Yam, R. (1999), "Approaches for reliability modeling of continuous-state devices", IEEE transactions on reliability, Vol. 48, No. 1, pp. 9-18, March 1999

APPENDIX A

A PV POWER PLANT VISUAL INSPECTION CHECKLIST

[A detailed report titled "Development of a Visual Inspection Data Collection Tool for Evaluation of Fielded PV Module Condition" on the checklist has been developed in 2012 by NREL (Packard, Wohlgemuth, & Kurtz, 2012) and it can be downloaded from the following website by using the form with the report title shown above: http://nrelpubs.nrel.gov/Webtop/ws/nich/www/public/SearchForm]

Documentation of module condition

Date _____ Name of data recorder_____

Location _____

Latitude_____ Longitude _____ Altitude _____

1. System Data

System design: ☐ single module ☐ multiple modules (a.) ☐ unknown

    (a.) Multiple module system:

      Module location/number in a series string (from negative) _____

      # of modules in series (string) _____ # of strings in parallel (array) _____

      # of bypass diodes_____ # of modules per bypass diode _____

System Bias: ☐ open circuit ☐ resistive load ☐ max. power tracked   ☐ short circuit

      ☐ unknown

System Grounding: ☐ grounded (a.)   ☐ not grounded   ☐ unknown

   (a.) ☐ negative   ☐ positive   ☐ center of string   ☐ unknown

BEGIN INSPECTION AT BACK SIDE OF MODULE

2. Module Data

Technology: ☐ mono Si ☐ multi Si ☐ a–Si ☐ CdTe ☐ CIGS/CIS

      ☐ other: _____

Certification: ☐ unknown ☐ UL 1703 ☐ IEC 61215 ☐ IEC 61646 ☐ IEC 61730

      ☐ other: _____

Estimated deployment date _____

Photo taken of nameplate: ☐ yes ☐ no

Manufacturer _____

Model # _____

Serial # _____

Installation Site/Facility Serial # _____

Width _____cm Length _____cm

Nameplate: ☐ nameplate missing

    P_{max} _____ V_{oc} _____ I_{sc} _____

    Sys Volt_____ V_{max} _____ I_{max} _____

    Bypass diode, I_r _____

    Series fuse _____

3. Rear-side Glass: ☐ not applicable ☐ applicable

Damage: ☐ no damage ☐ small, localized ☐ extensive

Damage Type (mark all that apply):
☐ crazing or other non--crack damage
☐ shattered (tempered) ☐ shattered (non-tempered) ☐ cracked (a.) ☐ chipped (b.)
(a.) Cracks (#):☐ 1 ☐ 2 ☐ 3 ☐ 4--10 ☐ >10
    Crack(s) start from: ☐ module corner   ☐ module edge   ☐ cell   ☐ junction box
        ☐ foreign body impact location
(b.) Chips (#): ☐ 1 ☐ 2 ☐ 3 ☐ 4--10 ☐ >10
    Chipping location: ☐ module corner ☐ module edge

4. Backsheet: ☐ not applicable ☐ applicable

Appearance: ☐ like new   ☐ minor discoloration   ☐ major discoloration
Texture: ☐ like new   ☐ wavy (not delaminated)   ☐ wavy (delaminated)   ☐ dented
Material quality --chalking: ☐ none   ☐ slight   ☐ substantial
Damage: ☐ no damage   ☐ small, localized   ☐ extensive
    Damage Type (mark all that apply):
    ☐ burn marks (a.) ☐ bubbles (b.) ☐ delamination (c.) ☐ cracks/scratches (d.)

    (a.)Burn marks (#):☐ 1 ☐ 2 ☐ 3 ☐ 4--10 ☐ >10
        Fraction of area burned:
        ☐ <5% ☐ 5--25% ☐ 50% ☐ 75% --100% (consistent overall)
    (b.) Bubbles(#):   ☐ 1 ☐ 2 ☐ 3 ☐ 4--10 ☐ >10
        Average bubble dimension: ☐ <5mm ☐ 5--30mm ☐ >30mm
        Fraction of area with bubbles > 5 mm:
        ☐ <5% ☐ 5--25% ☐ 50% ☐ 75% --100% (consistent overall)
    (c.) Fraction of area delaminated:
        ☐ <5% ☐ 5--25% ☐ 50% ☐ 75% --100% (consistent overall)
        Fraction of delamination that exposes circuit or cell(s)
        ☐ <5% ☐ 5--25% ☐ 50% ☐ 75% --100% (consistent overall)
    (d.) Cracks/scratches (#): ☐ 1 ☐ 2 ☐ 3 ☐ 4--10 ☐ >10
        Cracks/scratches location: ☐ random/no pattern ☐ over cells ☐ between cells
        Fraction of area affected by cracks/scratches (approx.):
        ☐ <5% ☐ 5--25% ☐ 50% ☐ 75% --100% (consistent overall)
        Fraction of cracks/scratches that expose circuit (approx.):
        ☐ 0% ☐ 25% ☐ 50% ☐ 75% ☐ 100%

5. Wires/Connectors:

Wires: ☐ not applicable ☐ like new ☐ pliable, but degraded ☐ embrittled
    (mark all that apply): ☐ cracked/disintegrated insulation ☐ burnt
    ☐ corroded ☐ animal bites/marks
Connectors: ☐ not applicable ☐ like new ☐ pliable, but degraded ☐ embrittled
    Type: ☐ unsure ☐ MC3 or MC4 ☐ Tyco Solarlok ☐ other _____

(mark all that apply): ☐ cracked/disintegrated insulation ☐ burnt ☐ corroded

6. Junction Box:

Junction box itself: ☐ not applicable/observable ☐ applicable
    Physical state: ☐ intact ☐ unsound structure
    (mark all that apply): ☐ weathered ☐ cracked ☐ burnt ☐ warped
    Lid: ☐ intact/potted ☐ loose ☐ fell off ☐ cracked
Junction box adhesive: ☐ not applicable/observable ☐ applicable
    Attachment: ☐ well attached ☐ loose/brittle ☐ fell off
    Pliability: ☐ like new ☐ pliable, but degraded ☐ embrittled
Junction box wire attachments: ☐ not applicable/observable ☐ applicable
    Attachment: ☐ well attached ☐ loose ☐ fell off
    Seal: ☐ good seal ☐ seal will leak
    other: ☐ arced/started a fire

7. Frame Grounding:

Original state: ☐ Wired ground   ☐ Resistive ground   ☐ No ground ☐ unknown
Appearance: ☐ Not applicable   ☐ Like new ☐ Some corrosion   ☐ Major corrosion
Function: ☐ Well grounded   ☐ No connection

Photos taken of ☐ back, label, and junction box

CONTINUE INSPECTION ON FRONT SIDE OF MODULE

8. Frame: ☐ not applicable   ☐ applicable

Appearance: ☐ like new   ☐ damaged (a.)   ☐ missing
    (a.) (mark all that apply): ☐ minor corrosion ☐ major corrosion ☐ frame joint separation
                             ☐ frame cracking ☐ bent frame   ☐ discoloration
Frame Adhesive: ☐ like new/not visible   ☐ degraded (a.)
    (a.) (mark all that apply): ☐ adhesive oozed out   ☐ adhesive missing in areas

9. Frameless Edge Seal: ☐ not applicable ☐ applicable

Appearance: ☐ like new   ☐ discoloration (a.) ☐ visibly degraded
    (a.) Fraction affected by discoloration:
    ☐ <5% ☐ 5--25% ☐ 50% ☐ 75% --100% (consistent overall)
Material problems:
    ☐ squeezed/pinched out   ☐ shows signs of moisture penetration
Delamination: ☐ none ☐ area(s) delaminated (a.)
    (a.) Fraction Delaminated:
    ☐ <5% ☐ 5--25% ☐ 50%   ☐ 75% --100% (consistent overall)

10. Glass/Polymer (front):

Material: ☐ glass ☐ polymer ☐ glass/polymer composite ☐ unknown
Features: ☐ smooth ☐ slightly textured ☐ pyramid/wave texture
    ☐ antireflection coating
Appearance: ☐ clean ☐ lightly soiled ☐ heavily soiled
    Location of soiling:
        ☐ locally soiled near frame:
            ☐ left ☐ right ☐ top ☐ bottom ☐ all sides
        ☐ locally soiled on glass /bird droppings
Damage: ☐ no damage ☐ small, localized ☐ extensive
    Damage Type (mark all that apply):
    ☐ crazing or other non--crack damage
    ☐ shattered (tempered) ☐ shattered (non--tempered) ☐ Cracked (a.)
    ☐ Chipped (b.) ☐ milky discoloration (c.)
    (a.) Cracks (#): ☐ 1 ☐ 2 ☐ 3 ☐ 4--10 ☐ >10
        Crack(s) start from: ☐ module corner ☐ module edge ☐ cell ☐ junction box
                ☐ foreign body impact location
    (b.) Chips (#): ☐ 1 ☐ 2 ☐ 3 ☐ 4--10 ☐ >10
        Chipping location: ☐ module corner ☐ module edge
    (c.) Fraction of area:
        ☐ <5% ☐ 5-25% ☐ 50% ☐ 75% -- 100% (consistent overall)

11. Metallization:

Gridlines/Fingers: ☐ not applicable/barely observable ☐ applicable
    Appearance: ☐ like new ☐ light discoloration(a.) ☐ dark discoloration(a.)
    (a.) Fraction of discoloration:
        ☐ <5%   ☐ 5-25%   ☐ 50%   ☐ 75% - 100% (consistent overall)
Busbars: ☐ not applicable/not observable ☐ applicable
    Appearance: ☐ like new ☐ light discoloration(a.) ☐ dark discoloration(a.)
    (a.) Fraction of discoloration:
        ☐ <5%   ☐ 5-25%   ☐ 50%   ☐ 75% - 100% (consistent overall)
    (mark all that apply): ☐ obvious corrosion ☐ diffuse burn mark(s) ☐ misaligned
Cell Interconnect Ribbon: ☐ not applicable/not observable ☐ applicable
    Appearance: ☐ like new ☐ light discoloration(a.) ☐ dark discoloration(a.)
        (a.) Fraction of discoloration:
        ☐ <5%   ☐ 5-25%   ☐ 50%   ☐ 75% - 100% (consistent overall)
    (mark all that apply): ☐ obvious corrosion ☐burn marks ☐ breaks
String Interconnect: ☐ not applicable/not observable ☐ applicable
    Appearance: ☐ like new   ☐ light discoloration(a.)   ☐ dark discoloration(a.)
        (a.) Fraction of discoloration:
        ☐ <5%   ☐ 5-25%   ☐ 50%   ☐ 75% - 100% (consistent overall)
    (mark all that apply): ☐ obvious corrosion ☐ burn marks ☐ breaks
        ☐ arc tracks (thin, small burns)

12. Silicon (mono or multi) module: ☐ not applicable ☐ applicable

Number of:
        Cells in module _____
        Cells in series/string _____
        Strings in parallel _____
Cell size: Width _____ cm Length _____ cm
Distance between frame and cell: ☐ >10 mm ☐ <10 mm
Distance between cells in a string: ☐ >1 mm ☐ <1 mm
Discoloration: ☐ none/like new ☐ light discoloration ☐ dark discoloration
      Number of cells with any discoloration: _____
      of those, average % discolored area:
      ☐ <5%   ☐ 5-25%   ☐ 50%   ☐ 75% - 100% (consistent overall)
      Discoloration location(s) (mark all that apply):
      ☐ module center   ☐ module edges   ☐ cell centers   ☐ cell edges
      ☐ over gridlines   ☐ over busbars   ☐ over tabbing   ☐ between cells
      ☐ individual cell(s)darker than others   ☐ partial cell discoloration
      Junction box area: ☐ same as elsewhere ☐ more affected ☐ less affected
Damage: ☐ none
      (mark all that apply): ☐ burn mark (a.) ☐ cracking (b.) ☐ moisture
                          ☐ worm marks/snail tracks (c.) ☐ foreign particle embedded
      (a.) Burns (#): ☐ 1   ☐ 2   ☐ 3   ☐ 4-10   ☐ >10
      (b.) Number of cells cracked: _____
      (c.) Number of cells with worm marks/snail tracks: _____
Delamination: ☐ none ☐ from edges ☐ uniform ☐ corner(s) ☐ near junction box
      ☐ between cells (a.) ☐ over cells (b.) ☐ near cell or string interconnect
      (a.) Fraction delaminated between cells:
      ☐ <5%   ☐ 5-25%   ☐ 50%   ☐ 75-100% (consistent overall)
      (b.) Fraction delaminated over cells:
      ☐ <5%   ☐ 5-25%   ☐ 50%   ☐ 75-100% (consistent overall)
      Likely interface (choose 2): _____
      ☐ glass   ☐ semiconductor   ☐ encapsulant   ☐ back sheet   ☐ busbar

13. Thin film module: ☐ not applicable ☐ applicable

Number of cells:
        Number of cells in module _____
        Number of cells in series/string _____
        Number of strings in parallel _____
Cell size: Width _____ cm Length _____ cm
Distance between frame and cell: ☐ >10 mm ☐ <10 mm
Appearance: ☐ like new   ☐ minor/light discoloration ☐ major/dark discoloration
      Discoloration type (mark all that apply):
      ☐ spotted degradation   ☐ haze (encapsulant browning)   ☐ other

Discoloration location (mark all that apply):
☐ overall/no location pattern ☐ module center ☐ module edge(s)
☐ cell center ☐ cell edges ☐ near crack(s)
Damage: ☐ no damage ☐ small, localized ☐ extensive
Damage Type (mark all that apply): ☐ burn mark(s) ☐ cracking
☐ possible moisture ☐ foreign particle embedded
Delamination: ☐ no delamination ☐ small, localized ☐ extensive
Location: ☐ from edges ☐ uniform ☐ corner(s) ☐ near junction box ☐ near busbar
☐ along scribe lines
Delamination Type: ☐ absorber delamination ☐ AR coating delamination ☐ other

Photos taken of ☐ front and defects

14. Electronic Records ☐ not applicable ☐ applicable
Photographs and I--V curves recorded electronically--list file names in blanks
Photo files _____
I--V curve _____
Connector function: ☐ functions ☐ no longer mates ☐ exposed
Irradiance _____Sensor _____
Temperature _____Sensor _____
EL picture _____
IR picture_____
Bypass Diode Test: ☐ not applicable ☐ applicable
Number of diodes:
In total_____, shorted_____, open_____

OTHER

APPENDIX B

B   EVOLUTION OF MODULE DESIGN QUALITY BETWEEN 1997 AND 2011

Figures B-1 and B-2) present the accelerated qualification test failure data of more than five thousand modules between 1997 and 2011 (TamizhMani et al., 2012). Figure B-1, corresponding to c-Si modules, indicates that the failure rate was low before 2005, became high in 2005-2007, and became low again after 2007 with lowest being between 2009 and 2011. Because the number of new manufacturers with limited module design and manufacturing experience became very high (from less than 50 old manufacturers to more than 200 new manufacturers) during 2005-2007 time period, the failure rate in the accelerated qualification testing dramatically increased. Ignoring the 2005-2007 data, the failure rates of various accelerated tests of the old modules (before 2005) and recent modules are nearly the same for the 2007-2009 period or even lower for the 2009-2011 period. If one assumes and proves that the accelerated qualification failure data for the periods after 2007 represent the infant/early field failure data (if made available) of the recent field installed modules (more than 80% of the cumulative installed modules have come from the modules produced after 2007), then one may tend to use the future qualification failure data (generated by independent test labs) to predict the infant failure rates of future field installed modules. In all these historical failure reporting years (1997-2011), the failure rates in the qualification testing of crystalline silicon modules were primary influenced by the change in the number of manufacturers with varied manufacturing experience. However, in future, the trend of failure rates in the qualification testing of crystalline silicon modules may strongly be influenced by the change in the module construction materials and radically different designs and manufacturing processes. As shown in Figure B-3, the SunShot program aims to reduce the price of the module from about $2/W to about $0.5/W by primarily reducing the costs of module construction materials and manufacturing processes (U.S. Department of Energy, 2012). The change in construction materials include the wafer (thickness), encapsulant, backsheet, edge seals, mounting hardware, cable

connectors, cell interconnections, bus bars, and junction boxes. All these material level changes are expected to have significant influence in the failure rates of future qualification testing programs.
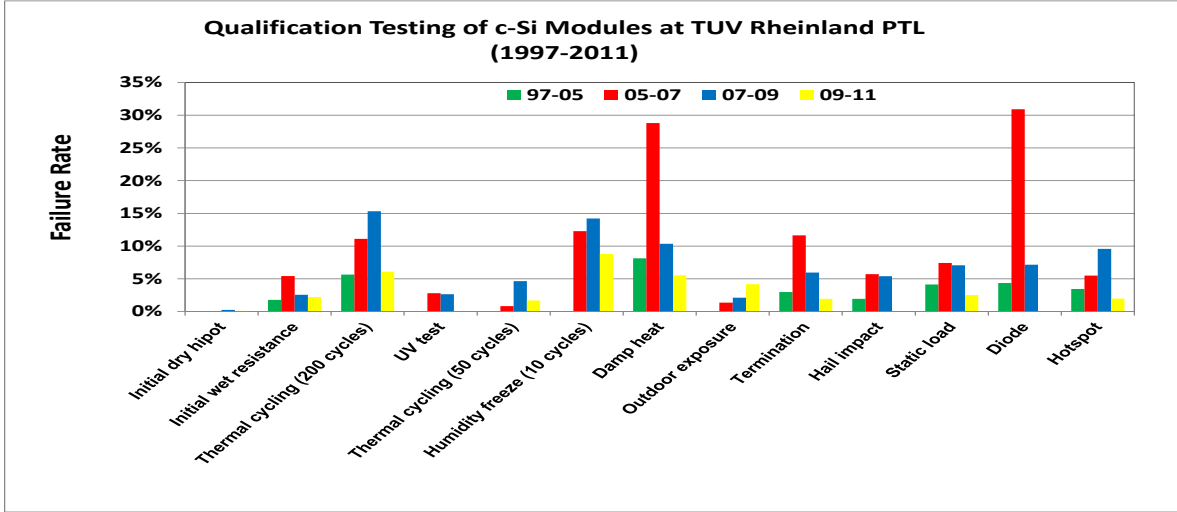

Figure B-1: Failure rates of crystalline silicon PV modules in qualification testing (TamizhMani et al., 2012).
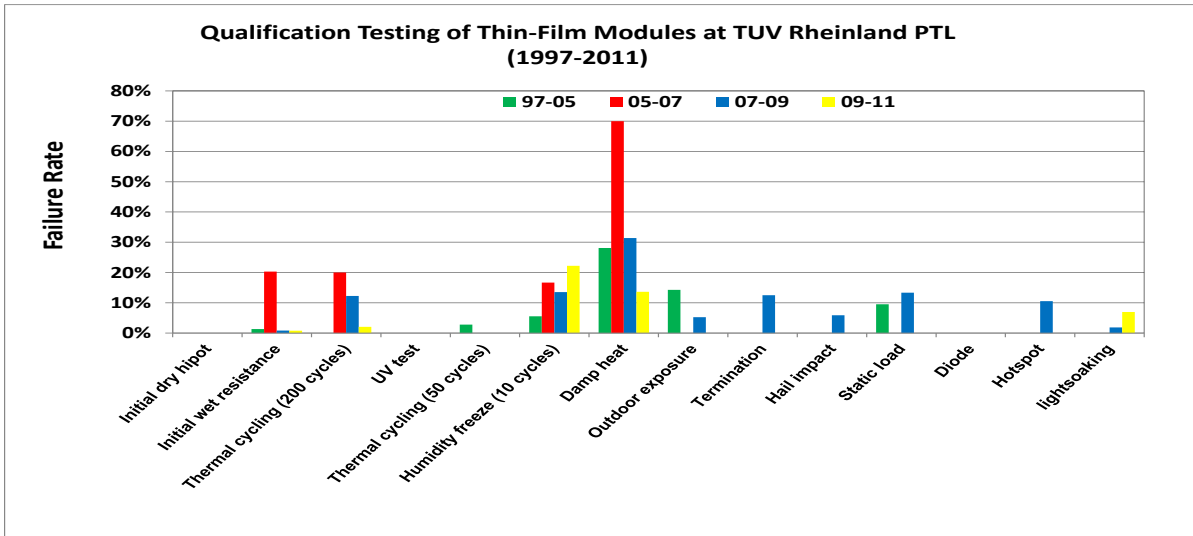

Figure B-2: Failure rates of thin film PV modules in qualification testing (TamizhMani et al., 2012).
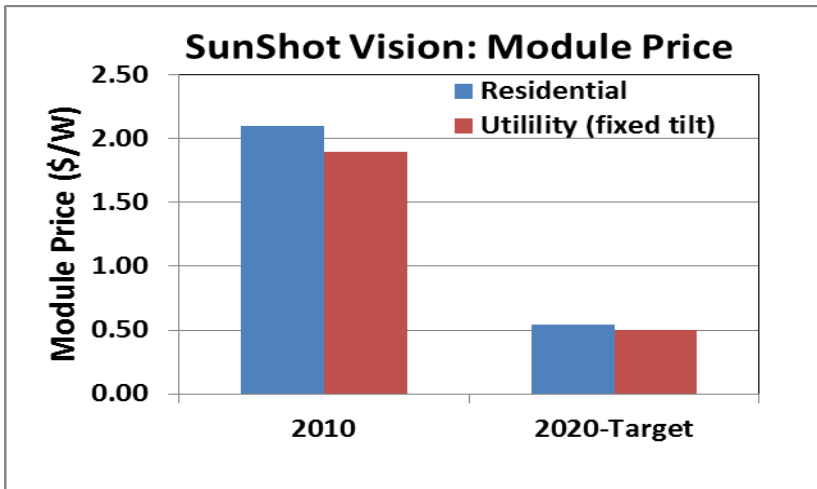
Figure B-3: Target reduction of module price by reducing cost of materials, manufacturing processes, and shipping (U.S. Department of Energy, 2012).

APPENDIX C

C   USING INFORMATION GAIN AS SPLITTING RULE

The algorithm below is from (Han & Kamber, 2006)

- ❖ Let D be the training set containing tuples of class Ci, i={1, 2, ..., m}

  The expected info required to classify any arbitrary tuple in D is:

  $$\text{Info}(D) = -\sum_{i=1}^{m} p_i \log_2(p_i)$$

  - ▪ p_i = probability that the tuple belong to class C_i

    $$p_i = \frac{|C_{i,D}|}{|D|} = \frac{\text{\# of tuples of class } C_i \text{ in D}}{\text{\# of tuples in D}}$$

  - ▪ Info(D) is also known as the Entropy of D

- ❖ Entropy of attribute A with values {a_1, a_2, ..., a_v} is

  $$\text{Info}_A(D) = \sum_{j=1}^{\upsilon} \frac{|D_j|}{|D|} \text{Info}(D_j)$$

  - ▪ D_j is the # of tuples in D with outcome a_j of A

- ❖ Info gained by branching on attribute A is:

  $$\text{Gain}(A) = \text{Info}(D) - \text{Info}_A(D)$$

- ❖ Splitting attribute = Attribute with highest Gain(A)

APPENDIX D

D   DECISION TREE ALGORITHM

The below algorithm was obtained from (Dunham, 2003)

Input: Training data – D

Output: Decision tree – T

DTBuild algorithm:

(1) T = Ø;

(2) Apply Attribute selection method;;

(3) T = Create root node and label with splitting attribute;

(4) T = Add arc to root node for each split predicate and label;

(5) For each arc do

D = Database created by applying splitting predicate to D;

If stopping point reached for this path, then
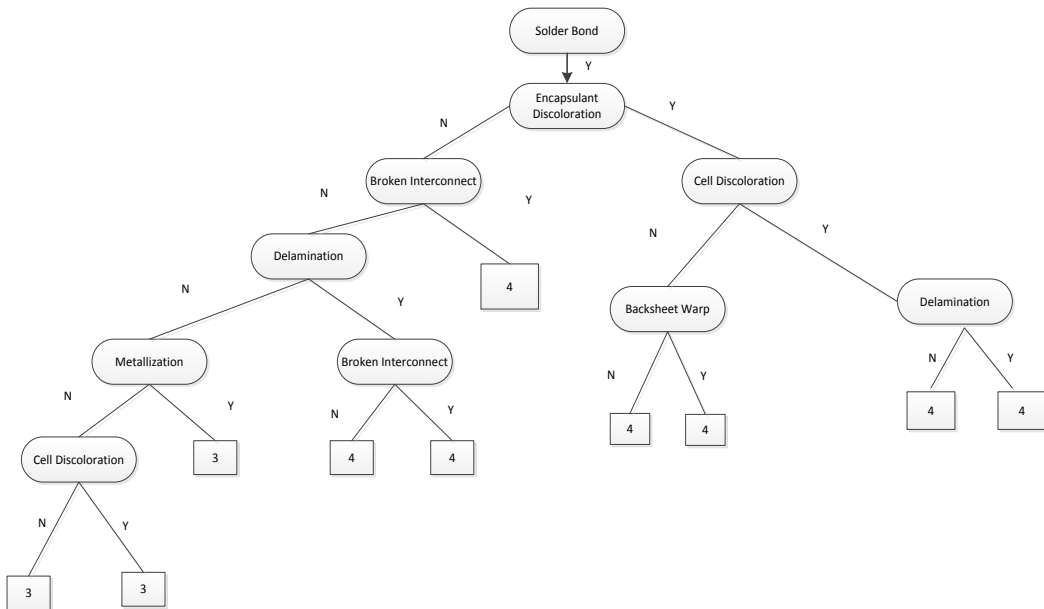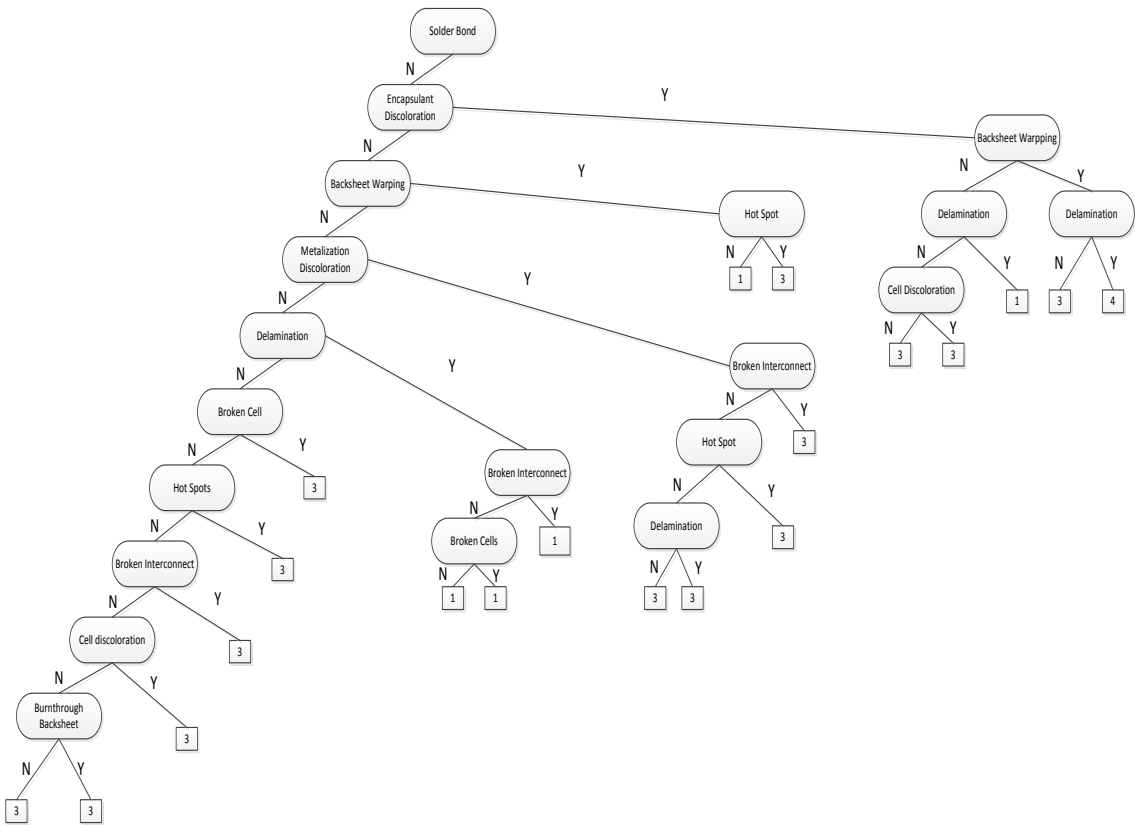
T' = Create leaf node and label with appropriate class;

Else

T' = DTBuild(D);

T = Add T' to arc;

APPENDIX E

E   A VISUALIZATION OF THE DECISION TREE

APPENDIX F

F   DECISION TREE ACCURACY

=== Stratified cross-validation ===

=== Summary ===

Correctly Classified Instances   1856   73.1284 %

Incorrectly Classified Instances   682   26.8716 %

Kappa statistic   0.4636

Mean absolute error   0.203

Root mean squared error   0.3205

Relative absolute error   67.5217 %

Root relative squared error   82.6693 %

Total Number of Instances   2538

=== Detailed Accuracy By Class ===

	TP Rate	FP Rate	Precision	Recall	F-Measure	ROC Area	Class
	0.963	0.58	0.698	0.963	0.809	0.744	III
	0.316	0.018	0.708	0.316	0.437	0.802	I
	0	0	0	0	0	0.682	II
	0.743	0.012	0.929	0.743	0.825	0.903	IV
Wted Avg.	0.731	0.342	0.658	0.731	0.671	0.772	

=== Confusion Matrix ===


```
  a    b    c    d   <-- classified as
1421  29    0   26   |  a = III
 210  97    0    0   |  b = I
 291   9    0    0   |  c = II
 115   2    0  338   |  d = IV
```